



Università  
Ca' Foscari  
Venezia

Corso di Dottorato di ricerca  
in Science and  
Technology of Bio  
and Nanomaterials  
ciclo XXXIV

Tesi di Ricerca

***Advanced bioelectrochemical  
sensors based on nanostructured  
surfaces***

SSD: CHIM/01

**Coordinatore del dottorato**  
ch. prof. Flavio Rizzolio

**Supervisore**  
Dott.ssa Najmeh Karimian, PhD

**Co-supervisori**  
ch. prof. Paolo Ugo, ch. Prof. Flavio Rizzolio

**Dottorando**  
Davide Campagnol  
Matricola 956451

# Index

ABSTRACT .....	7
CHAPTER 1: INTRODUCTION .....	8
1. INTRODUCTION TO BIOSENSORS .....	8
1.1. DEFINITION AND CLASSIFICATION .....	8
1.2. ELECTROCHEMICAL BIOSENSORS .....	9
1.3. ELECTROCHEMICAL NANO-BIOSENSORS .....	10
1.3.1. <i>Voltammetry with nanoelectrode arrays</i> .....	12
1.4. ADVANCES IN THE FUNCTIONALIZATION OF RECOGNITION ELEMENT .....	13
1.4.1. <i>Molecularly imprinted polymers (MIPs)</i> .....	14
1.4.1.1. <i>Imprinting of Proteins</i> .....	16
1.4.1.2. <i>MIP electropolymerization</i> .....	16
1.4.1.2.1. <i>Orto-phenylenediamine-based functional monomers</i> .....	17
1.4.2. <i>Electrochemical sensors based on MIPs</i> .....	19
1.5. AIM OF THE THESIS .....	20
CHAPTER 2: STUDY OF GLASSY CARBON NANOELECTRODE ARRAYS ON ENZYMATIC REDOX-MEDIATORS.....	21
1. INTRODUCTION .....	21
1.1. NANOELECTRODE ARRAYS: PRELIMINARY CONCEPTS AND FABRICATION TECHNIQUES.....	21
EXPERIMENTAL SECTION.....	23
2. MATERIALS AND METHODS .....	23
2.1. ELECTROCHEMICAL APPARATUS AND PROCEDURES.....	23
2.1.2. NEA MANUFACTURING .....	24
3. RESULTS AND DISCUSSION.....	25
3.1. MORPHOLOGICAL CHARACTERIZATION OF NEAS .....	25
3.2. ELECTROCHEMICAL CHARACTERIZATION OF THE NEA WITH FA <sup>+</sup> .....	26
3.3. CATHODIC ELECTROCHEMISTRY OF NEA WITH PHENOTHIAZINE REDOX MEDIATORS.....	29
4. CONCLUSION.....	35
CHAPTER 3: DEVELOPMENT OF MOLECULARLY IMPRINTED ELECTROCHEMICAL SENSOR FOR THE ULTRASENSITIVE DETECTION OF CYTOCHROME C .....	36
1. INTRODUCTION .....	36
1.1. CYTOCHROME C: STRUCTURE AND ROLE IN RESPIRATION.....	36
1.2. CYTOCHROME C: ROLE IN APOPTOSIS.....	37
1.3. CLINICAL ROLE OF <i>CYTOCHROME C</i> .....	39
1.4. ELECTROCHEMICAL DETECTION OF <i>CYTOCHROME C</i> .....	39
EXPERIMENTAL SECTION .....	41
2. MATERIAL AND METHODS .....	41
2.1. MATERIALS .....	41
2.2. APPARATUS AND MEASUREMENTS.....	42
2.3. FABRICATION OF MIP AND NIP ELECTRODES .....	43
2.4. ANALYTICAL MEASUREMENTS .....	43
3. RESULTS AND DISCUSSION.....	45
3.1. PREPARATION OF MIP AND NIP ELECTRODES.....	45
3.1.1. <i>Electrochemical characterization of the imprinted electrodes</i> .....	46

3.1.2. <i>Optimization of the MIP sensor preparation</i> .....	48
3.1.2.1. Optimization of the monomer concentration .....	48
3.1.2.2. Optimization of the template concentration.....	50
3.1.2.3. Optimization of number of cycles for electropolymerization .....	52
3.1.2.4. Template Removal .....	54
3.1.2.5. Optimization of the re-binding time .....	57
3.2. BINDING STUDY .....	59
3.3. ANALYTICAL PERFORMANCES .....	61
3.3.2. <i>Sensor performances in real condition: selectivity studies</i> .....	64
3.3.3. <i>Sensor performances in real condition: serum tests</i> .....	65
4. CONCLUSIONS .....	67
<b>CHAPTER 4: DEVELOPMENT OF AN ELECTROCHEMICAL SENSOR BASED ON SCREEN PRINTED ELECTRODE MODIFIED WITH MIP FOR THE DETECTION OF TROPONIN I</b> .....	<b>68</b>
1. INTRODUCTION .....	68
1.2. CARDIAC TROPONIN I: CLINICAL ROLE AND DETECTION .....	68
2. MATERIALS AND METHODS.....	73
2.1. MATERIALS.....	73
2.2. APPARATUS AND MEASUREMENTS.....	73
2.3 PREPARATION AND ELECTROCHEMICAL CHARACTERIZATION OF IMPRINTED SENSORS.....	74
3.RESULTS AND DISCUSSION.....	75
3.1. ELECTROCHEMICAL CHARACTERIZATION OF SPES .....	75
3.2. DETERMINING THE ELECTROACTIVE AREA USING CYCLIC VOLTAMMETRY .....	76
3.2.1. <i>Experimental measurement of the active area of Dropsens Gold 220AT</i> .....	76
3.2.3 <i>Dropsens Carbon 110AT</i> .....	82
3.2.4. <i>Micrux Carbon</i> .....	84
3.3. DEVELOPMENT OF PO-PD MODIFIED SCREEN PRINTED ELECTRODES (SPES) .....	88
3.3.1. <i>Electrochemical polymerization on SPES</i> .....	88
3.3.2. <i>Electrochemical characterization of PoPD@SPE</i> .....	89
3.4. PREPARATION OF POLY O-PD COATINGS IN THE PRESENCE OF TROPONIN I ON SPE MICRUX CARBON: FORMATION OF TNI-MIP-SPE .....	91
3.5. FABRICATION OF ELECTROCHEMICALLY SENSOR BASED ON DUMMY MOLECULARLY IMPRINTED POLYMERS USING CYTOCHROME C AS A TEMPLATE MOLECULE FOR TNI DETECTION .....	92
4.CONCLUSIONS .....	94
5. GENERAL CONCLUSIONS.....	95
REFERENCES.....	97

## List of Abbreviations

### **A**

AMI

Acute Myocardial Infarction .....20

ATP

Adenosin Tryphosphate.....41

### **B**

BDD

boron-doped diamond.....24

### **C**

CME

chemically modified electrode ..... 10

CNT

Carbon nanotubes ..... 12

COX

cyclo oxygenase .....39

cTnI

Cardiac Troponin I .....69

cTnT

Cardiac Troponin T .....69

CVD

Cardiovascular Disease .....20

*Cyt c*

Cytochrome C.....20

### **D**

Da

Dalton ..... 17

DPV

Differential Pulse Voltammetry .....45

### **E**

EBL

electron beam lithography ..... 12

ETC

mitochondrial respiration chain.....41

### **F**

FA<sup>+</sup>

(ferrocenylmethyl)trimethylammonium.....22

FA<sup>+</sup>PF<sub>6</sub><sup>-</sup>

Ferrocenylmethyl trimethylammonium hexafluorophosphate .....25

FcCOOH

Ferrocene carboxylic Acid .....	46
<b>G</b>	
GC	
Glassy Carbon .....	22
GC-NEAs	
Glassy Carbon Nano electrode Arrays .....	22
<b>H</b>	
HS	
Human Serum.....	67
<b>I</b>	
IMM	
Inner mitochondrial membrane .....	41
<b>M</b>	
MIPs	
molecularly imprinted polymers .....	10
<b>N</b>	
nanoMIPs	
MIP nanoparticles.....	16
NEAs	
nanoelectrode arrays.....	11
NEEs	
Nanoelectrode Ensembles .....	12
NIL	
Nanoimprint Lithography.....	23
NIP	
Not imprinted polymer .....	60
NP	
Nano particles.....	12
<b>O</b>	
o-PD	
o-phenylenediamine .....	18
<b>P</b>	
PBS 1X	
Phosphate Buffer Saline .....	25
PoPD	
Poly orthophenylenediamine.....	18
PTM	
post translational modifications.....	39
<b>R</b>	
ROS	
Reactive Oxygen Species .....	39

## **S**

### S/N

Signal-to-noise..... 13

### SAMs

self-assembled monolayers..... 11

### SEM

Scanning Electron Microscopy ..... 25

## **T**

### TnI

Troponin I..... 20

### TNIL

Thermal nanoimprinting..... 24

## **U**

### UV

Ultra violet..... 18

## **Abstract**

In this thesis the preparation and characterization of nanostructured polymer films on different electrode materials with focus on their potential application for biochemical analysis were studied. With this goal, both glassy carbon nanoelectrode arrays and electrodes coated with molecular imprinted polymers (MIPs) were examined. The analytes studied were some redox mediators used in bioelectrochemistry as well as proteins such as Cytochrome *c* and Troponin I. In particular the use of MIP showed very promising capabilities for the detection of Cytochrome *c* at trace concentration levels. Preliminary results indicate the possibility to extend this approach to the highly sensitive detection of Troponin I as a potential cardiac disease biomarker.

# CHAPTER 1: Introduction

## 1. Introduction to biosensors

### 1.1. Definition and classification

The analysis of biomolecules plays crucial role in biological and clinical studies [1], in particular of molecules which are considered as biomarkers of particular diseases and pathological conditions. Molecular recognition between a molecular receptor (host) and a substrate (guest) in a matrix containing structurally related molecules requires discrimination and binding; this can happen only if the binding sites of the host and guest molecules complement each other in size, shape, and chemical functionality. Biological systems, such as enzyme-substrate, antibody-antigen, and hormone-receptor systems, demonstrate molecular recognition properties developed by natural selection [2]. Chemical recognition systems are nowadays applied for analytical purposes and many analytical assays exploit the occurrence of a molecular recognition event between a reactant and the target analyte. Analyses can be performed in a qualitative or quantitative way, for determining the presence or absence of the analyte and its concentration, respectively. The use and practice of bioanalytical assays, in particular heterogeneous bioassays, together with the modern progress in sensitive and miniaturised analytical instrumentation, have evolved into the development of the so-called analytical biosensors [3]. According to the definition recommended by the International Union of Pure and Applied Chemistry (IUPAC) in 1999, a biosensor is a self-contained device that is capable of providing specific quantitative or semi-quantitative analytical information using a biological recognition element (biochemical receptor) which is retained in direct spatial contact with a suitable transduction element responsible for detecting the biological reaction and converting it into a measurable signal [4] (see Figure 1).

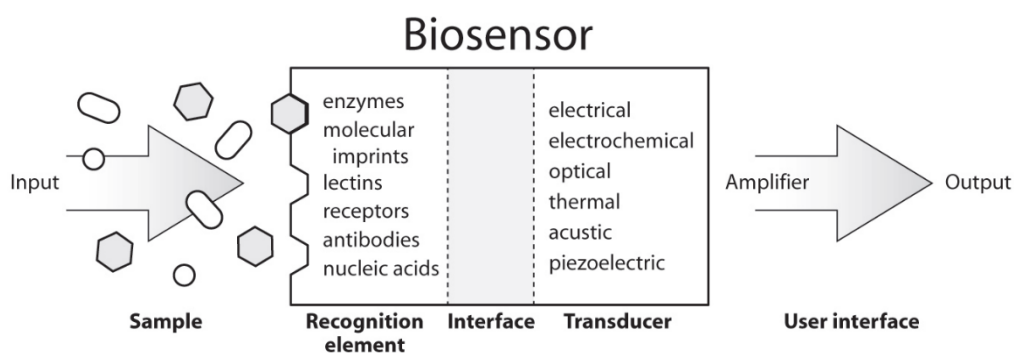


**Figure 1.** Schematic representation of a biosensor, showing biorecognition, interface, and transduction elements (reproduced from ref. [5]).



The biological recognition element of a biosensor can be of biological origin, such as an enzyme or an antibody, an antibody fragment, a nucleic acid, a whole microbial cell, or even a plant or an animal tissue, or abiotic such as synthetically produced host-guest molecules and molecularly imprinted polymers (MIPs). The main purpose of the recognition system is to provide the sensor with a high degree of selectivity necessary for the specific recognition of the analyte in a complex matrix. The transducer is typically a miniaturized device which transforms a form of energy into another. In an analytical sensor, the transducer transforms a change in energy associated with the recognition event (typically thermal, photonic or electrochemical energy) into a signal, typically an electrical signal such as an electrical current or a potential. The transducer can be a thermistor, an electrode, an optode or a resonator. Therefore, depending on the type of transducer employed, biosensors can be classified as optical, electrochemical, calorimetric and piezoelectric biosensors [3]. Figure 2 presents a scheme summarizing the classification of biosensors.

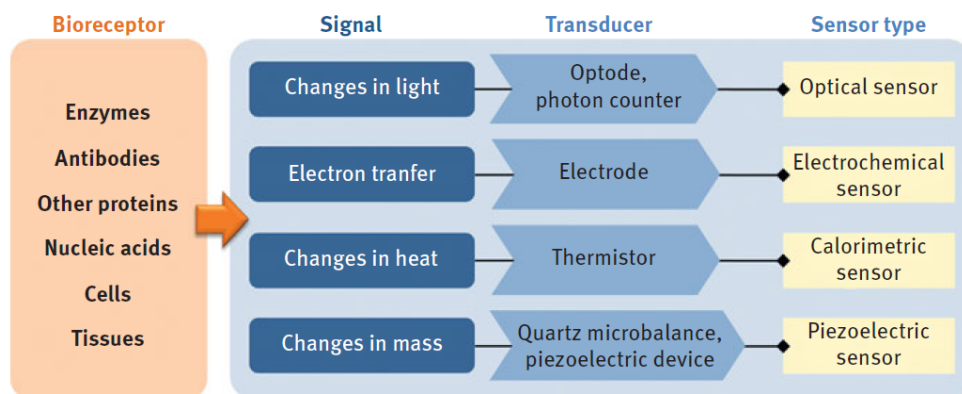


**Figure 2.** Classification of biosensors (reproduced from ref. [3]).

## 1.2. Electrochemical biosensors

An electrochemical biosensor is a biosensor with an electrochemical transducer that detects changes in electrical properties (redox potential, current or conductivity) related to a biorecognition event. An electrochemical biosensor can be considered as a chemically modified electrode (CME) [6,7] in which the electrode surface is typically functionalized by an electronic conducting, semiconducting or ionic material which incorporates the biorecognition element. Electrochemical biosensors are widely studied and applied for bioanalysis, thanks to the following advantages: they are user friendly,

have a low cost, are small in size, allow to achieve low detection limits, can be easily automatized, and they do not suffer any interference from coloured or turbid samples. All these properties make them applicable for *in situ* and decentralized monitoring [8]. Electrochemical biosensors can be classified into three main classes depending on the parameter that is measured [3]:

- potentiometric biosensors, when the transducer detects changes in electric(chemic)al potential;
- conductimetric biosensors that measure changes in conductivity;
- amperometric (or voltammetric) biosensors that measure the electrical current resulting from the electrochemical oxidation or reduction of an electroactive species which undergo a redox reaction during the analytical process.

### 1.3. Electrochemical nano-biosensors

Notwithstanding the above advantages, electrochemical biosensors still present some problems and limits which must be overcome. One crucial aspect is the optimization of the surface modification procedure to maximize the biorecognition capabilities and to minimize the sensitivity to non-specific adsorption and fouling [9]. In principle, the nano-structuration of the sensor surface can contribute to solve some of these problems, for example nanostructured surfaces can be exploited to increase the specific area of the sensor so that high amounts of biorecognition molecules can be immobilised, while keeping the overall size of the sensor very small [10]. Moreover, by separating biorecognition and transduction, at the nanoscale range, it is possible to engineer the sensor surface so that one can protect, by the use of self-assembled monolayers (SAMs) of thiols, the nanoelectrodes from undesired nonspecific adsorption while confining the biorecognition in the proximity of (but not on) the nanoelectrode [11,12]. As electrodes decrease in size, radial diffusion of the analyte to the electrode surface becomes dominant, finally resulting in a highly efficient mass transport. The high rate of mass transport (diffusion) at small electrodes produces steady-state voltammetric current responses. Under such conditions, chemical and electrochemical processes can become the limiting step of the sequence of processes involved in the heterogeneous electron transfer so that with nanoelectrodes the determination of kinetic parameters for very fast electrochemical reactions becomes possible [13,14]. Increased mass transport characteristics of nanoelectrodes reflects into shorter response times, obtaining increased faradaic to charging current ratio. In particular, the high signal/noise ratios typical of nanoelectrode arrays (NEAs) [9] in the form of nanodisks, nanowires, nanochannels and nanopores has allowed the ultrasensitive detection of analytes of biological interest, which can include both biomacromolecules (e.g., proteins, polynucleotides) and small molecules (e.g., drugs, metabolites, toxic metal ions) [13,15,16]. Improving the benefits of going “nano” in electrochemistry is related to the availability of suitable nanofabrication methods. Figure 3 schematizes the different geometries of

nanoelectrode arrays (NEAs). Top down techniques, such as ion beam lithography [13,17], electron beam lithography (EBL) [18], nanoimprint [19] or scanning probe lithography [20] allow one to obtain high resolution nanostructures, providing a precise positioning and sizing down to a scale of a few nanometers. These spatial resolution capabilities have been indeed exploited to prepare ordered arrays of nanoelectrodes [13,18,21]. In principle, disordered arrays can be obtained also by dispersing metal NPs or CNTs in a thin layer of a dielectric binder or an ink [3]. Another method to modify electrode surfaces that behaves like nanoelectrode ensembles (NEEs) is by coating the surface of a microelectrode with a discontinuous insulating layer, such as a defective self-assembled monolayer or nanoporous polymeric membranes as those used to prepare molecularly imprinted polymers.

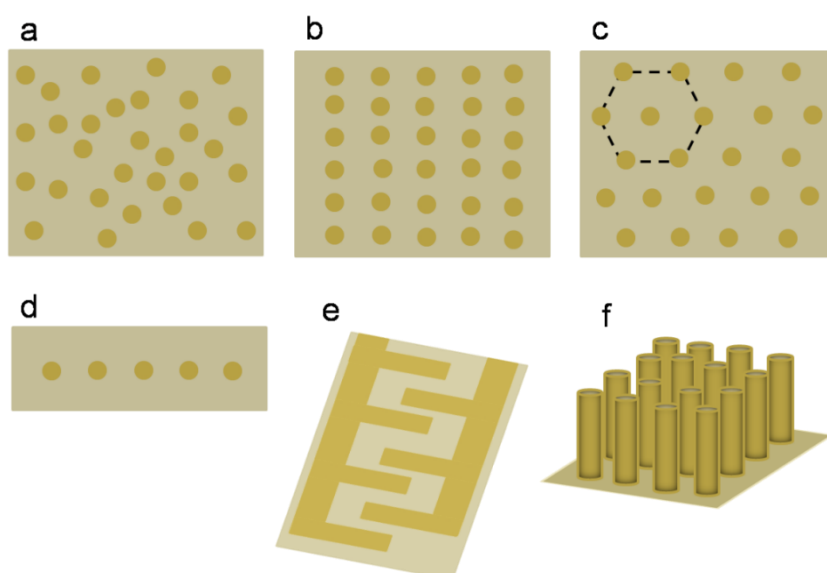


**Figure 3.** Different geometries for array of nanoelectrodes: (a) random array (ensemble), (b) square array, (c) hexagonal array, (d) linear array, (e) interdigitated nanoband array, (f) three-dimensional nanowire array (reproduced from ref. [22]).

Note that, in all these arrays, the nanoelectrodes are electrically shortened so that they all experience the same applied potential. For multiplexing analyses, in principle, it would be necessary to individually address each nanoelectrode or, alternatively, to develop arrays of arrays, where different groups of nanoelectrodes are addressed by distinct current collectors. However, such multiplexing potentialities are still under investigation [3].

### 1.3.1. Voltammetry with nanoelectrode arrays

NEAs distinguish from conventional macro (millimeter-sized) or even ultramicro (micrometer-sized) electrodes for some special characteristics, in particular for the dramatic increase of signal-to-noise (S/N) ratios due to low capacitive currents, which act as noise in voltammetry [23,24] and the extreme sensitivity to the kinetics of charge transfer processes [25]. Depending on the scan rate or the reciprocal distance between the nanoelectrodes [26,27] or the viscosity [28], three different diffusional regimes determine the voltammetric responses at NEAs, as summarized in Figure 4. When radial diffusion boundary layers overlap totally (radius of diffusion hemisphere larger than average hemi-distance between electrodes, Figure 4A), NEAs behave like planar macroelectrodes with respect to faradaic currents. When diffusion hemispheres become shorter (for higher scan rates, Figure 4B), the current response is dominated by radial diffusion at each single element. At very high scan rates, a linear active state is reached in which the current response is controlled by linear diffusion to each individual nanodisk (Figure 4C). Transition from one regime to the other as a function of distance between nanoelectrodes was experimentally demonstrated [16,27]. Figure 4 also reports the equations of the peak/limiting current recorded for each of these regimes, for a reversible redox couple.

The faradaic current at a NEA operating in total overlap regime (i.e., for the cases (a) and (c)) for a reversible redox system obeys the so called Randles-Sevcik equation (Equation 1.1)

$$i_p = 2.69 \times 10^5 \times A_{geom} \times n^{3/2} \times D^{1/2} \times v^{1/2} \times C \quad (1.1)$$

where  $i_p$  is the peak current in amp (A),  $n$  is the number of transferred electrons,  $A_{geom}$  is the overall electrode geometric area (area of the nanoelectrodes + insulator between them) in  $\text{cm}^2$ ,  $D$  is the diffusion coefficient of the reversible redox prob expressed in  $\text{cm}^2/\text{s}$ ,  $v$  is the scan rate in V/s, and  $C$  is the redox species bulk concentration is given in  $\text{mol}/\text{cm}^3$ . Note that for the total overlap case (a), the sensitivity depends indeed on the geometric area, while for the linear active regime (c), it depends on the active area (overall surface area of the nanoelectrodes,  $A_{act}$ ). For the pure radial regime (b), the overall current is the sum of the currents recorded at each nanoelectrode in the array, that is,  $A_{geom} q$  (where  $q$  is the number of nanodiscs per  $\text{cm}^2$ , or nanodisc density). For all these three cases, the noise determined by the capacitive current is always proportional to  $A_{act}$ , according to Equation 1.2:

$$i_c = v \times C_{dl} \times A_{act} \quad (1.2)$$

where  $v$  is the scan rate in V/s,  $C_{dl}$  is the double layer capacitance of the gold nanodisks of the NEA and  $A_{act}$  is the active area in  $\text{cm}^2$ .

It is evident that the two regimes that provide the highest currents and S/N ratios are the pure radial and the total overlap. Note that an inter-electrode distance of  $10r$  (where  $r$  is the radius of the

nanoelectrodes) is high enough to avoid cross talking between the nanoelectrodes [26]. At a NEA, the faradaic currents are equal to those at a macro-electrode of the same geometric area [23], but when  $A_{\text{act}}$  is kept suitably smaller than  $A_{\text{geom}}$ , NEAs can provide signal-to-noise ratios orders of magnitude larger than at macro-electrodes [29,30] so allowing one to use and to detect extremely small concentrations (in the nM range) of electroactive species.

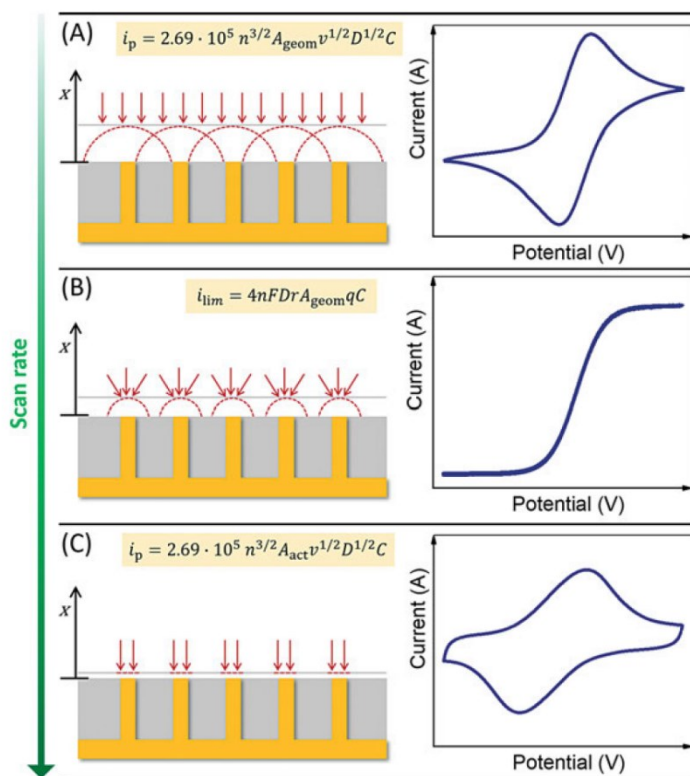


**Figure 4.** Schematic drawing illustrating the different diffusion regimes at nanoelectrode arrays (NEAs) made of shortened nanodisc electrodes (yellow), embedded in an insulator (grey): (A) total overlap; (B) pure radial; (C) linear active. The time scale decreases going from (A) to (C), while the scan rate increases. The relevant equations for peak currents (A) and (C) and plateau current (B) refer to reversible redox systems.  $A_{\text{act}}$  is the active area (nanodisc surface),  $A_{\text{geom}}$  is the total geometric area of the ensemble (nanodiscs and insulator),  $q$  is the density of nanodiscs (disc/cm<sup>2</sup>),  $x$  is the distance from the array surface (reproduced from ref. [3]).

#### 1.4. Advances in the functionalization of recognition element

From a general point of view, receptor design is perhaps the crucial step in the process of sensor development because it has to match the requirements of high selectivity and sensitivity for a target

with the particular characteristics of a given readout [31]. To furnish specific recognition capability for the analyte, the surface of the nanostructured electrode must be functionalized with a suitable modifier. Biomolecular recognition is the underlying principle of many biological processes. Like a hand in a glove, specialized structures such as antibodies, hormone receptors, and enzymes fit perfectly with their natural targets [32]. However, given the relatively poor chemical and physical stability of biomolecules and or not existing a natural receptor for a particular molecule of interest, artificial receptors have been gaining in importance as a possible alternative to applying biological receptors [33].

#### **1.4.1. Molecularly imprinted polymers (MIPs)**

Molecular imprinting technology has become an increasingly popular method for the design of artificial antibodies against a variety of analytes [34]. The strategies of molecular imprinting developed mainly by Wulff [35] and Mosbach [36, 37] in the seventies, have proven to be greatly suitable to be used as artificial receptors for designing biomimetic sensors [38]. Molecular imprinting of synthetic polymers involves arranging polymerizable functional monomers around the target analyte or a derivative thereof (the imprint molecule), which acts as a molecular template [37, 39]. The arrangement is achieved either by utilizing noncovalent interactions such as hydrogen bonds, van der Waals forces, ionic interactions (non-covalent imprinting) or reversible covalent interactions (covalent imprinting) between the template and the functional monomers. The complexes formed are then incorporated by polymerization into a highly crosslinked macroporous polymer matrix [37]. Subsequent removal of the template either by washing or by electrochemical removal, leaves binding sites with specific shape, size, and functional group complementarity to the analyte (Figure 5) [39]. By this way, a molecular memory is introduced into the polymer, which is now capable of rebinding the analyte with a very high specificity. As a generalization, covalent imprinting gives better defined and more homogeneous binding sites, while non-covalent imprinting is much more flexible in the range of functionalities which can be targeted and thus the range of templates which can be used [37]. The semi-covalent strategy is a hybrid of the former two, where the template and functional monomer(s) binding and analyte rebinding occur via covalent and non-covalent chemistries, respectively [40].

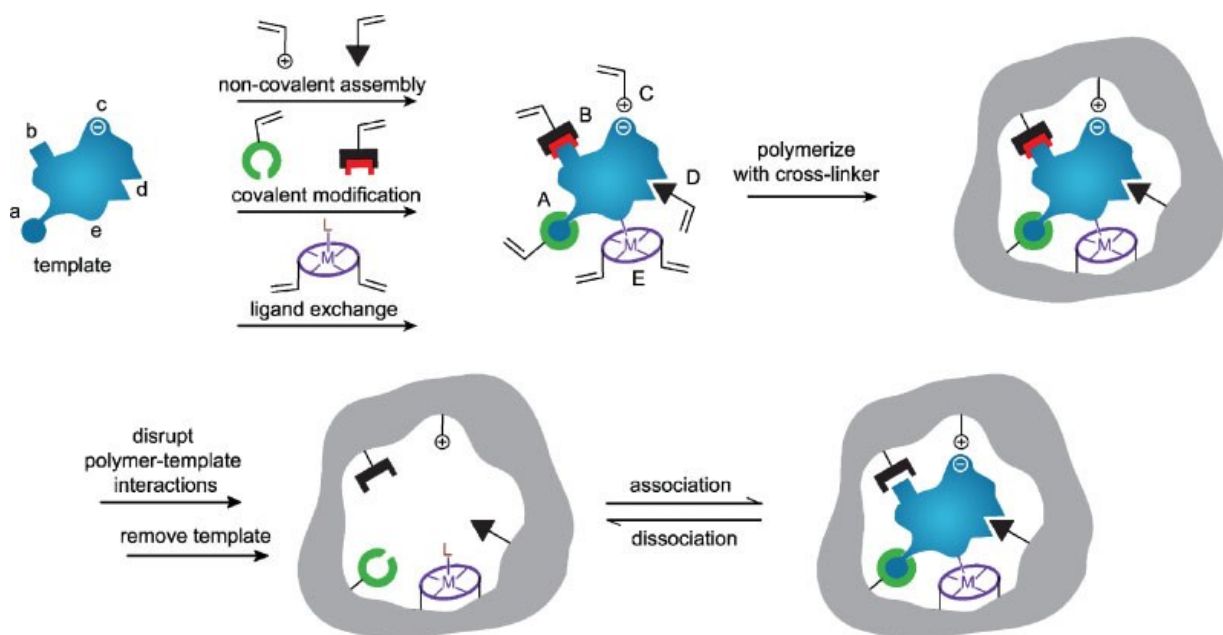


**Figure 5.** Schematic representation of the molecular imprinting process [41], reproduced with permission of the copyright owner.

In fact, MIPs are attractive not only for their recognition properties that are close to those of natural receptors and their availability for a wide range of targets but also for their superior chemical and physical stability compared to biological receptors [31]. Such high potentialities of MIPs find application in different fields such as immunoassays, separation, decontamination, sensing, cell imaging, therapy [42,43], catalysis, drug delivery and solid-phase extraction [44]. Indeed, molecular imprinting of synthetic polymers can be applied to a wide range of target molecules ranging from ions [45], small organic molecules (pharmaceuticals, steroids, sugars, amino-acids, etc.) [46,47] to peptides [48,49], proteins [50,51] and whole cells [52]. Depending on the application, MIPs come in different shapes and morphologies, such as monoliths, thin films, or nanoparticles [53] which can be synthesized in various ways, including free radical polymerization, electropolymerization, controlled/living polymerization, or sol gel synthesis [44]. A number of shortcomings have hindered the implementation of some of these synthesizing techniques in real-world applications. Indeed, the classical bulk methodologies, which were effective for low-molecular-weight compounds, generally can fail to address the peculiarities of macromolecular targets such as proteins [54]. A shift in MIP research from bulk polymers to MIP nanoparticles (nanoMIPs) provides a strategy to address some drawbacks including recognition site heterogeneity, template leakage, mass transfer limitations, and solubilities [55, 53]. In fact, using nanoMIPs can solve some of the problems associated with bulk MIPs; notably, nanoMIPs possess larger surface/mass ratio, have more easily accessible recognition sites and, importantly, they have lower heterogeneities and better solubilities [53].

### 1.4.1.1. Imprinting of Proteins

The protein imprints are necessary for the use of imprinted materials in several applications, such as diagnostics, drug delivery, environmental analysis, and proteomics. Indeed, proteins have size in the nm range with globular or ellipsoid structures, molar weights ranging up to several hundred kDa, moreover they can have poor solubility in organic solvents [34]. These features make the imprinting with protein templates very challenging when using bulk imprinting process. Furthermore, protein structure is sensitive to the non-physiological environment of radical polymerization such as the presence of organic solvent and functional monomers and changes in temperature or pH [53]. To overcome these challenges, several other approaches have been developed including: surface imprinting [56], epitope-mediated surface imprinting [57] and micro-contact imprinting [58]. Indeed, the surface imprinting approach ensures that most of the binding sites are at the surface of the generated materials, which provides improved template removal dynamics, decrease of mass transfer resistance and faster binding kinetics [59]. Synthesis of core-shell nanoparticles, where the imprints are located in the thin polymer shell, is one way to obtain this. By this approach, the advantages of surface imprinting are combined with a high surface area [60]. However, attaching the bulk powder-based polymers or surface imprinted nanoparticles to a sensor can be tricky and hard to accomplish in a reproducible manner [61]. This issue is addressed by synthesizing surface-imprinted polymers directly on the sensor surface. Different strategies are possible: depositing the pre-polymer (monomers/initiator/analyte) first and imprinting it with an analyte stamp or growing the polymer directly from the sensor surface in the presence of the analyte [61]. Electropolymerization allows the growth of polymers from the surface of the electrode in a highly controlled way.

### 1.4.1.2. MIP electropolymerization

An important aspect in the design of a sensor based on MIP is to find an appropriate approach for integrating the MIP layer with the transducer surface. In most cases, the MIP has to be brought into close contact with the transducer surface. An obvious advantage would be to integrate this step in an automated production process. Thereby, the polymer can either be synthesized *in situ* onto the transducer surface or the surface can be coated with a preformed polymer. *In situ* synthesis of a polymer can be done by electropolymerization on conducting surfaces [38, 36]. The thickness of film can be easily controlled by monitoring the amount of charge consumed during the electropolymerization process. This approach facilitates miniaturisation, one of the major goals of chemical sensor technology [62], and allows the quick formation of recognition sites as single elements or as arrays. Electropolymerization of MIPs can be a very practical tool for bioanalytes since



it combines several advantages including [63]: possibility to be performed in water or buffer; no need for an initiator nor activation by increasing the temperature, or by irradiating with UV light [64]. Furthermore, electropolymerization allows the easy tuning of the MIP thickness, that is a key aspect especially in the imprinting of proteins [54].

Another aspect which undoubtedly contributes to extend the fabrication of MIPs using an electropolymerization strategy, is the availability of a wide range of suitable monomers [64], allowing to control/increase the amount and the type of available functional groups involved in the monomer-template interaction [54]. Electroactive monomers can polymerize to form either conducting or nonconducting polymers. Several monomers such as *o*-phenylenediamine (*o*-PD) [65, 66], aniline [67, 68], pyrrole [69,70], 3-aminophenylboronic acid [71,72], and scopoletin [73–75] have gained popularity in MIP electrosynthesis.

#### **1.4.1.2.1. Orto-phenylenediamine-based functional monomers**

Orto-phenylenediamine (*o*-PD) is easily electropolymerized from acidic, neutral and alkaline solutions [76] on various substrate materials and forms films with good chemical and mechanical stability. It is widely used for biomolecules imprinting because its structure contains functional groups that allow multiple interactions, offering hydrophilic, hydrophobic and basic recognition sites via electrostatic interactions, hydrogen bond and  $\pi$  -  $\pi$  bond with the target molecules [38]. In fact, the presence of neutral or protonated  $-NH_2$  groups may be responsible for interactions with either single-stranded oligodeoxyribonucleotide, enzymes or molecules, when used as molecular templates [51]. The first example of electrochemically synthesized molecularly imprinted poly *o*-PD for a neutral template was reported by Malitesta et al. in 1999 [38]. Indeed, glucose-templated molecularly imprinted poly(*o*-phenylenediamine) film was prepared by potentiodynamic electropolymerization and applied as a recognition unit of a biomimetic chemosensor. Anodic oxidation of *o*-PD is strongly affected by the electropolymerization conditions such as pH and the potential range. Lusito et al. [77] for the first time, proposed the mechanism of formation of poly(*o*-phenylenediamine) (PoPD) at different pHs and potentials, using cyclic voltammetry and electrospray ionization-ion trap mass spectrometry for the characterization of the products. Figure 6 shows the schematic representation of the proposed polymerization mechanism.

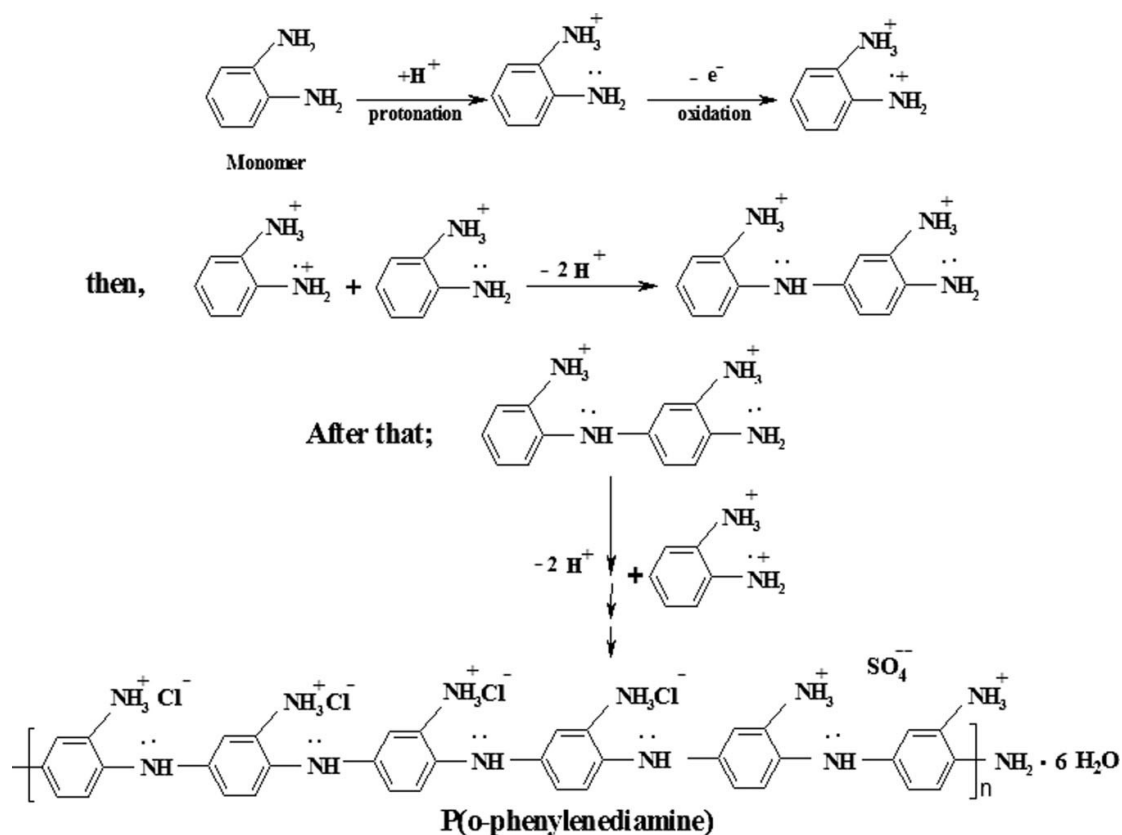


**Figure 6.** Schematic representation of the propagation and formation of PoPD [78].

The structure and properties of PoPD, strongly depend on the pH of the electrolyte solution used to oxidize the o-PD monomer [79]. Indeed, the polymer synthesized from strongly acidic solutions exhibits a phenazine-like structure (Figure 7a) and can be grown to  $>1\mu\text{m}$  thick films with moderate conductivity ( $10^{-4}$ - $10^{-2} \text{ S cm}^{-1}$ ). In contrast, electrodeposition from aqueous electrolytes with  $\text{pH} > 1$ , results in an insulating, ultrathin (typically  $<10 \text{ nm}$  thick) polymeric film. Under such conditions, the structure of the polymer backbone is disrupted by the presence of 1,4-substituted benzenoid-quinoid defects, which likely diminish the electronic conductivity of the polymer [80].

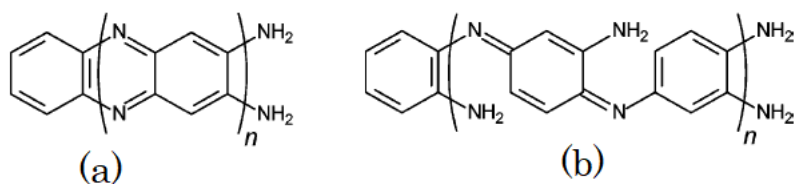


**Figure 7.** Different structures of the oxidized form of PoPD. (a) phenazine-like, (b) 1,4-substituted benzenoid-quinoid [80].

### 1.4.2. Electrochemical sensors based on MIPs

Electrochemical sensors represent one of the most successful applications of MIPs [51,81-84]. As explained above, electrochemical sensors are defined as devices wherein a sensing layer (which acts as recognition element) is coupled to an electrochemical transducer [85]. Depending on the electrical phenomenon used for transducing the binding event, different electrochemical sensors can be classified to potentiometric, conductimetric, impedimetric, and volt-amperometric [86]. Changes in the electrochemical properties of the analyte caused by the recognition event, are used for the detection. Indeed, if the target analyte has electrochemical activity, this property can be exploited for its electrochemical detection using MIP-based sensors [36]. However, a further interesting feature of MIP-based electrochemical sensors is that they even allow the detection of non-electroactive analytes. This is possible by exploiting the competition for the binding sites in the MIP between the analyte and a redox probe [82]. The probe should have characteristics similar to the analyte as far as molecular size, ionic charge, and binding interactions are concerned. When operating under these conditions, the probe signal will scale inversely with the analyte concentration because the analyte will compete with the probe (which produces the electrochemical signal) for the binding sites in the MIP.

Cardiovascular disease (CVD), cancer and sepsis are all classified as leading causes of death globally. The importance of rapid diagnosis is clearly demonstrated by evidence highlighting high mortality rates in the absence of prompt treatment [87]. Electrochemical immunoassays are the most commonly reported format of electrochemical biosensor for detecting two clinical biomarkers, namely, cytochrome *c* (*Cyt c*) and cardiac troponin I (TnI). *Cyt c* is indeed a possible biomarker for diseases related to defective apoptosis (i.e. programmed cellular death) which is involved in some tumors and auto-immune diseases, and TnI has proven to be a significant biomarker for acute myocardial infarction (AMI). This notwithstanding, up to now, no MIP-based sensor has been reported for the detection of these two biomarkers.

## 1.5. Aim of the Thesis

In this work we aim to develop simple, cost-effective and user-friendly electrochemical sensors suitable to maximize biorecognition capabilities, sensitivity and selectivity; to this goal both nanoelectrode arrays and molecularly imprinted polymers are studied.

Concerning NEAs, the present research work is focused on the electrochemical characterization of arrays of nanoelectrodes of glassy carbon with ordered geometry and their application as miniaturized transducers to stimulate voltammetric signals of some redox mediators, such as (ferrocenylmethyl)trimethylammonium ( $\text{FA}^+$ ), Azure A and B, that are widely employed in enzymatic electrochemical biosensor. This activity was developed in collaboration with ThunderNIL Srl, that provided the NEAs, prepared on glassy carbon (GC) substrates by nanoimprinting technology performed onto a thin layer of insulating polycarbonate. The obtained results show that the GC-NEAs are characterized by improved performances as far as background noise reduction, signal resolution and wide accessible potential window are concerned. These characteristics, together with their high reproducibility and sensitivity make GC-NEAs interesting candidates for the mass production of highly sensitive electrochemical biosensor.

On the other hand, our work is focused on another type of nanostructured electrodes based on MIP, using MIPs as suitable electrode coatings for biorecognition and bioanalytical purposes.

In this context, we studied the preparation and optimization of an electrochemical sensor based on molecularly imprinting technology for the trace detection of Cytochrome *c* (*Cyt c*) as possible biomarker for diseases related to defective apoptosis (i.e., programmed cellular death). The research shows that the sensitive and selective detection of *Cyt c* is possible by using electrodes modified by a thin layer of electrosynthesized molecularly imprinted poly (o-phenylenediamine). Different electrochemical methods such as cyclic voltammetry and differential pulse voltammetry were employed using ferrocenecarboxylic acid as the redox probe able to generate the analytical signal and to compete with *Cyt c* for the recognition sites in the MIP. Note that for this application, detection limits below the standard *Cyt c* concentration in human serum, that is  $< 2$  nM, should be achieved. The good results here achieved for *Cyt c* prompted us to investigate the development of a MIP-based voltammetric platform for the detection of troponin I, obtaining preliminary but promising results, at least in synthetic samples.

## **CHAPTER 2: Study of Glassy Carbon Nanoelectrode Arrays on Enzymatic Redox-Mediators**

### **1. Introduction**

#### **1.1. Nanoelectrode arrays: preliminary concepts and fabrication techniques**

The main disadvantage of using individual nanoelectrodes is the extremely small current recorded, so that high electronic amplification of signals and accurate shielding from external electric fields is required to record good quality voltammograms. This issue can be addressed by using ensembles of nanoelectrodes (NEEs, random distributed) or arrays of nanoelectrodes (NEAs, arranged in an ordered manner). A NEA is composed by a very large number of very small nanoelectrodes separated by an electrical insulator, with density between  $10^6$  and  $10^8$  electrodes/cm<sup>2</sup> [90]. Thanks to their geometrical and morphological features, NEAs present several advantages including: (i) the dramatic enhancement of diffusive mass fluxes to the nanoelectrodes in the array; (ii) very small double-layer charging (capacitive) currents; (iii) extreme sensitivity to the kinetics of the charge transfer process [24, 89, 91]. Different methods are used to fabricate high-resolution nanostructures with precise position and size. For instance, over the past decades, top-down lithographic methods have been applied to NEAs preparation, such as ion beam lithography [92], electron beam lithography (EBL) [18] or scanning probe lithography [93-95]. Among these nanofabrication techniques, electron beam lithography (EBL) showed to be able to produce ordered nanostructures with sub-50 nm spatial resolution and well-defined topographical features [94]. However, EBL process is expensive and time consuming, making this technique non suitable for large-scale production of electrochemical nanostructured sensors [90]. This limit can be overcome by using nanoimprinting lithography (NIL) as alternative nanofabrication method. NIL is a nonconventional lithographic technique for high-throughput patterning of polymer nanostructures with great precision and at a low cost [96]. The first report of NIL as a potential nanofabrication technique was reported in 1995 [97]. Unlike traditional lithographic methods, which achieve pattern definition through the use of photons or electrons to modify the chemical and physical properties of the resist, NIL relies on direct mechanical deformation of the resist material and can therefore achieve resolutions beyond the limitations set by light diffraction or beam scattering that are encountered in conventional approaches [96]. Tormen and co-workers presented the fabrication of nanoelectrodes on a polycarbonate (PC) resist film deposited on a boron-doped diamond (BDD) or Glassy Carbon (GC) electrodes through a thermal nanoimprinting (TNIL) process. In the imprint process, a mold with specific nanostructures on its surface is used to indent the same nanostructures in a thin thermoplastic film deposited on a substrate while the latter

is in a melt state, i.e., during a thermomechanical cycle. This approach leads to the formation of recessed nanoelectrodes in the polymeric film that can be subsequently transferred to the substrate by plasma etching, after the removal of a residual of resist that usually remains under the compressed areas. Figure 8 shows a schematic of the originally proposed NIL process [90].

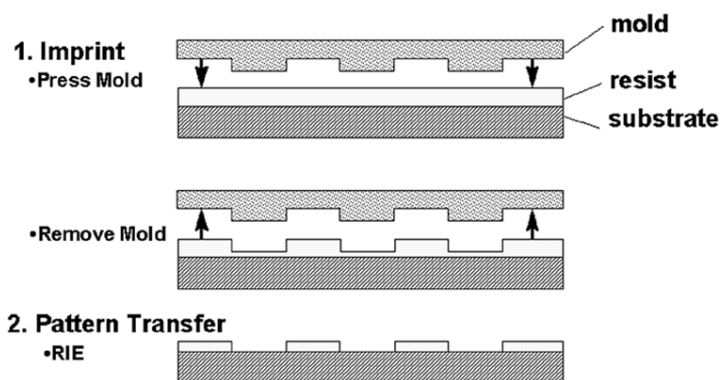


**Figure 8.** Schematic representation of the originally proposed NIL process [11].

Polycarbonate (PC) was used as resist by Tormen, Ugo and co-workers for the fabrication of NEAs by e-beam lithography on gold macroelectrodes [98] and BDD [94]. PC is characterized by interesting properties including high lithographic contrast, chemical stability and biocompatibility. Furthermore, PC is easily functionalized to immobilize biomolecules in order to produce integrated structures where bio-recognition takes place on the PC while the nanoelectrodes act as transducers. It was demonstrated that GC nanoelectrodes are characterized by great electrochemical stability and excellent conductivity [90]. NEA-based biosensors usually need redox mediators to connect the biocomponent with the nanoelectrodes [99], so generating an analytically useful voltammetric signal. The advantage of NEAs made of GC compared to NEAs made of gold is in the superior electrochemical properties of GC, in particular the wider potential window accessible; GC presents indeed a high overpotential towards the hydrogen evolution reaction and is very stable also at positive (anodic) potential values.

In this chapter, we characterized arrays of nanoelectrodes prepared on GC substrates by nanoimprint lithography performed onto a thin layer of insulating polycarbonate; these NEAs were provided by ThunderNIL Srl. In particular, the electrochemical properties of these GC-NEAs were examined with reference to some redox mediators, such as (ferrocenylmethyl)trimethylammonium ( $FA^+$ ) and Azure A and B, that are widely employed in enzymatic electrochemical biosensors.

## Experimental Section

### 2. Materials and methods

The two phenothiazines (Azure A and Azure B) were purchased from Sigma-Aldrich. The solution of phosphate buffer saline solution (PBS 1X) was prepared by dissolving PBS tablets in double distilled water in ratio of 1 tablet:200 mL of water as suggested by the manufacturer, using the pH meter to adjust the pH to 7.4. The final concentration of the components in the prepared PBS 1X were as 0.01 M phosphate, 0.137 M NaCl, 0.0027 M KCl. Ferrocenylmethyl trimethylammonium hexafluorophosphate ( $\text{FA}^+\text{PF}_6^-$ ) was prepared as follows: ferrocenylmethylamine (Aldrich) was first reacted with methyl iodide to form the quaternary ammonium iodide [100] to be later converted to  $\text{FA}^+\text{PF}_6^-$  by reaction with  $\text{AgPF}_6$ . A 0.1 mM  $\text{FA}^+$  solution was prepared in 0.01 M PBS 1X, pH 7.4. Standard stock solutions of Azure A and Azure B (2 mM) were prepared in double distilled deionized water. All other reagents were of analytical grade and solutions were prepared using double distilled deionized water.

#### 2.1. Electrochemical apparatus and procedures

Cyclic voltammetry (CV) measurements were performed at room temperature with CH Instruments potentiostats (CH660B and CH1222a), controlled via personal computer by CHI software. Measurements were performed in a three-electrode cell using either the NEA or a Glassy Carbon disk electrode (GC, 5.0 mm diameter) as the working electrode, a Pt spiral counter electrode, and an aqueous  $\text{Ag}|\text{AgCl}|\text{KCl}$  (sat.) reference electrode to which all here reported potential values are referred. The sample solution was purged with purified nitrogen for 15 min and was held under a nitrogen atmosphere during the measurements. Experiments at the NEA and GC were carried out in 10 mM supporting electrolyte solution (PBS 1X, pH 7.4). This relatively low electrolyte concentration was used because prior studies have shown that voltammetric signals at NEAs and NEEs can be flattened, and peak separations became larger, at higher concentrations of supporting electrolyte [101]. Low concentrations of electroactive species were also used here, and the electrolyte concentration was always at least 100 times the electroactive species concentration. Scanning electron microscopy (SEM) analyses were performed using a TM3000 Hitachi tabletop scanning electron microscope coupled with a Swift ED3000 X-ray microanalysis system.

### **2.1.2. NEA Manufacturing**

The used NEAs were manufactured by ThunderNIL company [102] and used as received. The fabrication process is property of ThunderNIL, so that only a general description can be reported here. Briefly, a polycarbonate film was spin-coated at 2000 rpm on a commercial pyrolitic GC substrate. The polycarbonate film was annealed for 30 min at 180 °C to remove residual solvent. The average film thickness of PC films prepared from solutions at 4% in cyclopentanone, measured by profilometry, was 220 nm. In order to ensure the indentation of the nanoarray structures, a pressure of 10 MPa was applied to the stack of stamp/polycarbonate film/macroelectrode on a 25 × 25 mm<sup>2</sup> for 10 min at 180 °C (release temperature of 80 °C). In order to remove any residual PC present in the holes, nanoarrays were cleaned by oxygen plasma for 4 seconds using an ICP-RIE system applying 4 mT pressure, 200 W coil power and 10 W platen power.



### 3. Results and discussion

#### 3.1. Morphological characterization of NEAs

Morphology of NEA was studied by SEM analyses. Figure 9 shows the SEM images of the surface of the NEA.

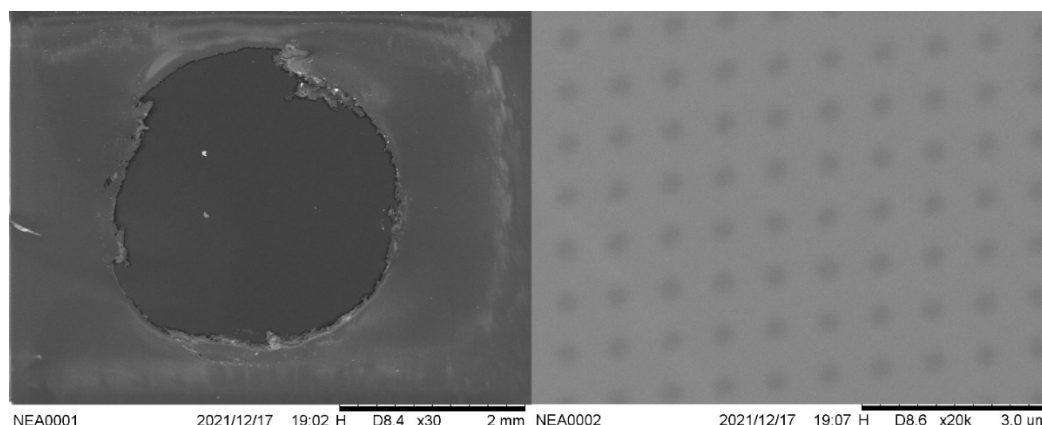


**Figure 9.** SEM Images of the NEA surface. On the left magnification of 30x, 10 kV of NEA surface, the black circle is the electrode surface. On the right zoom of the surface magnification 20000x, 10 kV, of the surface highlighting the dotted nanostructure of the surface.

The black circle at lower magnification describes the entire geometrical area of the array electrode, that is around 3 mm in diameter. The brighter surface was an insulating polymer material placed for insulating the surface of the chip apart the NEA area. The higher magnification image on the right reveals the nanostructured surface of the working electrode. The dark dots are the GC nanoelectrodes with 250 nm diameter, arranged in a square lattice with 800 nm side. The light gray layer is the polycarbonate film coating the electrode surface, apart the nanoimprinted holes through which bare GC dots can be seen. These results allowed us to calculate the theoretical *fractional area*,  $f$ , given as Equation 2.1:

$$f = A_{\text{act}}/A_{\text{geom}} \quad (2.1)$$

where  $A_{\text{act}}$  is the GC surface exposed to the electrolyte solution and  $A_{\text{geom}}$  is the overall geometric area composed by the GC nanoelectrodes and the PC around them.

By applying simple geometrical considerations, using the SEM data, the  $f$  value calculated for these NEAs is  $f = 0.11$ .

### 3.2. Electrochemical Characterization of the NEA with FA<sup>+</sup>

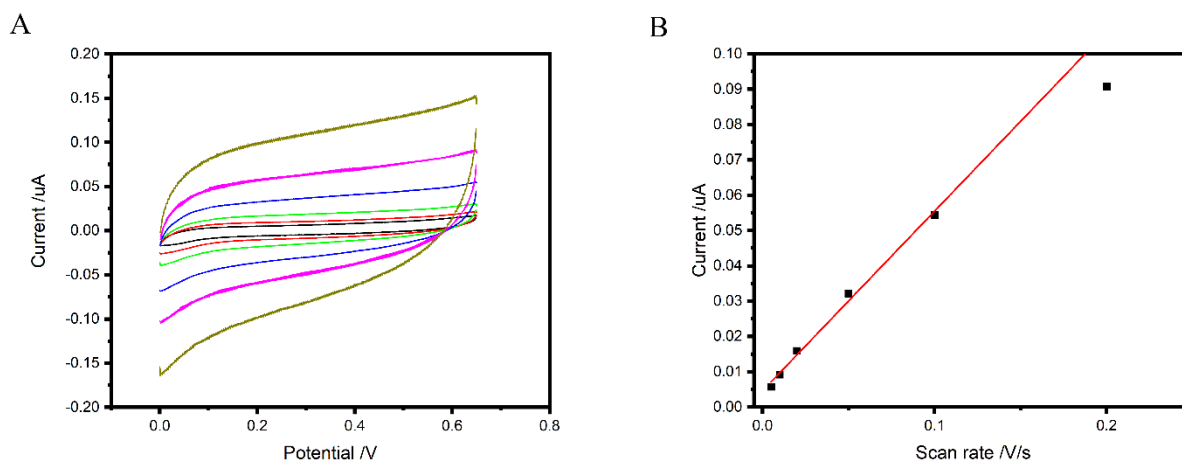


**Figure 10.** (A) Background cyclic voltammograms recorded at PBS 1X (10 mM, pH 7.4) at a NEA at different scan rates; from the outer to the inner 200 mV/s, 100 mV/s, 50 mV/s, 20 mV/s, 10 mV/s, 5 mV/s (B) Linear correlation between capacitive currents and scan rate.

In order to measure experimentally the electrochemically active area of the NEA, a series of cyclic voltammograms were recorded at different scan rates in a blank solution containing only supporting electrolyte (10 mM PBS 1X, pH 7.4). Figure 10A shows the voltammograms recorded in such conditions at a NEA. Under these conditions, the current recorded is the capacitive current ( $I_c$ ) which circulates in the electrochemical cell to build the electrical double layer at the nanoelectrodes/solution interface. The equation relating the capacitive current with cyclic voltammetric parameters is given by Equation 2.2 [103]:

$$I_c = A_{act} \times v \times C_{dl} \quad (2.2)$$

where  $I_c$  is the capacitive current,  $A_{act}$  is the active area,  $v$  the scan rate and the  $C_{dl}$  the double layer capacitance. The latter parameter is not exactly known for the GC used here for NEAs preparation, therefore in the following the  $C_{dl}$  reported in the literature for conventional glassy carbon was used, that is  $5 \mu\text{F cm}^{-2}$  [104,105].

The capacitive current was calculated as half the sum of the forward and the backward background current [103], measured from the CVs in Figure 10A at the potential of +0.45 V, according to Equation 2.3.

$$I_c = \frac{i_{forward} + i_{backward}}{2} \quad (2.3)$$

where  $i_{forward}$  is the current measured in the forward scan at 0.45 V and  $i_{backward}$  is the current measured in the reverse scan at 0.45 V.

Considering Equation 2.2, the value of the experimental active area can be calculated dividing the slope value (provided by Figure 10 B) by the double layer capacitance. The calculated experimental active area was 0.0125 cm<sup>2</sup>.

The characterization of the NEA was continued by examining the cyclic voltammetric behaviour of a classical redox mediator, namely FA<sup>+</sup> (chemical structure in Figure 11).

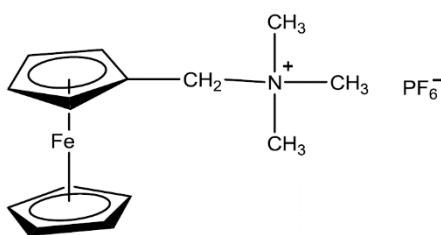


**Figure 11.** Chemical structure of FA<sup>+</sup>.

This redox probe undergoes a well-known one electron reversible oxidation at electrode surfaces which corresponds to the oxidation of the Fe(II) to Fe(III). Note that FA<sup>+</sup>, as well as other ferrocenyl derivatives, are widely used as redox mediators for enzymatic biosensors, in particular for shuttling electrons in sensors which employ oxidase enzymes, such as glucose oxidase [106].

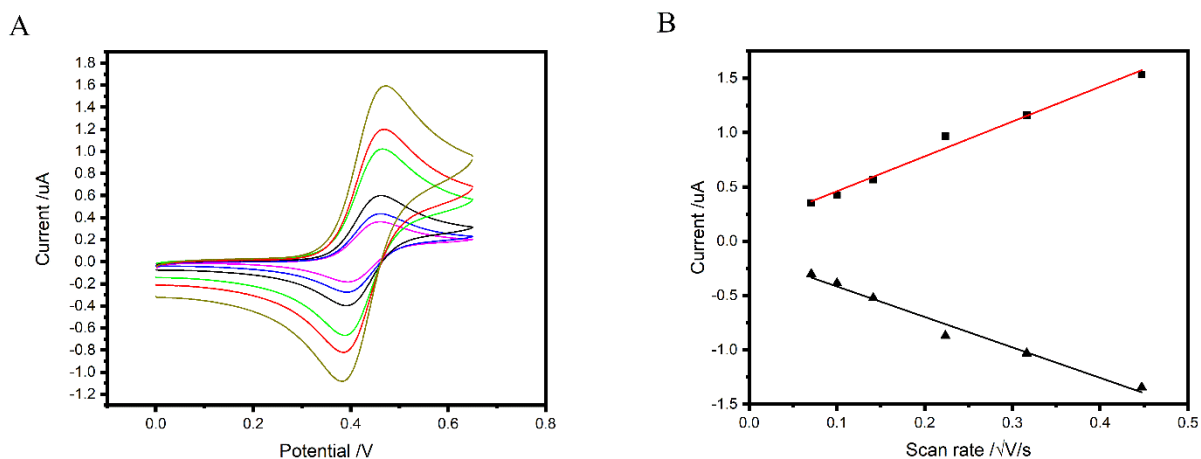


**Figure 12.** (A) Voltammograms recorded at a solution of 0.1 mM FA<sup>+</sup> in 10 mM PBS, pH 7.4 at a NEA at different scan rates; from the outer to the inner 200 mV/s, 100 mV/s, 50 mV/s, 20 mV/s, 10 mV/s, 5 mV/s. (B) Linear correlation between faradic peak currents and square root of scan rate.

Figure 12A reports the peaks shaped cyclic voltammograms recorded at a NEA in a solution containing 0.1 mM FA<sup>+</sup> in 10 mM PBS, pH 7.4 at different scan rates. Relevant voltammetric parameters measured from these CVs are listed in Table 1. The plot  $I_p$  vs  $v^{1/2}$  in Figure 12B shows a linear trend, typical for an electrochemical process controlled by semi-infinite linear diffusion.

**Table 1.** Relevant voltammetric parameters measured from voltammograms recorded in Figure 12A.

V [V/s]	E <sub>pa</sub> [V]	E <sub>pc</sub> [V]	ΔE <sub>p</sub> [V]	E <sub>1/2</sub> [V]	I <sub>pa</sub> [µA]	I <sub>pc</sub> [µA]	I <sub>pc</sub> /I <sub>pa</sub>
0.005	0.459	0.395	0.064	0.427	0.3540	- 0.3007	0.85
0.010	0.459	0.393	0.066	0.426	0.4250	- 0.3853	0.91
0.020	0.462	0.390	0.072	0.426	0.5690	- 0.5216	0.92
0.050	0.465	0.389	0.076	0.427	0.9669	- 0.8684	0.90
0.100	0.469	0.386	0.083	0.427	1.160	- 1.030	0.89
0.200	0.469	0.382	0.087	0.425	1.534	- 1.343	0.87

All these evidences indicate that the GC-NEAs operate under total overlap diffusion conditions and the electrochemical oxidation of FA<sup>+</sup> at the NEA has the characteristics of a typical reversible

(Nernstian) electrochemical process in which the rate of reaction is governed by the diffusion of the electroactive species to the surface of a planar electrode.

Under these conditions, the peak current  $I_p$  obeys the Randles-Sevcik equation (Equation 2.4) [103]:

$$I_p = 2.69 \times 10^5 \times n^{3/2} \times D^{1/2} \times C \times v^{1/2} \times A \quad (2.4)$$

where  $I_p$  is the faradaic peak current,  $n$  is the number of transferred electrons, that for the  $\text{FA}^+$  is one,  $v$  is the scan rate,  $C$  is the bulk concentration of the electroactive species ( $\text{FA}^+$ ),  $A_{\text{geom}}$  is the geometric area and  $D$  is the diffusion coefficient of the  $\text{FAPF}_6$ , that is  $(4 \pm 1) \times 10^{-6} \text{ cm}^2 \text{ s}^{-1}$ . [107].

Considering the plot in Figure 12B and equation (2.4), the linear correlation of the data was described by the general equation  $y=mx+k$ , where  $y=I_f$ ,  $x=v^{1/2}$  and  $m=2.69 \times 10^5 \times n^{3/2} \times D^{1/2} \times C \times A$ . The anodic peak was used to calculate the geometric area that resulted  $7.0 \times 10^{-2} \text{ cm}^2$ .

The experimental fractional area was calculated, as described above, from the ratio between the active area and the geometric area, calculated from the scan rate dependence of the capacitive and faradic current, respectively. The experimental fractional area results:

$$f = A_{\text{active}}/A_{\text{geom}} = 0.0125/0.070 = 0.17$$

Interestingly, this  $f$  value obtained from electrochemical data is in satisfactory agreement with the  $f$  value evaluated by geometrical calculations. These results confirm the reliable electrochemical characteristics of the GC-NEAs here examined.

### 3.3. Cathodic Electrochemistry of NEA with Phenothiazine Redox Mediators

The electrochemistry of two electron-transfer mediators used for biosensors based on reductase enzymes, namely the two phenothiazines Azure A and Azure B, was investigated with the GC-NEA.

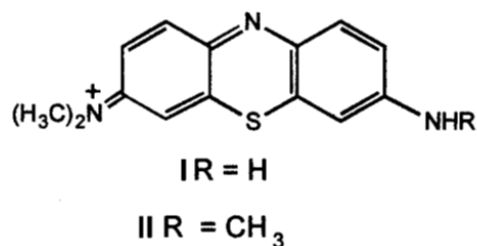


**Figure 13.**Chemical structure of Azure A (I) and Azure B(II) [101].

The electrochemical behavior of these mediators is more complex and less “ideal” than the one of FA<sup>+</sup> for the following reasons [101]:

- i) The electrochemical reduction of the mediators occurs at negative potential values, so that it can overlap with the reduction of the H<sub>3</sub>O<sup>+</sup> ion of water, in particular on electrode materials with low hydrogen evolution overpotential, such as Au or Pt;
- ii) Azure A and Azure B can adsorb on electrode surfaces;
- iii) The electrochemical reduction of these mediators is influenced by the pH of the solution since it obeys the following equation:

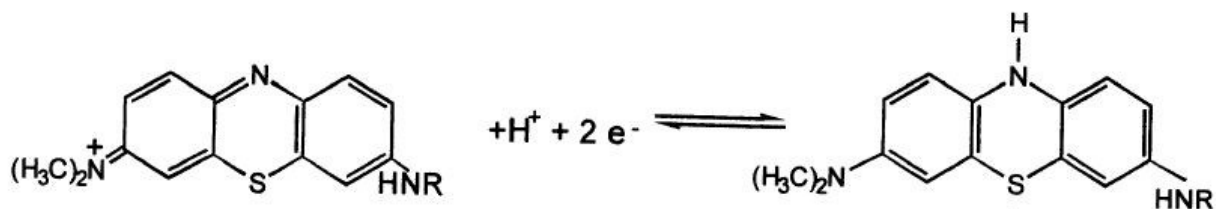


**Figure 14.** Chemical reaction of the mediators Azure A and Azure B [101].

Figure 15 reports the cyclic voltammograms for Azure B recorded with a GC-NEA at 20 mV/s operating at different solution concentration of the redox mediator, including the blank in pure supporting electrolyte.

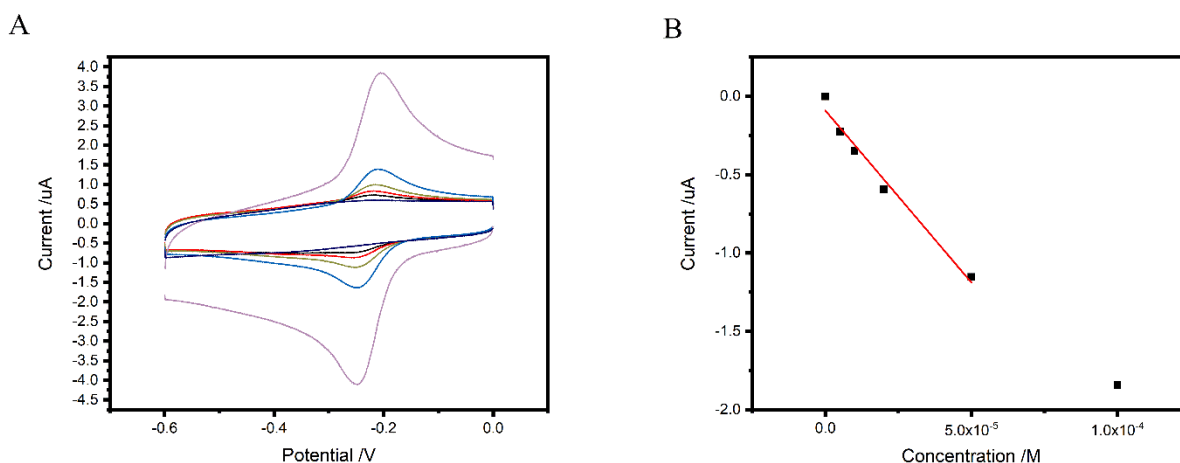


**Figure 15.** (A) Cyclic voltammograms recorded at a NEA in the presence of 0, 5, 10, 20, 50, 100  $\mu\text{M}$  Azure B; scan rate = 20  $\text{mV/s}$ ; supporting electrolyte: 10 mM PBS 1X, pH 7.4. (B) Dependence of the cathodic peak current on the Azure B concentration (relevant calibration plot).

The blank CV recorded in PBS at pH 7.4 shows that at a potential value as negative as -0.6 V vs Ag/AgCl, no proton reduction occurs at the GC-NEA. Note that, in a similar study performed previously using ensembles of gold nanoelectrodes (NEEs) [101], in PBS, pH 7.4, the water proton reduction started to occur already at -0.2 V vs. Ag/AgCl. This result confirms the wide cathodic limit for the potential window accessible with the GC-NEAs.

The CV recorded in the presence of Azure B is characterized by a reduction peak with associated anodic peak in the return scan, with  $E_{1/2}$  of -0.225 V vs Ag/AgCl. The current of the cathodic peak increases, in absolute value, linearly with the Azure B concentration up to 50  $\mu\text{M}$ , while tending to flatten at higher redox probe concentrations.

Figure 16A shows the scan rate dependence of the CV while keeping the concentration of Azure B constant at 100  $\mu\text{M}$ . Relevant CV parameters measured from these voltammograms are listed in Table 2.

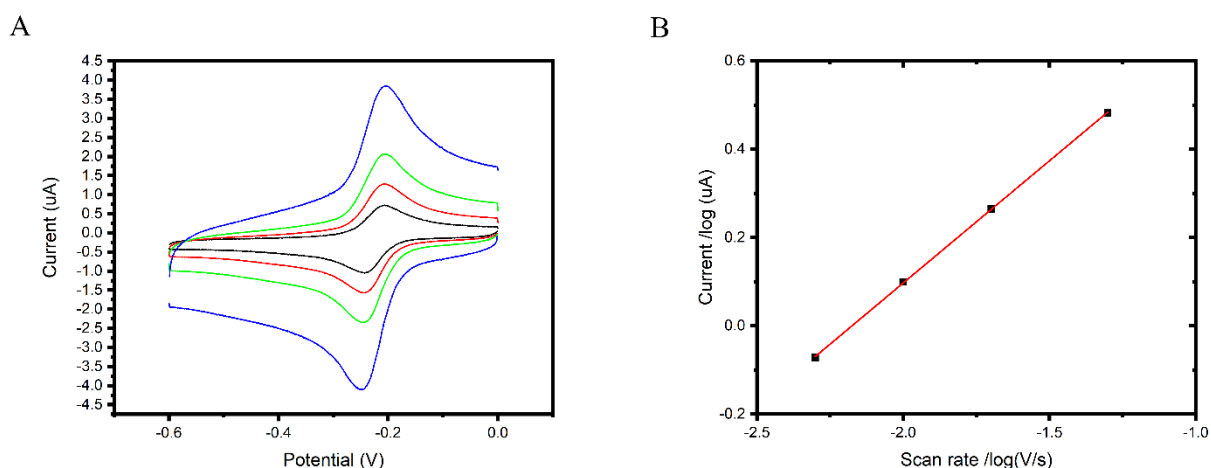


**Figure 16.** (A) Cyclic voltammograms recorded at a NEA in the presence of 100  $\mu\text{M}$  azure B in 10 mM PBS 1X, pH 7.4 at different scan rates from inner to outer 5, 10, 20, 50 mV/s. (B) Linear correlation between logarithm of the cathodic current over the logarithm of the scan rate.

**Table 2.** Relevant parameters obtained from the CVs in Figure 16.

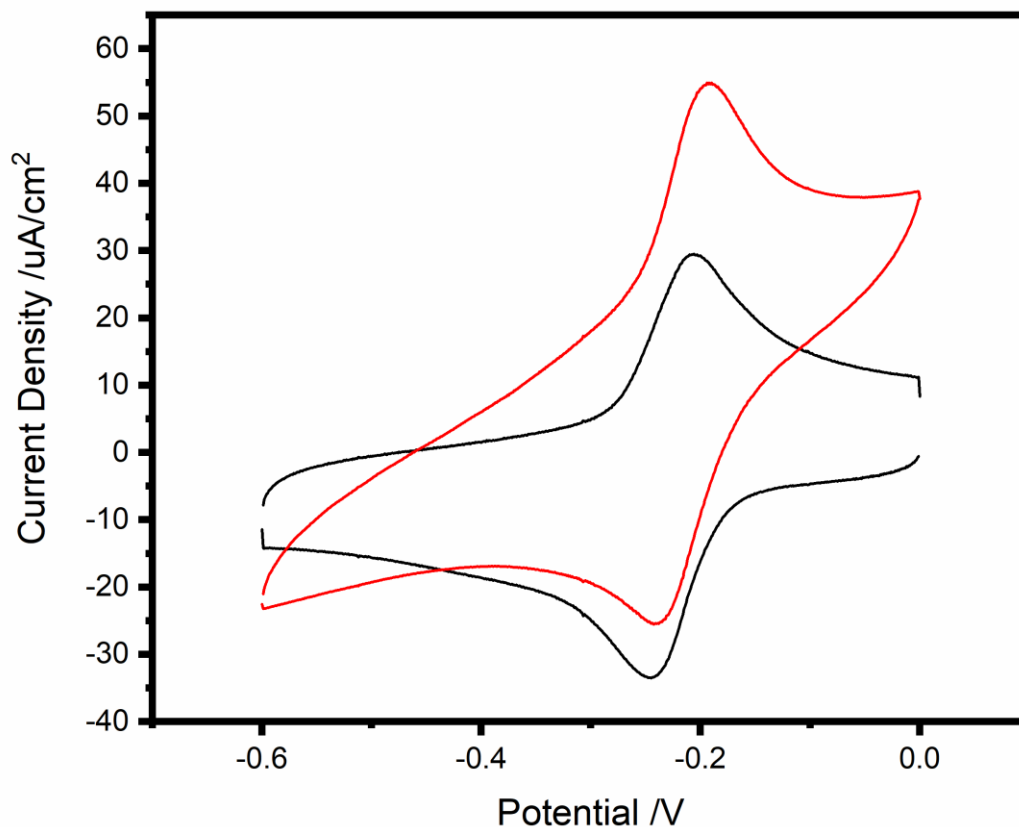
$v$ [V/s]	$E_{pa}$ [V]	$E_{pc}$ [V]	$\Delta E_p$ [V]	$E_{1/2}$ [V]	$I_{pa}$ [ $\mu\text{A}$ ]	$I_{pc}$ [ $\mu\text{A}$ ]	$I_{pc}/I_{pa}$
0.005	-0.207	-0.242	0.035	-0.225	0.8146	-0.8474	1.04
0.010	-0.207	-0.244	0.037	-0.226	1.174	-1.257	1.07
0.020	-0.207	-0.244	0.037	-0.226	1.696	-1.842	1.09
0.050	-0.207	-0.248	0.041	-0.228	2.608	-3.037	1.16

Figure 16B reports the plot for  $\log I_{pc}$  vs.  $\log v$ . The slope of this plot provides information of the mass transport regime which rules the electron transfer process. In fact, the slope is expected to be 0.5 for linear diffusion control, it is 1 for adsorption control or, finally, assumes intermediate values for mixed adsorption/diffusion control. In our case the slope is 0.55, indicating a linear diffusion-controlled process. Data in Table 2 confirm the occurrence of a two electrons reversible reduction process.

In comparison with the CV reported in Figure 3 of ref. [101], the CV signal for the Azure mediator recorded with the GC-NEA is significantly better resolved from the background current than the



signals recorded with the Au-NEE, so confirming the superiority of the GC-NEA in eliminating the interference of the hydrogen evolution reaction.



**Figure 17.** Comparison between the recorded CVs at GC (red line) and NEA (Black line) at 20 mV/s in the presence of 100  $\mu\text{M}$  Azure A in 10 mM PBS 1X, pH 7.4.

Figure 17 shows the comparison of the CVs recorded at 20 mV/s in 10  $\mu\text{M}$  Azure A recorded with a GC-NEA and a regular glassy carbon disk electrode (GCE). Because the two electrodes have different geometric area ( $0.07 \text{ cm}^2$  and  $0.19 \text{ cm}^2$  for GC-NEA and GCE, respectively) the current on the Y axis are reported as current densities, being normalized for  $A_{\text{geom}}$ . The result obtained demonstrates a better signal resolution and reversibility with the GC-NEA.

Data in Figure 18 and Table 3 report the results obtained with the GC-NEA for Azure A solutions,

These results substantially compare with those obtained for Azure B, even if the slightly larger peak-to-peak separation and slightly smaller peak current indicate a lesser degree of reversibility for Azure A. Anyhow, the CVs obtained confirm the satisfactory behavior of the GC-NEA in promoting the cathodic electrochemistry of this class of redox mediators.

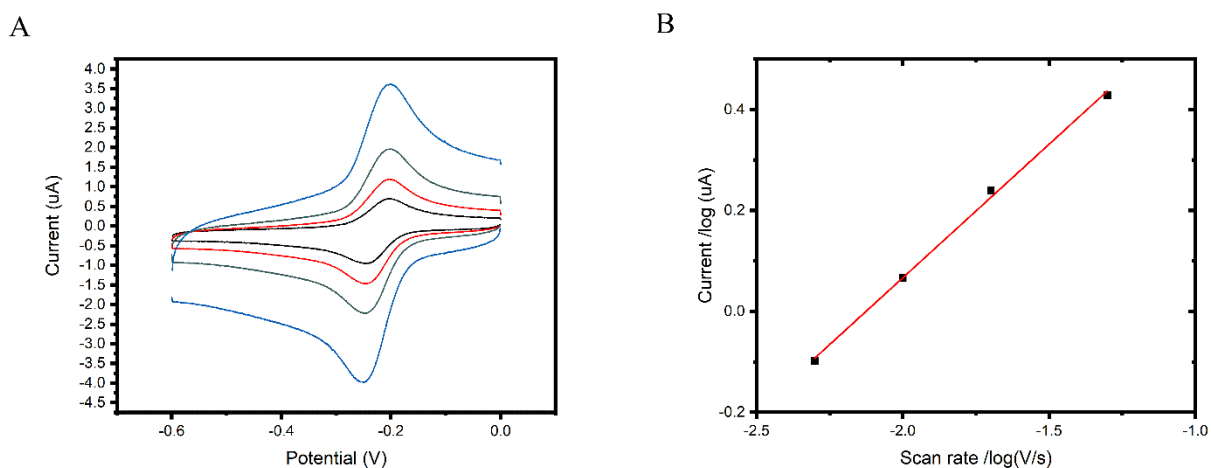


**Figure 18.** (A) Cyclic voltammograms recorded at a NEA in the presence of 100 μM Azure A in 10 mM PBS 1X, pH 7.4 at different scan rates from inner to outer 5,10, 20, 50 mV/s. (B) Linear correlation between logarithm of the cathodic current over the logarithm of the scan rate.

**Table 3.** Relevant parameters obtained from the CVs in Figure 18.

v [V/s]	E <sub>pa</sub> [V]	E <sub>pc</sub> [V]	ΔE <sub>p</sub> [V]	E <sub>1/2</sub> [V]	I <sub>pa</sub> [μA]	I <sub>pc</sub> [μA]	I <sub>pc</sub> /I <sub>pa</sub>
0.005	-0.203	-0.247	0.044	-0.225	0.7134	-0.7982	1.12
0.010	-0.204	-0.247	0.043	-0.225	1.067	-1.165	1.09
0.020	-0.204	-0.250	0.046	-0.227	1.542	-1.737	1.13
0.050	-0.200	-0.248	0.048	-0.224	2.457	-2.682	1.09

## 4. Conclusion

GC-NEAs prepared by nanoimprinting lithography present interesting features, in particular for their use as sensing platforms for enzymatic (as well as for other kind of) electrochemical biosensors. The fabrication procedure provides indeed perfectly ordered arrays of nanodot electrodes with geometrical features which fit well with the expected electrochemical characteristics, as far as capacitive and faradic current are concerned.

The value of the fractional electrode area, in the 0.1 range, indicates that these sensors allow improvement in limit of detection of one order of magnitude with respect to conventional electrodes with the same geometric area.

Moreover, the use of GC as material for the nanoelectrodes allow a significant widening of the accessible potential window, that is a feature of particular interest for sensors operating at cathodic potential values, such as those working with dehydrogenase or reductase enzymes in the presence of suitable redox mediators, such as the phenothiazines here examined.

## CHAPTER 3: Development of molecularly imprinted electrochemical sensor for the ultrasensitive detection of Cytochrome *c*

### 1. Introduction

#### 1.1. Cytochrome *c*: Structure and Role in Respiration

Cytochrome *c* (*Cyt c*) is a water soluble metalloprotein with relatively small molecular weight (Mw=12.4 kDa, 104 amino acids) which contains a redox active heme group and is involved in electron transferring in respiratory chain. Figure 19 shows the secondary structure of *Cyt c*.

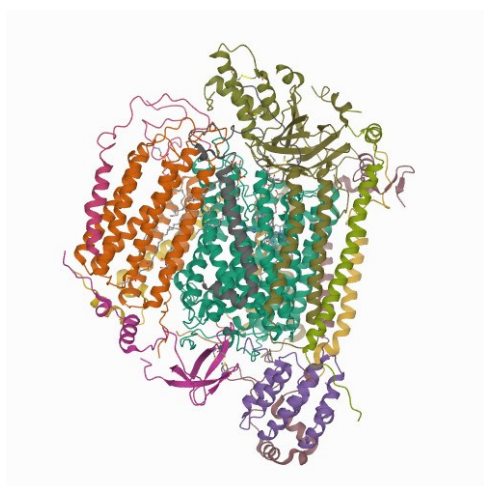


**Figure 19.** Secondary structure of Cytochrome *c*, from Protein Data Base.

*Cyt c* is located in the intermembrane space of mitochondria, where it operates electron transfer between complex III (coenzyme D-*Cyt c* reductase) and Cytochrome *c* oxidase [108–110]. In particular the electron transfer is carried out by the heme group where a  $\text{Fe}^{3+}$  ion is reduced to  $\text{Fe}^{2+}$  in order to accept an electron to be transferred to cytochrome *c* oxidase (COX). While the heme group is responsible for electron transfer, the aminoacidic structure regulates the rate of electron transfer, via post translational modifications (PTM). Phosphorylation on specific residues, such as Tyrosin 97 [111] and Tyrosin 48 [112], has been investigated as pivotal in decreasing of energy generation to avoid an excess of reactive oxygen species (ROS) formation. Thus, phosphorylation in both cases

(Tyr97 in heart, Tyr48 in liver) causes partial, but not full, inhibition of the reaction between *Cyt c* and COX. This PTM regulations is consistent with what is known as differential regulation of COX from tissue type to tissue type. Figure 20 shows schematic representation of the role of *Cyt c* in respiration.

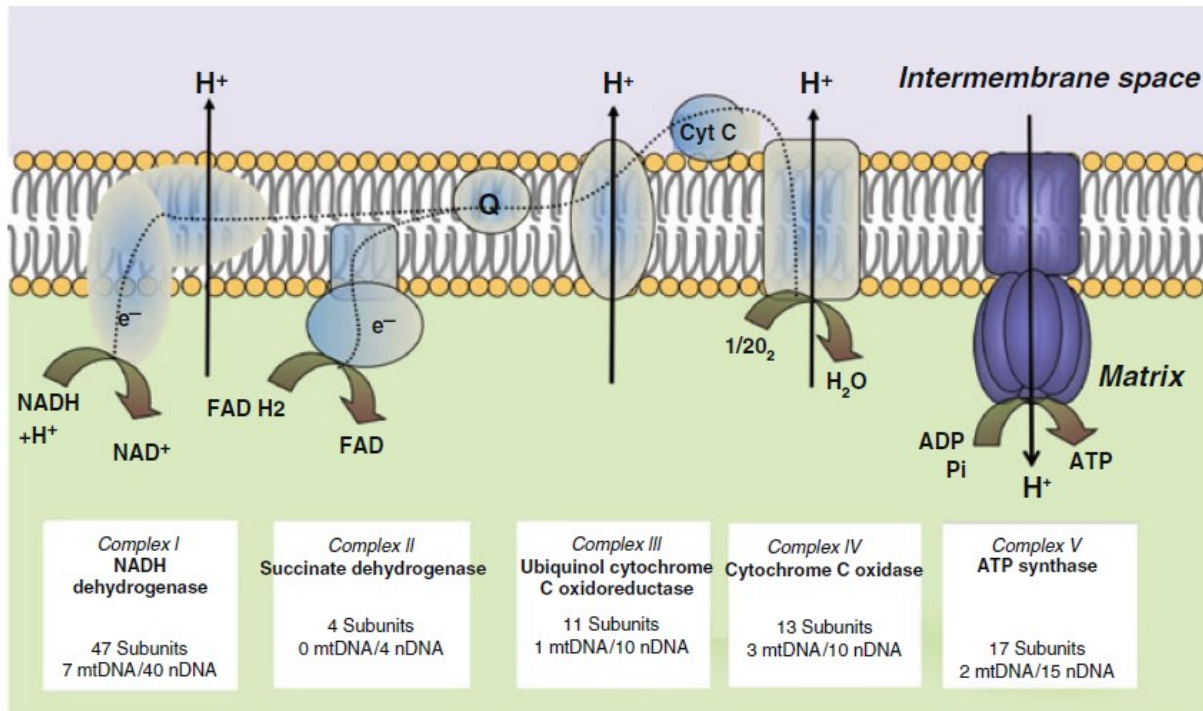


**Figure 20.** Cartoon of *Cyt c* function in mitochondrial respiration [113], reproduced with permission of the copyright owner.

## 1.2. Cytochrome *c*: role in Apoptosis

Over the regular function of *Cyt c* in mitochondrial respiration chain (ETC), *Cyt c* is involved in the regulation of apoptosis of the cell. Apoptosis is the programmed cell death after the compromise of the normal cell functions. The localization of the *Cyt c* in the inner mitochondrial membrane (IMM) is pivotal in healthy cell. A schematic representation of the *Cyt c* function in apoptosis is shown in Figure 21.

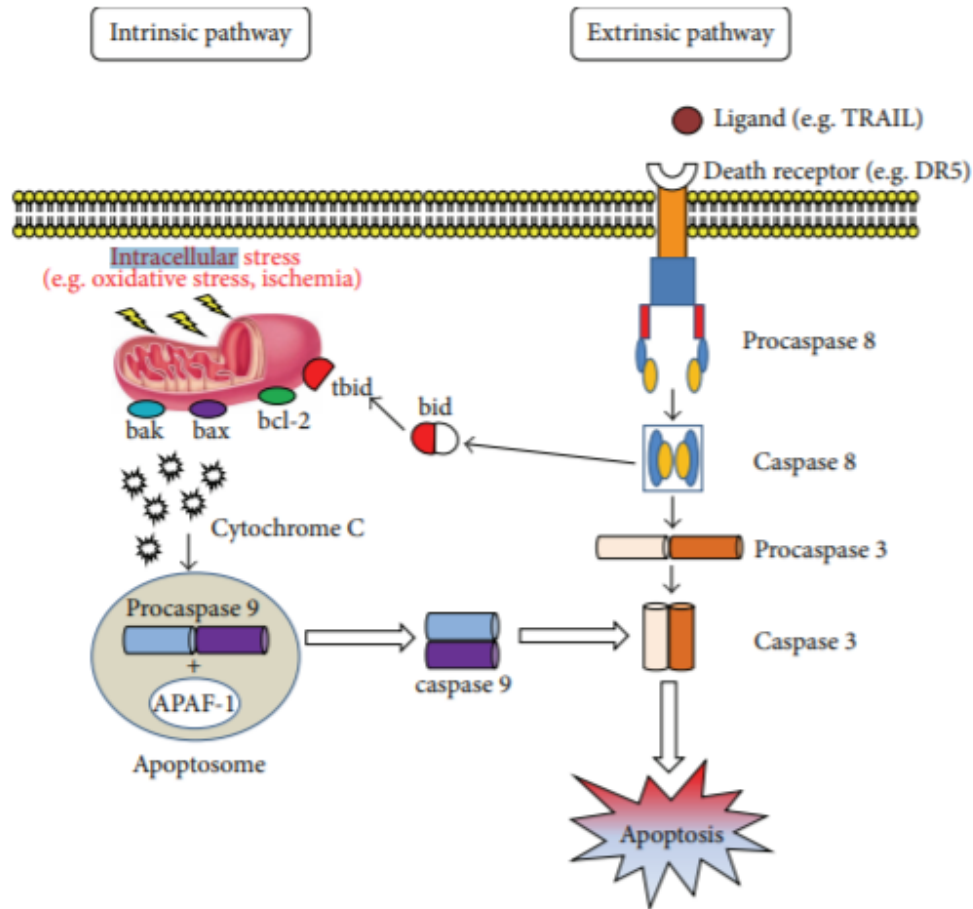


**Figure 21.** Apoptotic pathway activated via *Cyt c* [114], reproduced under Creative Commons Attribution License.

After a mitochondrial damage via external stimulus, such as intracellular stress, uncontrolled ROS production, ischemia, that is irreversible for the mitochondrial recovery, leads to a change in the permeability of the mitochondrial membrane causing the uncontrolled leakage of *Cyt c* in the cytosol. The *Cyt c* uncontrolled translocation in cytosol compartment activates the Apaf 1. In particular in presence of dATP or ATP causes a conformational change in the Apaf 1/cytochrome *c* complex that exposes the CARD domain of Apaf 1, allowing caspase-9 to bind [110]. These initiates the cascade pathway leading the Activation of the Caspase 3 and subsequently the cell death.

### **1.3. Clinical role of *Cytochrome c***

After apoptosis event, *Cyt c* is released by the cellular debris in the intercellular environment. *Cyt c* is then distributed in the organism through the lymphatic system and reaches the plasma in the normal blood circulation system.

For this reason, in recent years the potential role of the *Cyt c* as biomarker of cellular damage has been highlighted. In particular, in regular living conditions, apoptosis regulates cell homeostasis, while excess or defect apoptosis characterize several pathological situations. In fact, defect apoptosis does not allow a sufficiently fast turn-over of eventually abnormal cells that cannot be adequately replaced by regular cells; this mechanism is involved in some cancers such as tumors characterized by p53 mutations or hormone-dependent ones, some autoimmune diseases and type I diabetes. On the other hand, excess apoptosis is involved in some neurodegenerative diseases such as spinal muscle atrophy, amyotrophic lateral sclerosis, Alzheimer and Parkinson diseases and Ischemic damage. Release of excess *Cyt c* into the circulation system has been confirmed also in patients with myocardial infarction [115]. The concentration of *Cyt c* in human serum under regular conditions is quite low, around 2 nM [116], therefore to monitor possible decrease of *Cyt c* concentration in the case of pathologies related to defect apoptosis, detection methods with high sensitivity and low detection limits are required. Several studies have indicated a possible role of serum *Cyt c* as a prognostic marker in various types of cancer and different disease such as liver hepatitis [117], liver disease [118], liver drug-induced injury [119], lung cancer [120].

### **1.4. Electrochemical detection of *Cytochrome c***

Considering that excessive or insufficient apoptosis is a marker of disease, *Cyt c* quantification in human serum is being considered of increasing importance in early clinical diagnosis [109,121,122] and tumor therapy follow-up. Various methods have been developed for the detection of *Cyt c* in serum. These include electrochemiluminescence [123], chemiluminescence [124], high performance liquid chromatography [125], ELISA [126], Western blotting [127], spectrofluorimetry [122], spectrophotometry [128] to name some.

Some of these methods are highly reliable and sensitive, however, since they require the use of complex instrumentation managed by specialized personal combined with time consuming and complex analytical procedures, they can be performed only in the laboratory. In a prospect of an increasing role of first-level screening methods suitable for decentralized analysis and point-of-care

diagnostics, there is increasing interest for novel sensing devices which could allow the quick and relatively simple, but always adequately sensitive and selective, detection of the analyte of interest. Among the other, electrochemical sensors allow decentralized or automated analysis with several advantages as far as sensitivity, simplicity, rapidity, low cost and quick response times are concerned [129]. Indeed, the change in oxidation state from Fe(III) to Fe(II) of the heme group of *Cyt c* could be exploited for the voltammetric detection of the protein, but at bare metal electrodes poor voltammetric responses are typically obtained because of random adsorption of *Cyt c* on metal surfaces with consequent random orientation of the electroactive heme center, which is buried in the protein polypeptide chain, such a condition being unfavourable for electron transfer with the metal surface [130–132]. Indeed, direct electron transfer between *Cyt c* and the electrode surface can be achieved by using suitable promoters [133–140], typically 4,4'-bipyridyl (4,4'-bipy) [133,134] or 4,4'-dipyridyl sulfide [135,136] or others [137,138], or applying electrodes modified with thin polymeric membranes [139–142]. Some studies demonstrating the possibility of avoiding the use of promoters have also been published. This was observed for graphite and carbon [143,144], glassy carbon [145,146], tin and indium oxide [146]. Direct voltammetry of *Cyt c* was also possible with gold ultramicroelectrodes [147], microelectrode arrays [148], screen-printed electrodes [149], electrodes coated with Au nanoparticles [150–152] and with ensembles of gold nanoelectrodes [153]. In any case, the use of bare electrodes or electrodes modified simply with promoters does not allow one to achieve the selectivity required for analysis in complex biological matrices such as blood serum or other biological fluids. For this kind of sample, the electrode surface needs to be functionalized with specific recognition elements, such as enzymes, antibodies and or molecularly imprinted polymers as plastic antibodies [65], in order to make the electrode able to interact selectively with the target analyte, so generating a specific transduction signal [154] also in the presence of possible interferences.



## Experimental Section

### 2. Material and methods

#### 2.1. Materials

*o*-Phenylenediamine (*o*-PD,  $\geq 98\%$ ), ferrocenecarboxylic acid (FcCOOH,  $\geq 97\%$ ), cytochrome *c* (*Cyt c*,  $\geq 95\%$ , Mw = 12.384 kDa, from horse heart), Hemoglobin, Albumin, Lysozyme, were purchased from Sigma–Aldrich and used as received. Standard stock solution of *Cyt c* (30  $\mu\text{M}$ ) was prepared in double distilled deionized water and stored at 4 °C if not in use, Table 4 and Table 5 provide a summary of the preparation of the solutions. Human Serum Plasma (HSP, Sigma) was diluted in phosphate buffer saline solution (PBS 1X: 10 mM Phosphate Buffer,  $1.37 \times 10^{-1}$  M NaCl,  $2.7 \times 10^{-3}$  M KCl, pH 7.4 @ 25 °C). A 1 mM FcCOOH solution was prepared in PBS 1X at pH 7.4. All other reagents were of analytical grade and solutions were prepared using double distilled deionized water.

**Table 4.** Summary of solutions preparation

Solution No.	Name	Concentration of <i>Cyt c</i> [xxM]	Concentration of <i>Cyt c</i> [xxg/ mL]	Quantity weighted [mg]	Volume solution [ml]	Volume used for dilution	Process of preparation
1	Stock Solution	30 $\mu\text{M}$	0.38 mg/ mL	1.9 mg	5 mL		
2	Intermediate stock solution	0.3 $\mu\text{M}$	0.0038 mg/ mL		5 mL	50 $\mu\text{L}$	Prepared by dilution from solution 1
3	Polymerization solution	1 $\mu\text{M}$	12.7 $\mu\text{g/ mL}$	//	20 mL	667 $\mu\text{L}$	Prepared by dilution from solution 1
4	Solution <i>Cyt c</i> 100 ng/mL	8.06 nM	100 ng/ mL	//	2.5 mL	66 $\mu\text{L}$	Prepared by dilution from solution 2
5	Solution <i>Cyt c</i> 1 ng/mL	80.6 pM	1 ng/ mL	//	2.5 mL	25 $\mu\text{L}$	Prepared by dilution from solution 4
6	Solution <i>Cyt c</i> 0.05 ng/mL	4.03 pM	0.05 ng/ mL	//	2.5 mL	125 $\mu\text{L}$	Prepared by dilution from solution 5

**Table 5.** *Cyt c* addition's protocol for evaluation of performance MIP sensor

Addition in cell No.	Volume added	Solution used for addition	Volume of Cell	Final concentration of <i>Cyt c</i> in the cell [ng/mL]	Final concentration of <i>Cyt c</i> in the cell [M]	Final actual concentration [ng/mL]
1	120 $\mu$ L	Solution 6 from <b>Table 4</b> (0.05 ng/mL)	6 mL	0.001 ng/mL	$8.06 \times 10^{-14}$ M	0.001 ng/mL
2	48 $\mu$ L	Solution 5 from <b>Table 4</b> (1 ng/mL)	6.12 mL	0.009 ng/mL	$7.25 \times 10^{-13}$ M	0.0088 ng/mL
3	192 $\mu$ L	Solution 5 from <b>Table 4</b> (1 ng/mL)	6.17 mL	0.04 ng/mL	$3.22 \times 10^{-12}$ M	0.0399 ng/mL
4	3.2 $\mu$ L	Solution 4 from <b>Table 4</b> (100 ng/mL)	6.36 mL	0.09 ng/mL	$7.25 \times 10^{-12}$ M	0.09 ng/mL
5	21 $\mu$ L	Solution 4 from <b>Table 4</b> (100 ng/mL)	6.36 mL	0.4 ng/mL	$3.22 \times 10^{-11}$ M	0.42 ng/mL
6	27.6 $\mu$ L	Solution 4 from <b>Table 4</b> (100 ng/mL)	6.38 mL	0.8 ng/mL	$6.44 \times 10^{-11}$ pM	0.85 ng/mL
7	459 $\mu$ L	Solution 4 from <b>Table 4</b> (100 ng/mL)	6.41 mL	7.6 ng/mL	$6.13 \times 10^{-10}$ nM	7.96 ng/mL

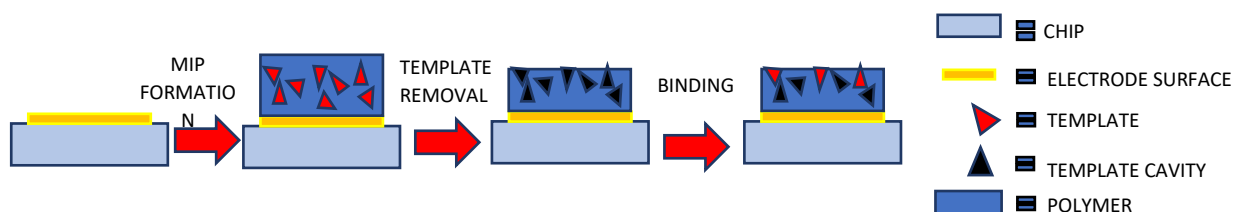
## 2.2. Apparatus and Measurements

Cyclic voltammetry (CV) and differential pulse voltammetry (DPV) measurements were performed at room temperature with CH Instruments Potentiostats (CH660B and CH1222a) controlled via personal computer by its own software. A standard three-electrode configuration was used. The working electrode was a gold disk electrode (2.0 mm diameter), the counter electrode was a platinum wire and the reference electrode was an Ag|AgCl|KCl (1 M), with respect to which all potential values reported hereafter are referenced.

### 2.3. Fabrication of MIP and NIP electrodes

Gold disk electrodes were used for the imprinted film-synthesis and the electrochemical measurements. Prior to electropolymerization of *o*-PD, the surface of the gold electrode was polished with 1.0, 0.3, and 0.05  $\mu\text{m}$  wet alumina slurry and then washed in an ultrasonic bath with double distilled water for 5 min, followed by electrochemical activation via cyclic voltammetry, by sweeping the potential between 0.2 and 1.5 V vs. Ag/AgCl in 0.5 M  $\text{H}_2\text{SO}_4$  at 0.05 V/s, until a stable cyclic voltammogram was recorded. Electrosynthesis of the molecularly imprinted poly(*o*-phenylenediamine) (Po-PD) was performed by cyclic voltammetry (20 scans), by scanning the potential between 0 and 1.1 V vs Ag/AgCl at 50 mV/s in a solution of acetate buffer (0.1 M, pH 5.2) containing 10.0 mM *o*-PD. *Cyt c* was added in a solution as a template molecule before polymerization at concentration of 1  $\mu\text{M}$ . A control electrode modified with non-imprinted polymer (NIP) was obtained in the same way, but without *Cyt c* being added as a template. The modified electrodes were dried under air flow and stored at room temperature. The resulting MIP-modified electrode was rinsed with water and dipped in template removal solution (0.1 M  $\text{H}_2\text{SO}_4$ ) for 60 min under mild stirring, followed by subsequent washing with double distilled water before further electrochemical characterization.

A schematic diagram of sensor working principle is shown in Scheme 1.



**Scheme 1.** Schematic view of MIP modified sensor preparation.

### 2.4. Analytical measurements

The interaction between *Cyt c* and imprinted Po-PD was evaluated by incubating the electrode in a solution containing appropriate concentrations of *Cyt c*, for 10 min with stirring. Electrochemical measurements to characterize the MIP electrode were carried out in a 1 mM  $\text{FcCOOH}$  in PBS 1X solution at room temperature. Cyclic voltammograms (CVs) of the imprinted membranes were recorded within the potential range 0.0–0.5 V vs Ag/AgCl, at a scan rate of 50 mV/s. Differential pulse voltammetry (DPV) runs for the modified electrodes at each concentration of test analyte were

quantified over a potential range of 0.0–0.5 V vs. Ag/AgCl with pulse width 25.0 ms, pulse amplitude 25.0 mV, increment potential 4.0 mV; scan rate 20 mV/s. Human serum samples ( stored at -20 °C) were diluted 1:20 or 1:50 in PBS 1X. Bovine Serum Albumin, Hemoglobin, Streptavidin and Lysozyme were selected as competitor compounds in order to evaluate the recognition specificity of the prepared MIP modified electrode.

### 3. Results and discussion

#### 3.1. Preparation of MIP and NIP electrodes

Fabrication of the MIP film was achieved by the anodic deposition of o-phenylenediamine (o-PD) in the presence of *Cyt c* on a gold substrate. The voltammograms recorded during electrodeposition of o-PD are shown in Figure 22A. The CV demonstrates an oxidative polymerization of o-PD detected by an anodic peak at approximately 0.4 V, followed by a shoulder during the first scan. The consecutive decreases in oxidation current over the following cycles i.e., from the 1st cycle to the 20<sup>th</sup> cycle, indicating the formation of an insulating polymer film on the surface of the electrode. Typical voltammograms recorded during electrodeposition of o-PD show the features expected for the electropolymerization of o-PD [38, 82]. No significant difference was observed between cyclic voltammograms observed in the presence of *Cyt c* and those obtained in its absence (NIP), Figure 22B, which reveals that *Cyt c* does not have any electrochemical behaviour under the applied potential range for electrodeposition, and the structure of the template was not changed during the imprinting process.

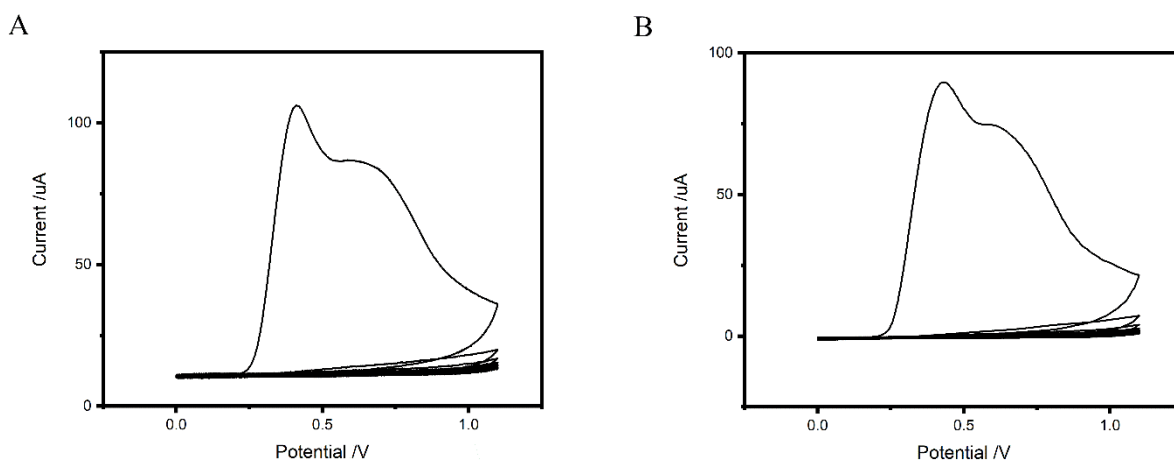


**Figure 22.** Cyclic voltammograms for o-PD electropolymerization on a gold electrode in acetate buffer (pH 5.2). (A) containing 10 mM o-PD and 1  $\mu\text{M}$  *Cyt c*, (B) only 10 mM o-PD; scan rate 50  $\text{mV s}^{-1}$ ; number of scans 20.

### 3.1.1. Electrochemical characterization of the imprinted electrodes

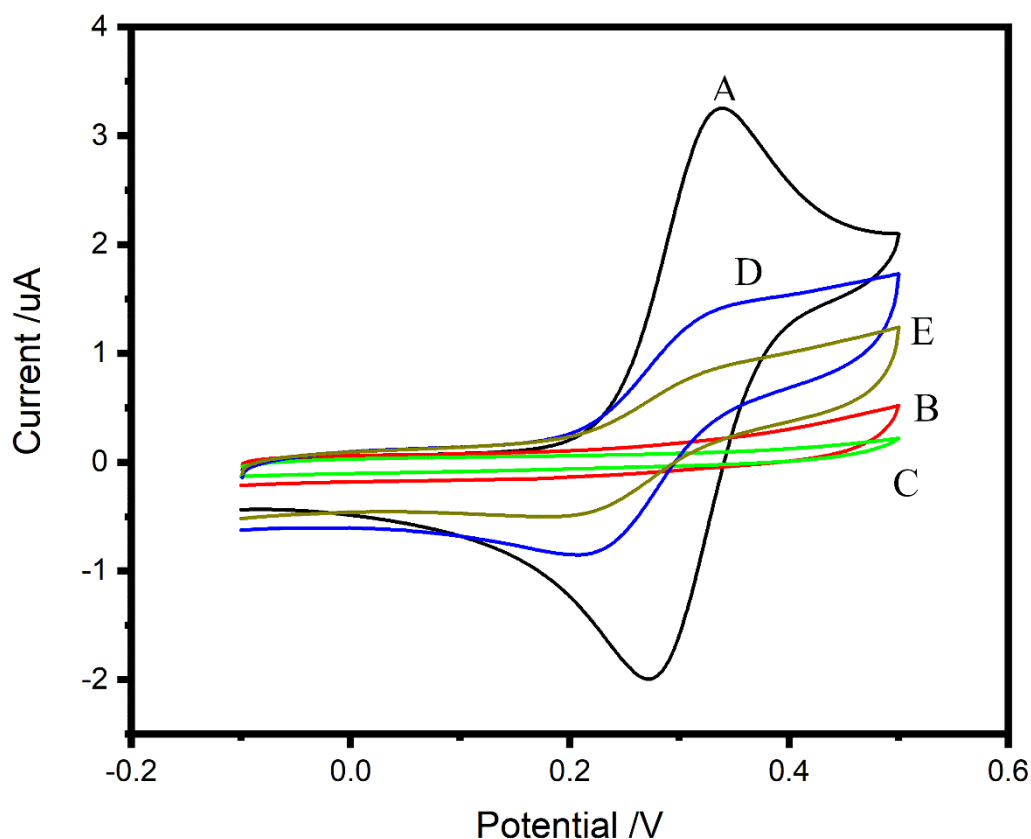


**Figure 23.** Cyclic voltammograms of 1 mM FcCOOH in PBS 1X, pH 7.4 at bare and modified electrodes. (A) bare Au electrode, (B) MIP-modified electrode, (C) NIP-modified electrode, (D) MIP-modified electrode after removal of *Cyt c*, (E) MIP-modified electrode after 10 min incubating in 1 mM FcCOOH (pH 7.4) containing  $8.06 \times 10^{-14}$  M *Cyt c*, scan rate  $50 \text{ mV s}^{-1}$ .

The stepwise modification of the developed MIP sensor was electrochemically characterized. Whereas the voltammetric response of *Cyt c* at trace levels is quite poor at bare metal electrodes, most likely due to protein denaturation at the metal electrode surface leading to extremely slow electron-transfer kinetics [155, 156]. Therefore, to characterize the MIP sensor, electrochemical analyses were performed in the presence of FcCOOH, used as an electrochemical redox probe. Changes in the FcCOOH voltammetric behavior were monitored upon modification of the gold electrode during the preparation of the MIP sensor. A reversible couple of typical redox peaks was observed on the bare gold electrode, as shown in Figure 23, curve A. After poly(o-PD) deposition, a sluggish response to the redox probe is observed. No peak is observed on the MIP (Fig. 23, curve B) and NIP electrodes prior to the template removal, this effect being explained by the presence of a compact and non-

conductive film, electropolymerized on the surface of the electrode [38, 62, 82]. Following the removal of *Cyt c* using 0.1 M H<sub>2</sub>SO<sub>4</sub> for 60 min, the FcCOOH signal is again detected, although with an almost sigmoidal pattern (Fig. 23, curve D). This result demonstrated that removal of templates left some imprinted cavities that enable FcCOOH to diffuse through the polymer towards the electrode surface. This is not the case for the NIP modified electrode (Figure 23, curve C) even after treatment with sulphuric acid. After incubation of the MIP electrode in solution containing  $8.0 \times 10^{-14}$  M *Cyt c* for 10 min, the current response of the electrode decreases (Figure 23E), which reveals that some cavities are occupied by *Cyt c*, hindering the electron transfer of the redox probe on the surface of electrode.

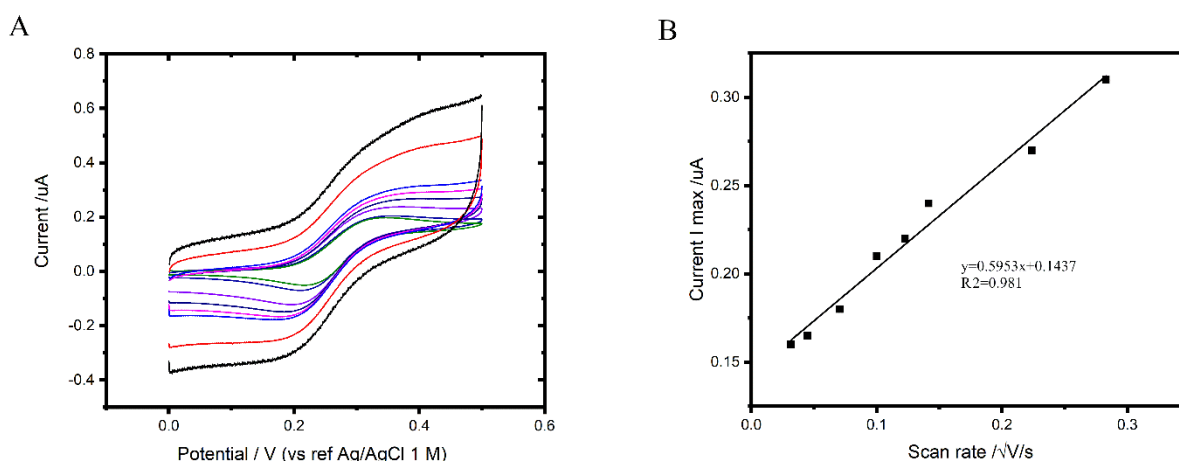


**Figure 24.** (A) Cyclic Voltammograms of 1 mM FcCOOH in PBS 1X at MIP-modified electrode. Scan rates from outer to inner: 80, 50, 20, 15, 10, 5, 2, 1 mV s<sup>-1</sup>, (B) Linear correlation between Current  $I_{\max}$  and square root of scan rate.

After template removal, MIP-modified electrode was dipped in solution containing 1 mM FcCOOH in PBS 1X and to characterize the MIP-modified electrode, the CVs were recorded at different scan rates (1-80 mV/s). Figure 24A shows the dependence of the FcCOOH pattern at the MIP-modified electrode to the scan rate. The voltammograms show a substantially sigmoidal shape, but with an evident hysteresis between the forward and backward scan. The recorded CVs at very low scan rates (between 1 and 5 mV/s) demonstrated a flattened peak tends to emerge from the sigmoidal pattern which this peak being slightly more evident in the return scan. Figure 24B illustrates the plots for  $I_{\max}$  vs the square root of the scan rate ( $v^{1/2}$ ), where  $I_{\max}$  is the plateau or peak current measured in the

forward scan, after subtraction of the background current. This plot results linear in the range of scan rates explored. The hysteresis between forward and backward scan can be ascribed to the capacitive current (which is evident at the potential of scan reversal), such hysteresis scaling directly with the scan rate. This could be due to the presence of an ultrathin polymeric film at the interface between the underlying electrode and some cavities, this layer hindering but not blocking completely the electron transfer. All these evidences indicate that the MIP-modified electrodes behaves like electrodes with partially blocked surface [157], where the cavities in the MIP-modified surface act as individual electrodes of nanometric dimension [9, 158]. The shape of the CVs, which looks intermediate between sigmoidal and peak shaped, as well as the scan rate dependence on  $v^{1/2}$ , suggest that the MIP-sensor operates under diffusive control, with a diffusion regime intermediate between pure radial and linear. Such behaviour was described in the literature for arrays of nanoelectrodes [89, 8, 28] when the diffusion layers to the individual nanoelectrodes partially overlap so that the overall diffusion regime is something midway between the so-called total overlap and pure radial diffusion regimes. Note that at arrays of nanoelectrodes, the shape of the voltammetric patterns is peak-shaped for total overlap diffusion conditions to become sigmoidal under pure radial diffusion conditions [89]. Indeed, the evidence that for the MIP-sensor a partially peak shaped pattern appears at very low scan rates agrees with the progressive broadening of the diffusion layers to each individual nanocavity electrode when working with a longer timeframe, so that cross talking between the nanoelectrodes becomes progressively more important.

### **3.1.2. Optimization of the MIP sensor preparation**

In order to obtain the best analytical performance of the MIP sensor, different influencing factors including the amount of o-PD, *Cyt c* concentration, number of cycles for electropolymerization of o-PD, template removing conditions and the incubation time were investigated. For analytical purposes, differential pulse voltammetry (DPV) was preferred to CV because it allows a better resolution of the signals, higher sensitivity and minimization of double layer charge current effects [159].

#### **3.1.2.1. Optimization of the monomer concentration**

The monomer concentration in the polymerization process affects the thickness of the deposit layer and the amount of imprinted molecule in the polymer matrix, which in turn further affects the electrochemical behavior of the sensor [160]. To evaluate the effect of the o-PD concentration on the response of MIP to *Cyt c*, the MIPs were electropolymerized using a constant *Cyt c* concentration (1.0  $\mu\text{M}$ ) and varying the o-PD concentration. The sensitivity and linear range of the prepared MIP-



sensors were evaluated by DPV, under pH 7.4 using 1 mM FcCOOH as the probe. The changes of peak current before and after rebinding were evaluated. Comparing the results reported in the Table 6, the highest sensitivity was obtained with 10 mM of monomer. As further evidence to determine the optimal monomer concentration, the change of current response of the FcCOOH probe ( $\Delta I = i_0 - i$ ) was calculated by subtracting the current recorded in the presence of  $8.0 \times 10^{-14}$  M *Cyt c* (*i*) from the current recorded in the absence of *Cyt c* (*i*<sub>0</sub>). As shown in Figure 25, the highest  $\Delta I$  value was again obtained at 10 mM o-PD. A decrease in the current response was observed for o-PD concentrations lower than 10 mM, probably because *Cyt c* cannot be captured during the electropolymerization process and, consequently, causing a poor formation of cavities. On the other hand, at too high o-PD concentration (>10 mM), the imprinted polymer membrane becomes too thick, and the template molecules located in the central area of the polymer membranes cannot be completely removed from the polymer matrix [161].

**Table 6.** Comparison of the analytical performance (sensitivity) of prepared MIP sensors using 1  $\mu$ M *Cyt c* and different concentration of o-PD as monomer.

Concentration o-PD [mM]	Delta I slope [ $\mu$ A/M]	R squared	Delta I/I <sub>0</sub> slope	R squared
5	0.486	0.919	0.166	0.919
7.5	0.131	0.929	0.139	0.929
10	1.497	0.999	0.277	0.999
12.5	0.755	0.946	0.113	0.946
15	0.166	0.911	0.158	0.911

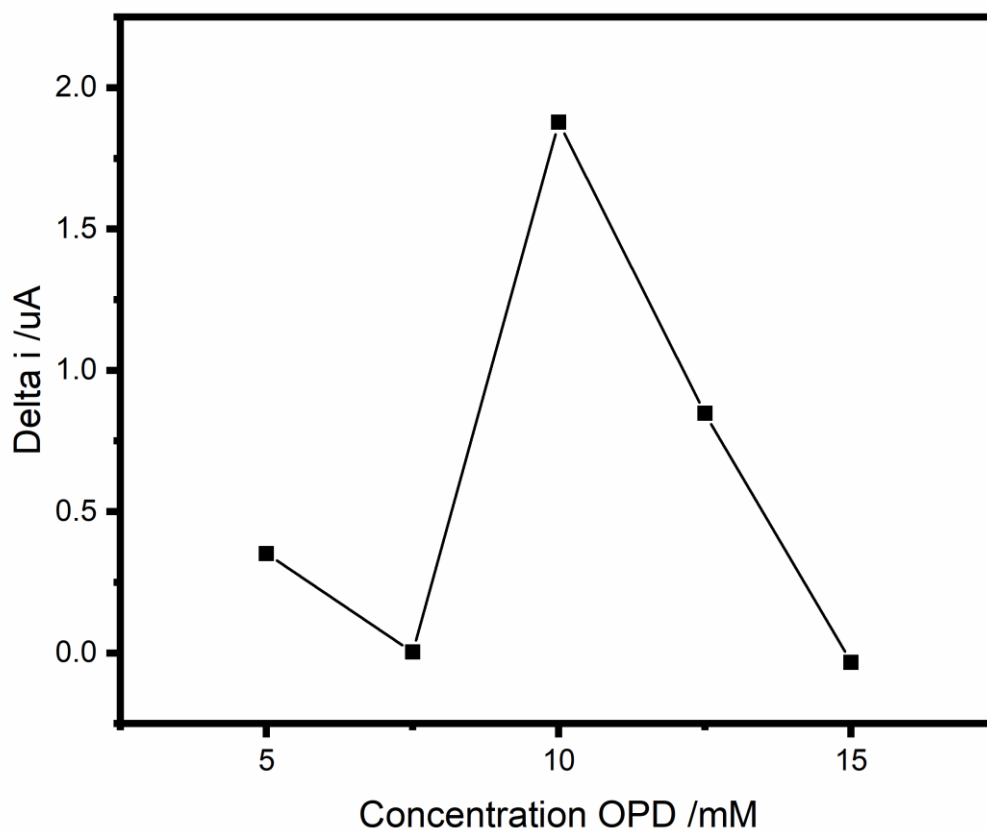


**Figure 25.** Optimization of o-PD concentration affecting the performance of the MIP electrode. Effect of the o-PD concentration on  $\Delta I$  at the prepared MIP electrode in the solution containing 1 mM FcCOOH in PBS 1X in the presence of  $8.06 \times 10^{-14}$  M *Cyt c* after 10 min incubation time.

### 3.1.2.2. Optimization of the template concentration

The quantity and quality of the molecularly imprinted polymer recognition sites is a direct function of amount of template [162]. Therefore, the effect of different concentration of template in the process of electropolymerization was studied and the corresponding results are listed in Table 7. The highest sensitivity was obtained using 1  $\mu$ M *Cyt c*, suggesting this as the best template concentration for cavities formation in the conditions tested. Furthermore, all the fabricated sensors have been compared with the slope  $\Delta I$ , not normalized to  $I_0$ , to verify the value of the current for every condition. Moreover, all the values of R-square were above 0.90 indicating a small dispersion of the data analyzed.

**Table 7.** Comparison of the analytical performance (sensitivity) of prepared MIP sensors using 10 mM o-PD and different concentration of *Cyt c* as template.

<b>Concentration <i>Cyt c</i> [<math>\mu</math>M]</b>	<b>Delta I slope [<math>\mu</math>A/M]</b>	<b>R squared</b>	<b>Delta I/I<sub>0</sub> slope</b>	<b>R squared</b>
<b>0.5</b>	0.425	0.938	0.065	0.938
<b>1</b>	0.709	0.937	0.122	0,937
<b>2</b>	0.534	0.895	0.073	0.895
<b>4</b>	0.148	0.943	0.107	0.943

Further analysis of data relevant to optimization of the template concentration is shown in Figure 26, where the highest  $\Delta I$  value was obtained at 1  $\mu$ M *Cyt c*. The current decreases at smaller template concentration indicates a decrease in the formation of imprinted sites while, on the other hand, an excess of template can hinder the formation of a stable MIP film.

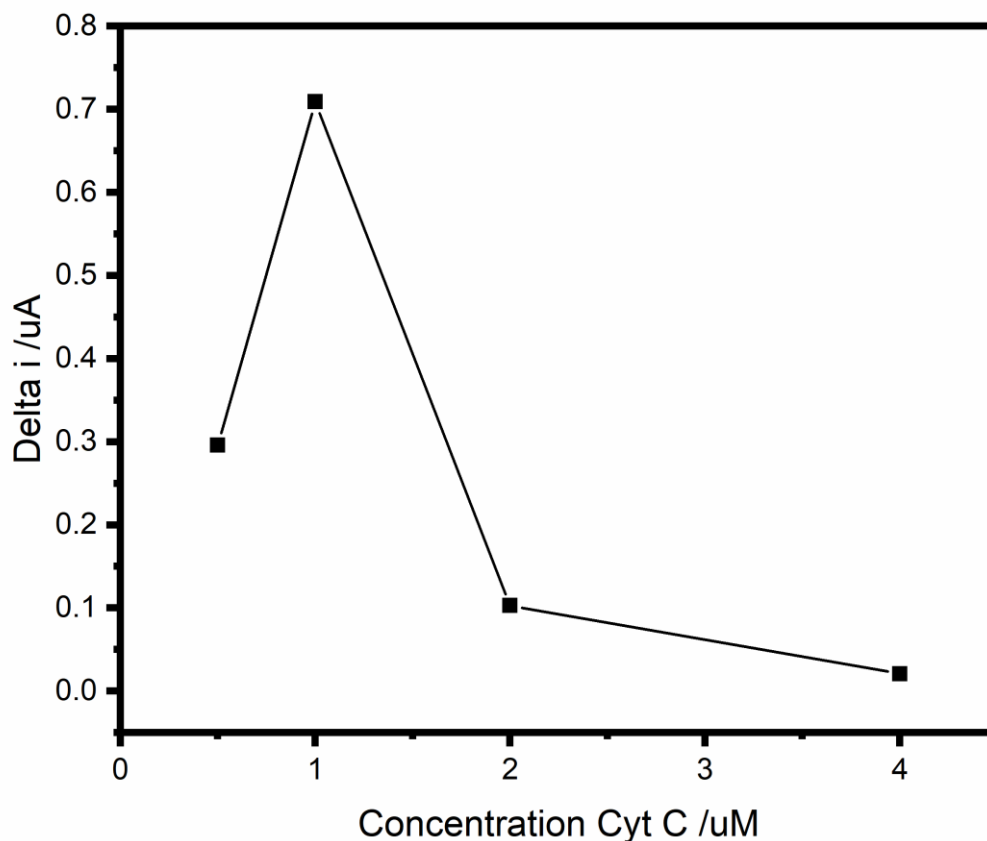


**Figure 26.** Optimization of *Cyt c* concentration affecting the performance of the MIP electrode. Effect of the *Cyt c* concentration on  $\Delta I$  at the prepared MIP electrode in the solution containing 1 mM FcCOOH in PBS 1X in the presence of  $8.06 \times 10^{-14}$  M *Cyt c* after 10 min incubation time.

### 3.1.2.3. Optimization of number of cycles for electropolymerization

The number of cycles was found to directly affect the sensor sensitivity. Data shown in Figure 27, indicate that the best  $\Delta I$  value was obtained after 20 voltammetric cycles, at 50 mV/s in the potential range 0.0-1.1 V. Lower and higher number of cycles seem to produce too thin or too thick coatings, respectively. In fact, above 20 cycles, too thick films with poor accessibility to the cavities are obtained; on the other hand, below 20 cycles, thinner films could not incorporate enough template to form cavities, resulting again in a loss of sensor sensitivity.

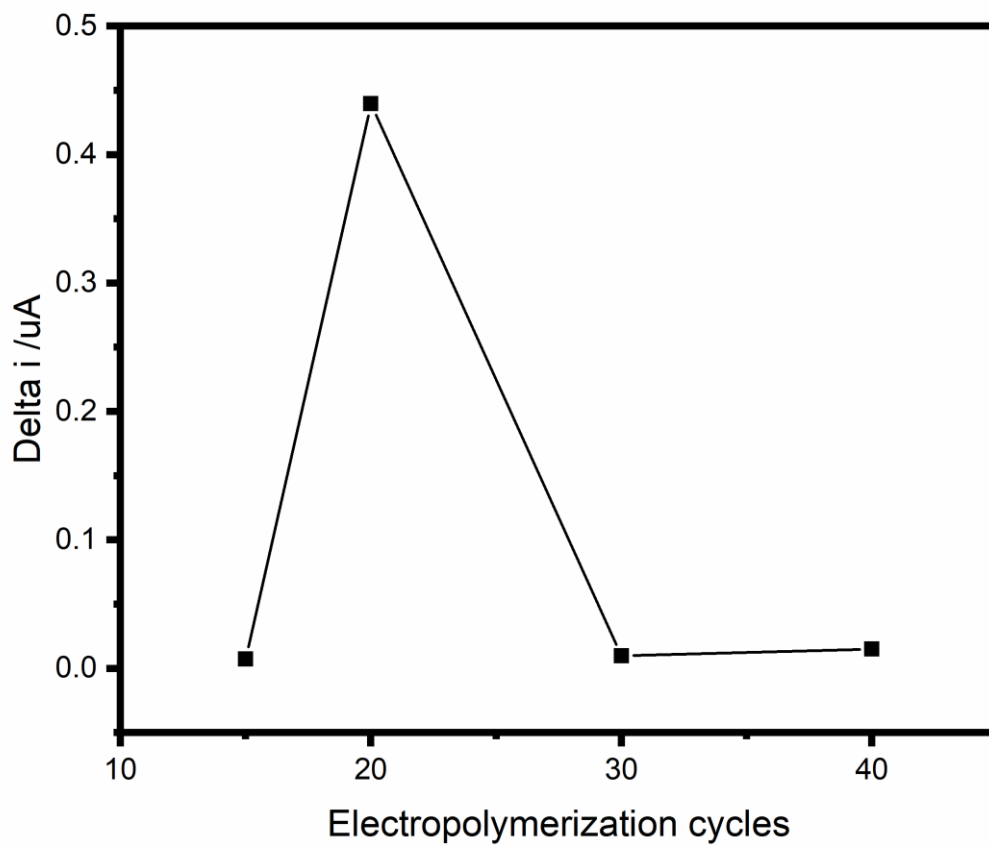


**Figure 27.** Optimization of number of cycles for electropolymerization affecting the performance of the MIP electrode. Effect of the cycles on  $\Delta I$  at the prepared MIP electrode in the solution containing 1 mM FcCOOH in PBS 1X in the presence of  $8.06 \times 10^{-14}$  M *Cyt c* after 10 min incubation time.

### 3.1.2.4. Template Removal

One of the most important parameters in the fabrication of an efficient MIP-electrode is template removal process. The ideal extraction solvent should interact with the polymer causing its swelling (necessary for the template release) without serious damage of the polymeric network [163]. Pure or mixed extraction solvents in the various treatment conditions were tested for extracting the *Cyt c* template. The electrochemical characterization of template removal process was performed in the presence of 1 mM FcCOOH (pH 7.4) using CV and DPV techniques. Using standard addition method, the calculated  $\Delta I$  after rebinding with a series of concentrations of *Cyt c* solutions, was used to evaluate the optimum conditions. Figure 28 shows the obtained results after acidic and basic treatments of MIP electrodes i.e., using  $H_2SO_4$  (1M for 3h) and NaOH (1M for 3h) respectively.

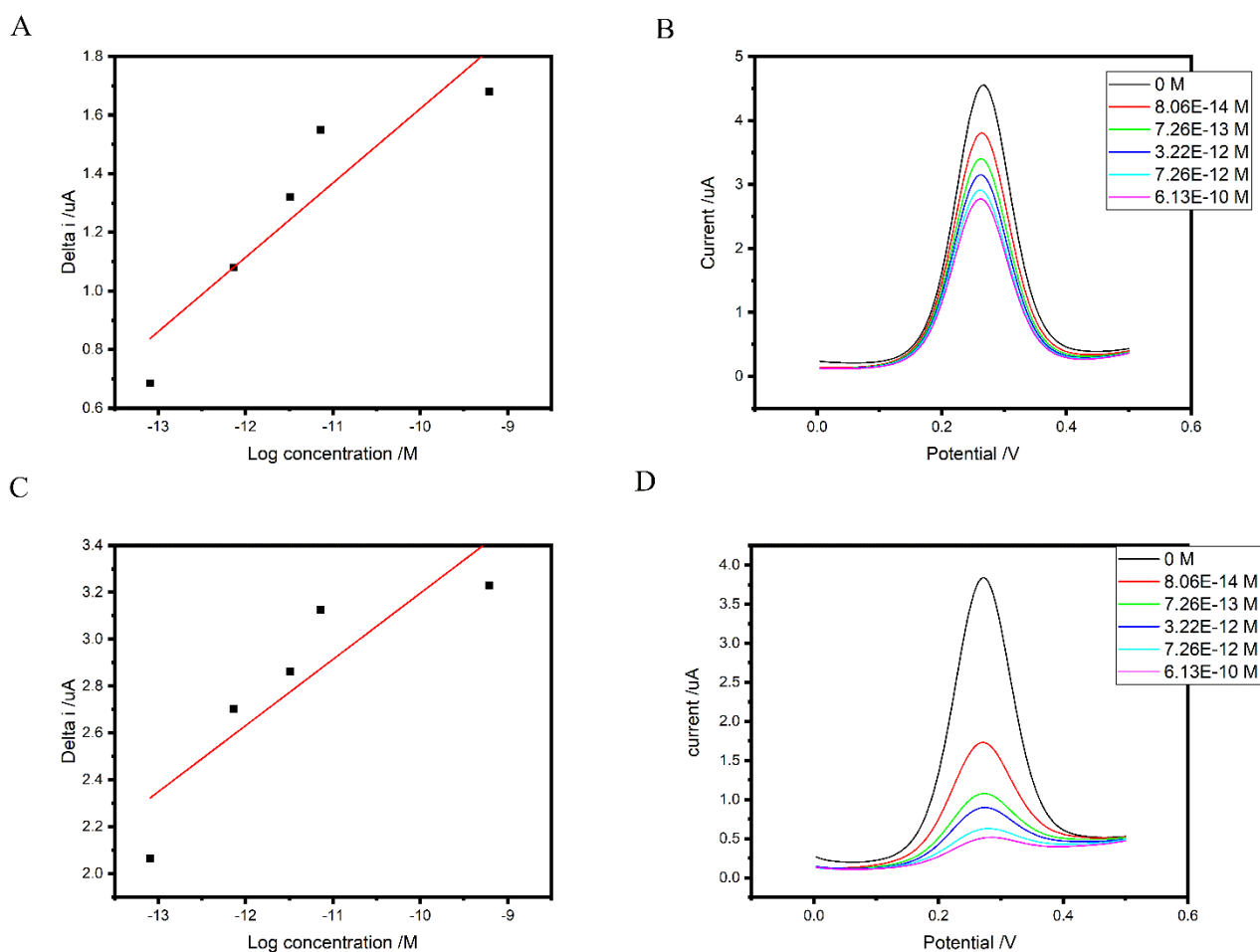


**Figure 28.** Effect of template removal treatment on the MIP sensor performances. In the upper part (A) the calibration plot and (B) DPVs graph of the MIP treated with 1 M NaOH for 3 hours. In the lower part (D) the DPV voltammograms and (C) calibration plot obtained with treated MIP with  $H_2SO_4$  1 M for 3 hours.

The obtained results demonstrate a successful extracting of the template molecules using acidic environment, in particular using  $H_2SO_4$  solution. The molecules of the solvent penetrate the polymeric layer, promoting swelling of the polymer and the release of the template molecule by virtue of the weakening of the hydrogen bonds between the polymer and the template molecule [81] probably by operating the protonation both of the amine group of poly-o-PD and glutamic and aspartic acid groups of *Cyt c*. A possible hydrolytic action of the strong acid on the protein backbone cannot be excluded. For the selective formation of the cavities, the effect of the different concentrations of acidic solution and wash times were investigated. Figure 29 shows the variation of the current ( $\Delta I$ ) at different extraction times.

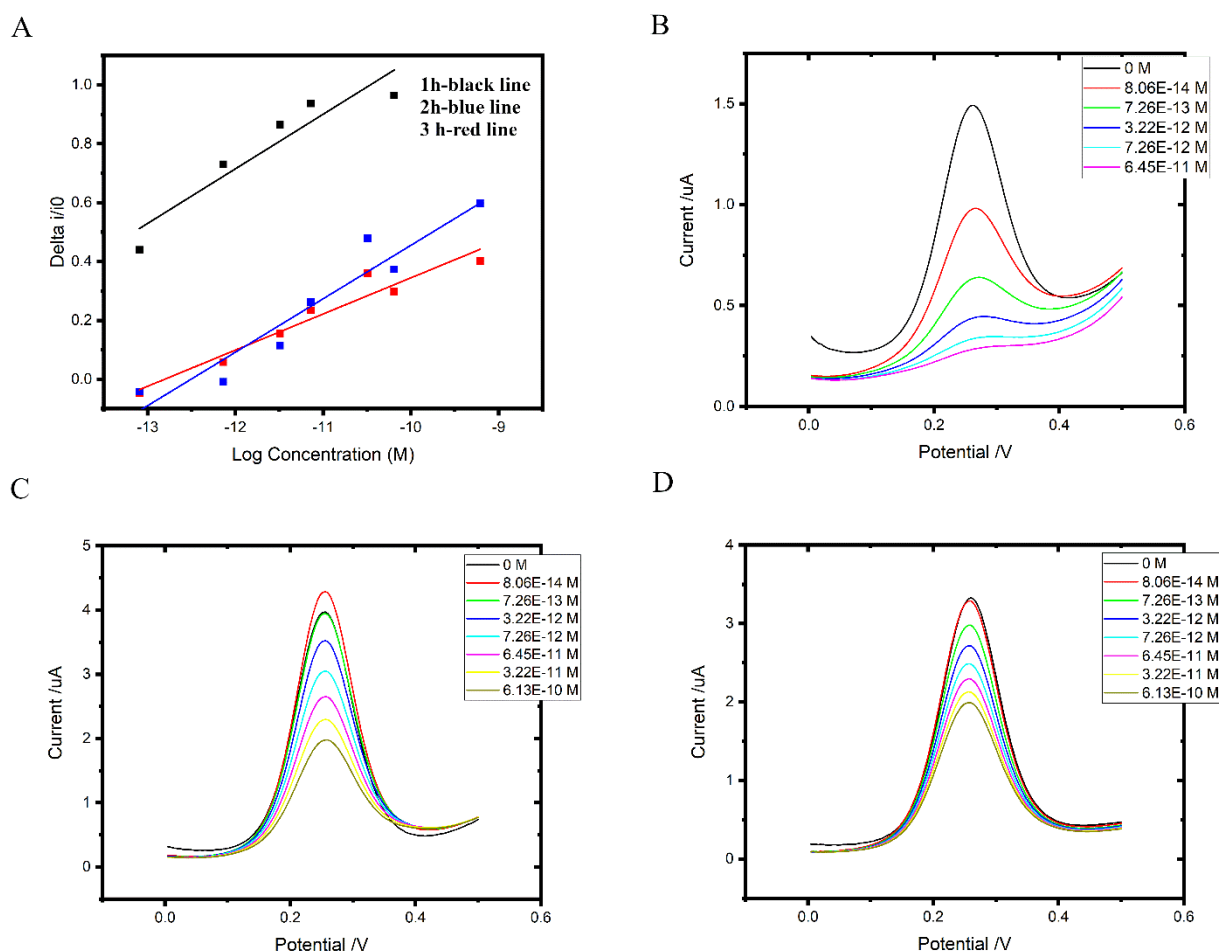


**Figure 29.** Effect of different extraction times on *Cyt c* removal using  $H_2SO_4$  1M. (A) Calibration plot of different times tested: 1h (black line), 2h (blue line), 3h (red line) at MIP modified electrodes. DPVs at the MIP modified electrodes prepared in different extracting time using  $H_2SO_4$  1M, after incubation in 1 mM FcCOOH in PBS 1X, containing different *Cyt c* concentrations: (B) 1h, (C) 2h, (D) 3h. MIP preparation: 10 Mm o-PD, 2  $\mu$ M *Cyt c*

Considering the slope of linear correlation between the logarithm of concentration and normalized  $\Delta I$  ( $\Delta I/I_0$ ), the greatest slope was referred to the condition of 1 hour in  $H_2SO_4$  1 M (black line).

The data plotted in Figure 30 show that the optimized template removal time was 1 hour.

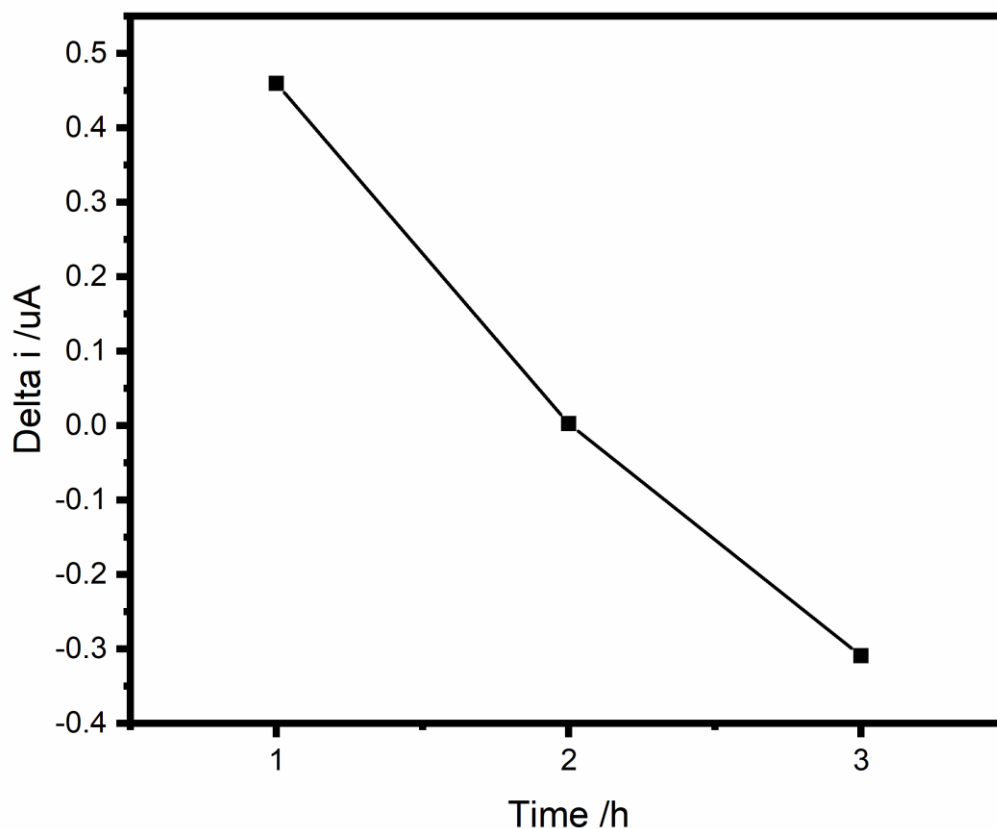


**Figure 30** .Correlation of the MIP current response after the addition of  $8.06 \times 10^{-14}$  M *Cyt c* in PBS 1X for tuning the extraction time.

The effect of the different concentrations of the  $H_2SO_4$  is shown by data in Figure 31. The best concentration obtained on the basis of the plot in Figure 31A is 0.5 M  $H_2SO_4$ , but this concentration tested on the NIP showed to cause some damages to the PoPD structure (see Figure 31B). Consequently, 0.1 M  $H_2SO_4$  was finally chosen as the best operative  $H_2SO_4$  concentration.



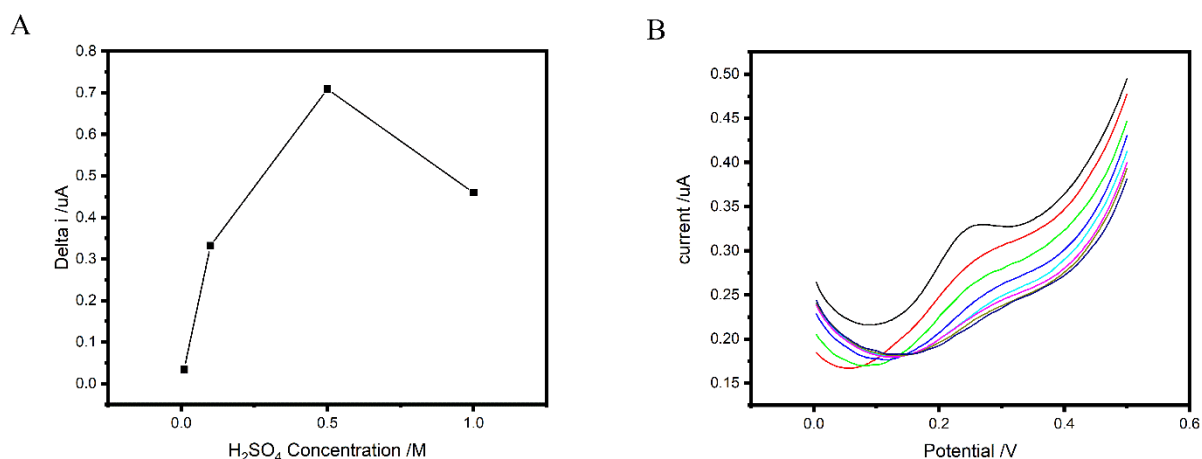


**Figure 31.** Effect of different conditions for template extraction. (A) effect of different concentration of H<sub>2</sub>SO<sub>4</sub> at MIP-modified electrode response, (B) DPVs at NIP-modified electrode treated by H<sub>2</sub>SO<sub>4</sub> 0.1M. The addition of *Cyt c* solution follows these concentrations 0 M,  $8.06 \times 10^{-14}$  M,  $7.27 \times 10^{-13}$  M,  $3.22 \times 10^{-12}$  M,  $7.27 \times 10^{-12}$  M,  $3.22 \times 10^{-11}$  M,  $6.45 \times 10^{-11}$  M,  $6.13 \times 10^{-10}$  M from the higher to the lower, respectively.

### 3.1.2.5. Optimization of the re-binding time

The influence of rebinding time on the MIP response was investigated. The time of accumulation in *Cyt c* solution using both MIP- and NIP-modified electrodes was optimized. Following the template removal process, the imprinted electrode was incubated in a stirred solution containing  $8.0 \times 10^{-14}$  M *Cyt c* for a certain time interval. As shown in Figure 32, the results obtained with the NIP electrode (squared dot line) indicate the almost-not-interaction between the *Cyt c* and the NIP-modified electrode. On the contrary, the  $\Delta I$  measured with the MIP-modified electrode increased with the time, indicating interaction between *Cyt c* and the cavities in the MIP. According to the results, a high current difference between the MIP and NIP electrodes was obtained already after 10 min, therefore, 10 min was evaluated as the best compromise between high sensitivity and short analysis time.

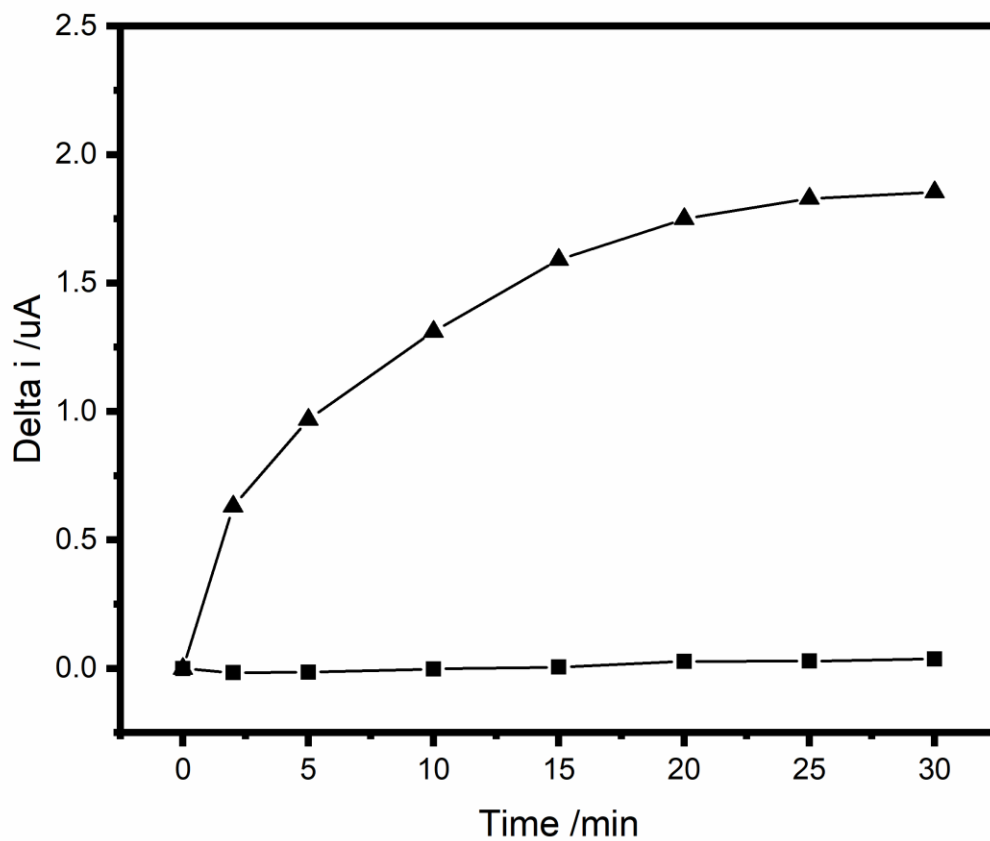


**Figure 32.** Effect of re-binding time on the response of MIP and NIP modified electrodes. MIP- and NIP-modified electrodes were prepared using 10 mM o-PD in the presence of 1  $\mu\text{M}$  *Cyt c* (MIP) and absence of *Cyt c* (NIP) in acetate buffer (pH 5.2); scan rate 50  $\text{mV s}^{-1}$ ; number of scans 20.

### 3.2. Binding Study

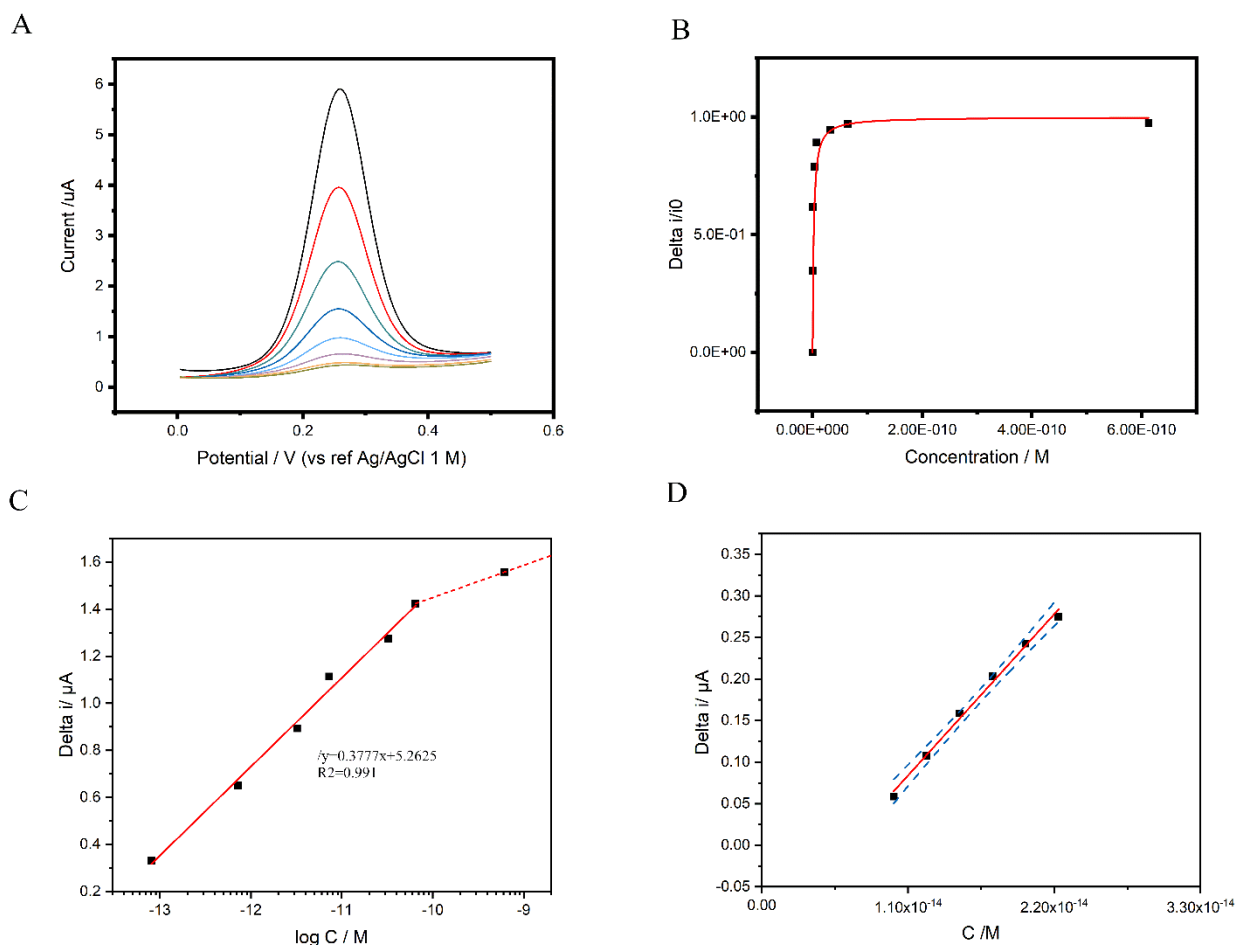


**Figure 33.** (A) DPVs of the MIP after the addition of *Cyt c* in the solution, from higher to lower voltammograms 0 M,  $8.06 \times 10^{-14}$  M,  $7.27 \times 10^{-13}$  M,  $3.22 \times 10^{-12}$  M,  $7.27 \times 10^{-12}$  M,  $3.22 \times 10^{-11}$  M,  $6.45 \times 10^{-11}$  M,  $6.13 \times 10^{-10}$  M of *Cyt c*, (B) Correlation between concentration and  $\Delta i/i_0$ , the theoretical fitting was reported in red, (C) Calibration plot of between  $\Delta i$  and the logarithm of the concentration, (D) Calibration plot (with 95% confidence interval) of the first linear tract of the sensor response to *Cyt c*, the linear fitting was reported in black.

In order to perform the quantitative evaluation of the affinity of the MIP for *Cyt c*, the dependence of DPV peak currents in Figure 33A on *Cyt c* concentration was analyzed in detail. Assuming that each individual binding side (BS) or cavity in the MIP can bind only one *Cyt c* molecule, the binding process between *Cyt c* and the MIP obeys the following equilibrium equation:



where  $\text{Cyt } c@BS$  is the  $\text{Cyt } c$  bound with a MIP binding site.

The formation constant  $K_a$  for  $\text{Cyt } c@BS$  is:

$$K_a = [\text{Cyt } c@BS]_{\text{pol}} / ([\text{Cyt } c]_{\text{sol}} \times [\text{BS}]_{\text{pol}}) \quad (3.2)$$

where subscripts “pol” and “sol” indicate concentrations in the polymer layer and in solution, respectively.

The total concentration of binding site in the polymer  $[\text{BS}]_0$  is always:

$$[\text{BS}]_0 = [\text{BS}]_{\text{pol}} + [\text{Cyt } c@BS]_{\text{pol}} \quad (3.3)$$

By substituting in Equation (2) and rearranging:

$$[\text{BS}]_0 / [\text{Cyt } c@BS]_{\text{pol}} = K_a [\text{Cyt } c]_{\text{sol}} / (1 + K_a [\text{Cyt } c]_{\text{sol}}) \quad (3.4)$$

$[\text{BS}]_0$  and  $[\text{Cyt } c@BS]_{\text{pol}}$  are directly proportional to  $i_0$  and  $(i_0-i)$  measured for the  $\text{FcCOOH}$  probe. Such a proportionality factor will depend on the diffusion rate of the  $\text{FcCOOH}$  probe to the nanocavities/electrode interface, so that, at constant  $\text{FcCOOH}$  solution concentration, this factor is expected to be constant. Under these conditions, simplifying the proportionality factor between numerator and denominator, then equation (4) becomes:

$$(i_0-i) / i_0 = K_a [\text{Cyt } c] / (1 + K_a [\text{Cyt } c]) \quad (3.5)$$

Figure 33B shows that equation (3.5) fits very well the trend obtained from DPV peaks currents vs. *Cyt c* solution concentration, when  $K_a = 5 \times 10^{11} \text{ M}^{-1}$ . Note also that when  $K_a [Cyt c] \ll 1$  (that is for very small *Cyt c* solution concentrations), equation (3.5) can be simplified to

$$(i_0 - i) / i_0 = K_a [Cyt c] \quad (3.6)$$

Note that at variance with other fitting equations recently proposed for other electrochemical MIP sensors ( see e.g. eq.(1) in ref. [164]), equation (3.1) has a more general applicative character, since it does not require the calculation of  $[BS]_0$  nor the knowledge of the exact equation relating voltammetric current signals to the specific diffusive regime (e.g. pure radial vs. total overlap vs. others) which rules mass transport of the redox probe to the array of electrochemically active nanocavities composing the MIP-sensor.

### 3.3. Analytical performances

DPV peak current signals recorded with the optimized MIP are plotted as a function of the logarithm of *Cyt c* solution concentration. As it has been shown in Figure 33C, the observed peak current decrease is proportional to the *Cyt c* concentration, identifying two linear ranges with different slopes, i.e., sensitivities. Figure 33D report the  $\Delta I$  vs.  $[Cyt c]$  plot for the higher sensitivity region. From these data, the limit of detection (LOD) for *Cyt c* with the MIP-sensor is calculated to be  $1.4 \times 10^{-15} \text{ M}$  ( $1.75 \times 10^{-2} \text{ pg/mL}$ ), using the equation  $\text{LOD} = 3.3\sigma/m$ , where  $\sigma$  is the standard deviation of y intercept in calibration curve, and  $m$  is the slope of the calibration curve. In comparison with chromatographic, spectrophotometry and other electrochemical techniques and sensors, the present MIP sensor is characterized an extremely low detection limit, even if such a small detection limit is achieved operating within a relatively limited linearity range.

#### 3.3.1. Reproducibility and reusability of MIP modified electrodes

The reproducibility of sensor fabrication was investigated by preparing four MIP modified electrodes independently by using the same optimized procedure. The prepared MIP sensors were evaluated by analyzing *Cyt c* standard solutions, using different concentrations, all selected to be within in the first portion of the linear range of the calibration plot. The sensitivities of the obtained calibration plots were compared and relevant results are reported in Figure 34.

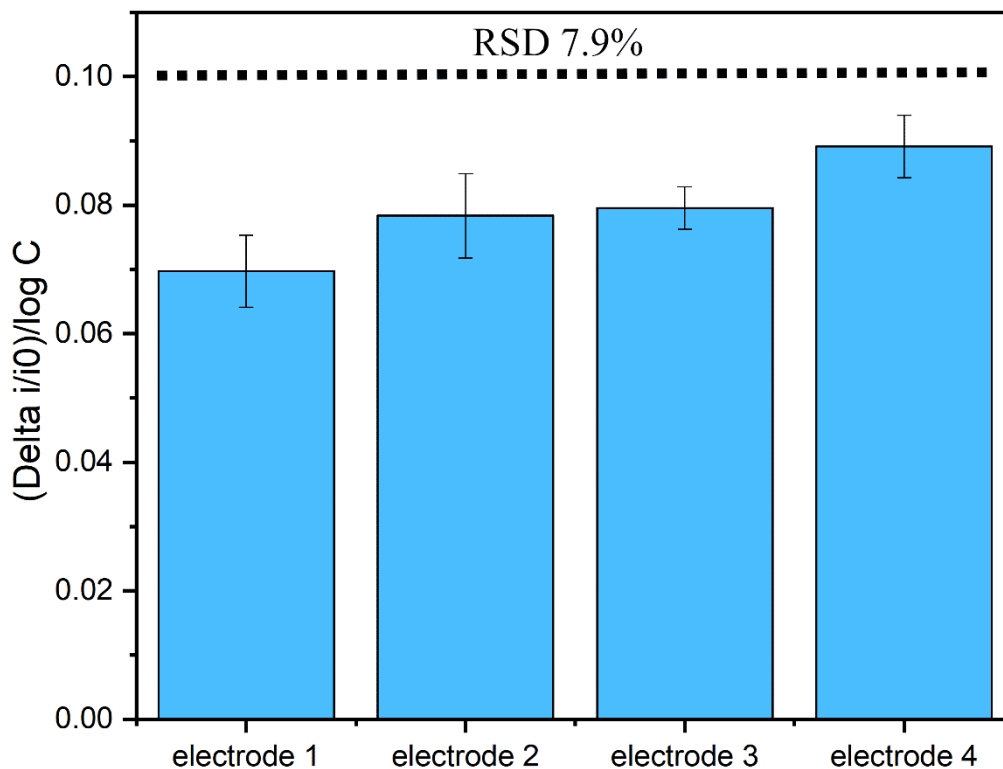


**Figure 34.** The charts show the sensitivities obtained from four fabricated MIP-electrodes.

The columns describe the value of the slope obtained by linear interpolation of the experimental data. The error bars represent the error of the slope given, calculated by the interpolation algorithm used. The reproducibility was reported in terms of relative standard deviations (RSDs) between the mean value with a result of 7.9% which indicates a good reproducibility of the fabrication of the MIP modified electrode.

Concerning the reusability of the developed sensor with an individual sensor, two successive measurements were performed with the same MIP electrode, after regeneration with  $H_2SO_4$  for 1 hour before each measurement.

The results obtained are reported on Figure 35.

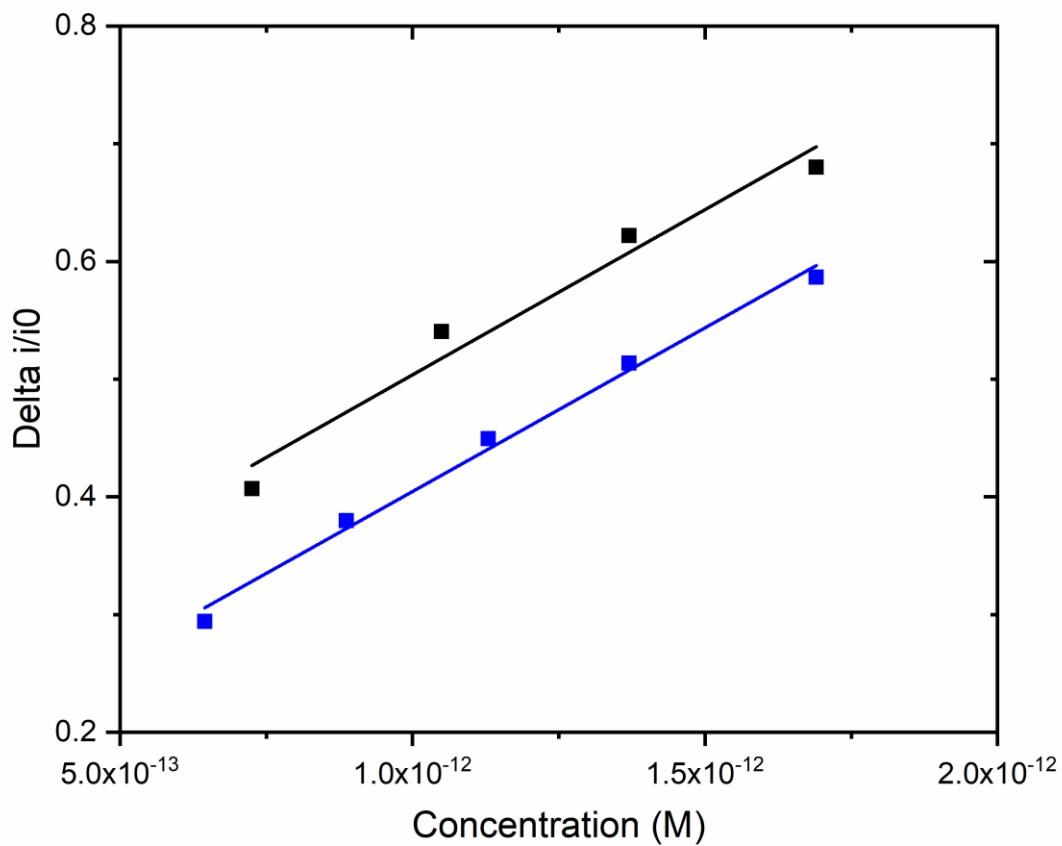


**Figure 35.** Comparison the sensitivity of sensor performance after regeneration of the imprinted cavities. Calibration plots of freshly-prepared MIP electrode (Black line) and Re-generated MIP electrode (Blue line).

The sensitivities of the *Cyt c* analyses were evaluated by the slopes of the calibration plots  $\Delta i/i_0$  vs. *Cyt c* concentration, obtained using a freshly-prepared MIP electrode (Fig. 35, black line) and a re-generated MIP electrode (Fig. 35, blue line); the values measured were  $2.81 \times 10^{11} \text{M}^{-1}$  ( $R^2=0.950$ ) and  $2.78 \times 10^{11} \text{M}^{-1}$  ( $R^2=0.990$ ), respectively. The obtained results indicated that the MIP-sensor exhibits good reusability (repeatability) and stable sensitivity.

### 3.3.2. Sensor performances in real condition: selectivity studies

Considering the real environment of *Cyt c* testing, the sensor selectivity was evaluated in presence or absence of possible interfering compounds, added in the same concentrations (molar ratio 1:1) with respect to *Cyt c* concentration  $4.03 \times 10^{-13}$  M. The rational idea of the molecule choice was to take in consideration proteins with similar isoelectric point of *Cyt c* (IP=10.8 at pH 7.00) or because of their natural abundance in the serum such as bovine serum albumin, albumin family member, Haemoglobin, hem-protein family member, Streptavidin and Lysozyme. The determination of *Cyt c* was performed by the MIP-modified electrode using the standard addition method. The results obtained with the MIP sensor are presented in the Table 8.

**Table 8.** Recovery data between *Cyt c* spike and *Cyt c* found experimentally.

<b>Interfering materials</b>	<b>Added <i>Cyt c</i> (M)</b>	<b>Found <i>Cyt c</i> (M)</b>	<b>Recovery (%)</b>
--	$4.03 \times 10^{-13}$	$3.94 \times 10^{-13}$	97.2
Lysozyme	$4.03 \times 10^{-13}$	$4.08 \times 10^{-13}$	101.2
Hemoglobine	$4.03 \times 10^{-13}$	$4.35 \times 10^{-13}$	108
Albumin	$4.03 \times 10^{-13}$	$5.24 \times 10^{-13}$	130

So, as reported in the Table 8, the recovery of 97.2% was found in the absence of any interference, while the recovery in the presence of the interference molecules spans from 101.2 % to 130 % for lysozyme and Albumin, respectively. In other word, noticeably, the foreign species, Lysozyme, Streptavidin and Hemoglobin showed little influence on the determination of *Cyt c*. This might be attributed to that the selective cavities which located in the imprinted polymer film could avoid the binding of foreign molecules with imprinted polymer film. Among all of foreign molecules being investigated, only Albumin can affect the determination of *Cyt c* seriously, which can be ascribed to the fact that it can absorb on the surface of polymer where the FcCOOH probe is impeded to reach on the surface of electrode for exchanging the electrons. The decay of FcCOOH signal was used as reference for the presence of *Cyt c* in the sample. The influence of recovery was also a straight correlation between the competition of the molecules at the same concentration. Finally, it can be



concluded that the proposed electrochemical sensor exhibits good selectivity to the electrochemical determination of *Cyt c*.

### 3.3.3. Sensor performances in real condition: serum tests

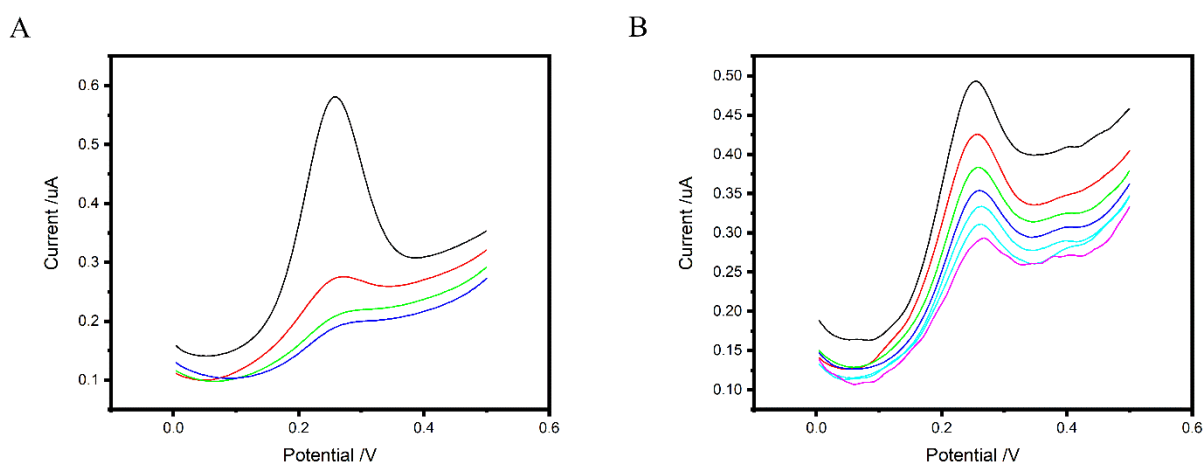


**Figure 36.** DPVs recorded at (A) MIP modified electrode with pure Fetal Bovine Serum (FBS) in ratio 1:20, from higher to lower voltammograms in 1 mM FcCOOH after 0 M,  $8.06 \times 10^{-14}$  M,  $7.27 \times 10^{-13}$  M,  $3.22 \times 10^{-12}$  M of *Cyt c* additions, respectively, (B) NIP modified electrode in solution of 1mM FcCOOH in PBS 1X with pure Fetal Bovine Serum (FBS) in ratio 1:20, DPV of the NIP after the addition of *Cyt c* in the solution, from higher to lower voltammograms in 1 mM FcCOOH after 0 M,  $8.06 \times 10^{-14}$  M,  $7.27 \times 10^{-13}$  M,  $3.22 \times 10^{-12}$  M,  $7.27 \times 10^{-12}$  M,  $3.22 \times 10^{-11}$  M,  $6.45 \times 10^{-11}$  M of *Cyt c* addition, respectively.

In order to investigate the usability of the developed sensor in the presence of interfering components, diluted human serum (HS) was used. The serum contains over then 10000 types of different proteins, where the Albumins range from 60% to 67% of the total proteins content [165]. Figure 36 demonstrated the analytical behavior of MIP and NIP electrodes in the solution serum containing different concentrations of *Cyt c*. The MIP was capable of detect the *Cyt c* also in this condition, whereas the NIP showed a limited recognition of the target only by non-specific interactions.

**Table 9.** Application of the MIP-modified sensor to the detection of *Cyt c* in human serum.

<b>Sample</b>	<b>Added <i>Cyt c</i> in diluted serum (M)</b>	<b>Found <i>Cyt c</i> in diluted serum (M)</b>	<b>Calculated <i>Cyt c</i> in undiluted serum <sup>a</sup> (M)</b>	<b>Recovery <sup>b</sup> (%)</b>
Diluted Serum (1:20)	$4.0 \times 10^{-13}$	$3.2 \times 10^{-13}$	$6.4 \times 10^{-12}$	80
Diluted Serum (1:50)	$4.0 \times 10^{-13}$	$3.9 \times 10^{-13}$	$1.9 \times 10^{-11}$	96
Diluted Serum (1:50)	$8.0 \times 10^{-15}$	$6.4 \times 10^{-15}$	$3.2 \times 10^{-13}$	80

Using the linear regression equation for *Cyt c* found through the calibration curve (Figure 33D), the diluted human serum was monitored with given amounts of *Cyt c* and the recoveries were evaluated. The determination results are listed in Table 9. Initially the matrix effect on the response of MIP-sensor was studied as function of dilution of HS with a dilution 1:20 and later, 1:50 using PBS 1X. As a result, increasing the dilution, the performances of sensor in HS were improved. The concentration of *Cyt c* in HS: PBS1X (1:50) were found  $3.86 \times 10^{-13}$  M (4.80 pg/mL) over a spiked value of  $4.03 \times 10^{-13}$  M (5.00 pg/mL) and  $6.45 \times 10^{-15}$  M (0.08 pg/mL) over a spike of  $8.06 \times 10^{-15}$  M (0.1 pg/mL). The satisfactory recovery results summarized in Table 9, indicate that the here prepared MIP sensor can be suitable for more extended application for ultratrace *Cyt c* analyses in biological samples.

## 4. Conclusions

The MIP-sensor here developed shows impressive sensitivity and extremely low detection limit, that make it suitable for the determination of *Cyt c* at trace concentration level, in the femtomolar range in synthetic samples and in the picomolar range in diluted blood serum.

The high affinity of the sensor for *Cyt c* was confirmed by the quantitative evaluation of the characteristics of the MIP-sensor, measuring a binding constant between *Cyt c* and the imprinted cavities in excess to  $10^{11} \text{ M}^{-1}$ . Interestingly, the detailed electrochemical characterization of the sensor supported, in agreement with previous studies [60,68], that MIP coated electrodes behave indeed as arrays of nanoelectrodes, where the imprinted cavities are to the nanoelectrodes.

The achieved results can open interesting perspectives for studying quantitatively the role of *Cyt c* in diseases associated with insufficient apoptosis, for which the serum concentration of *Cyt c* is expected to be below the regular nanomolar level.

The significant analytical performances of this MIP-sensor can open new prospect not only for developing a highly sensitive electrochemical sensor for *Cyt c*, but also for extending the application of MIP-sensor to trace detection of other proteins.

# **CHAPTER 4: Development of an electrochemical sensor based on screen printed electrode modified with MIP for the detection of Troponin I**

## **1. Introduction**

Cardiovascular diseases (CVDs) are classified in the group of heart and blood vessels disorders. According to the report from the World Health Organization (WHO), over 23.3 million of people are expected to die annually from CVDs by 2030 [166]. One of the most common types of CVDs is acute myocardial infarction (AMI). After blockage of a coronary artery and lack of blood supply (ischemia), myocardial muscle gets damage this damage leading to the AMI [167]. Due to outstanding specificity and high sensitivity for acute myocardial cell damage, cardiac Troponin I (TnI) and cardiac Troponin T (TnT) are the biomarkers considered as “gold standard” for AMI diagnosis [168,169]. Troponin I is a small protein belonging to the troponin-tropomyosin complex. Note that Troponin I is found only in the cardiac muscle whereas Troponin T is present in cardiac and skeletal muscles and troponin C (TnC) is selectively expressed in skeletal muscular cells [170]. The most important isoform of Troponin I is the cardiac troponin I (TnI). This type of troponin has the same function of other proteins of the troponin I family but has the unique feature to be expressed in the cardiac muscular tissue uniformly throughout atrial and ventricular chambers. The slow skeletal TnI isoform is mainly expressed in the embryonic stage of heart development. During the last weeks of human fetal development, the rate of cTnI expression increases [171] and by the ninth month after birth skeletal TnI is completely substituted by the cardiac isoform [171,172]. Starting from a normal cardiac muscle form by filaments of actin (double helical actin filaments), the Troponin-tropomyosin complex is associated every 7 actin monomers and is in charge for the muscle contraction through the shifting of the filaments. Troponin I is the subunit of this complex that prevents the contraction in absence of calcium release and TnC, through the inhibition of the actomyosin ATPase.

## **1.2. Cardiac Troponin I: clinical role and detection**

During the development of the cardiac tissue the mitosis rate decreases over the commitment of the tissue to his contractile function. Thus, in the early post-natal has been seen complete functional recovery after myocardial infarction; on the other hand, has a consequence of this the rate of adult human cardiomyocytes in the healthy heart is only about 0.5% to 1% per year and the majority of cardiomyocytes are never exchanged. In this tissue evolutionary scenario, the commonly protein founds in circulation deputed to cardiac tissue has been related to tissue damage and tissue necrosis.

Among them, cTnI, because of its specific localization in the cardiac tissue has been used as golden standard for the early diagnosis of myocardial acute injury. Note that abnormal concentration of cTnI protein is not detected in the case of injuries to skeletal muscles or other tissues [167,173]. The concentration of cTnI in serum increases up to 0.7–1.4 ng/mL from the normal level of <0.4 ng/mL within 3–12 h of AMI and may remain elevated for 5–9 days [167]. Despite its pivotal role in determination of the acute myocardial infarction, the clinical outcome of using cTnI as biomarker is under debate, because in recent years new high-sensitivity (<5 ng/ml) test methods have been developed demonstrating the need of new common practice clinical rules in stratifying the population who do have acute myocardial infarction (AMI). Indeed, international guidelines recommend using the sex-specific 99<sup>th</sup> centile from a healthy reference population as the diagnostic threshold for myocardial infarction, it is increasingly evident that the use of lower thresholds to risk-stratify patients and rule-out myocardial infarction at presentation is safer and more effective [174].

Along with the performance of test also the issue of standardization has been widely discussed by Bagai and colleagues [175] where the 99<sup>th</sup> percentile rule leads to very different values, even 20-fold, on thresholds levels of cTnI as limit value for identifying AMI.

The diagnosis of AMI, unstable angina, post-surgery myocardium trauma, as well as several other diseases related to cardiac muscle injury can be made possible by means of easy, rapid, sensitive and selective methods for detection of TnI [176]. Existing methods of diagnosis for TnI rely on expensive and time-consuming laboratory tests, including immunoenzymometric assays (ELISA) [177], chemiluminescence [178], chemiluminescent-immunoassays [179], fluorescence immunoassay [180], surface plasmon resonance[181] and colorimetric protein array [197].

However, to meet the increasing demand of quick diagnosis and clinical therapeutics, the development of devices characterized by fast response time, high sensitivity, stable characteristics as well as ease of operation and fabrication is essential. Electrochemical biosensors attracted considerable attention because of special features like simplicity, high sensitivity, low cost, rapid and reliable determination and miniaturization [182]. Generally, in affinity biosensors, the interaction between antigens and antibodies, which are immobilized on electrodes, are converted into an electrical signal. This signal can be amplified by enzymatic reaction. Special attention has been paid to electrochemical detection of cTnI based on electrochemical immunosensors [183,184] and electrochemical aptasensor [185,186].

The main characteristics of commercially available tests are summarized in Table 7, adapted from reference [56].

**Table 10.** Commercially available test for Troponin I and Troponin T.

<b>Manufacturer</b>	<b>Assay Model</b>	<b>Assay Type (I or T)</b>	<b>Assay Sensitivity</b>	<b>Manufacturer-determined 99<sup>th</sup> percentile</b>
<b>Abbott</b>	Architect	I	Standard	0.028 ng/mL
	AxSYM ADV	I	Standard	0.04 ng/mL
	I-STAT	I	Standard	0.08 ng/mL
	Architect	I	High	26 ng/L; (15.6ng/L for women; 34.2ng/L for men)
<b>Alere</b>	Triage Cardio 3	I	Standard	0.022 ng/mL
<b>Beckman-Coulter</b>	Accu TnI	I	Standard	0.04 ng/mL
	AccuTnI+3 Access	I	Standard	0.02 ng/mL
	AccuTnI+3 Dxi	I	Standard	0.03ng/mL
<b>bioMerieux</b>	VIDAS	I	Standard	0.01 ng/mL
<b>Ortho Clinical Diagnostics</b>	Vitros	I	Standard	0.034 ng/mL

<b>Radiometer</b>	AQT90	T	Standard	0.017 ng/mL
<b>Roche</b>	Cobas Elecsys	T	Standard	0.01 ng/mL
	Cobas h232	T	Standard	Not applicable/Qualitative assay*
	Cobas 600	T	High	14 ng/L
<b>Siemens</b>	Advia Centaur	I	Standard	0.04 ng/mL
	Dimension Vista	I	Standard	0.045 ng/mL
	Dimension EXL	I	Standard	0.056 ng/mL
	Dimension RXL	I	Standard	0.070 ng/mL
	Immulite 1000	I	Standard	0.3 ng/mL
	Immulite 2000	I	Standard	0.29 ng/mL
<b>Tosoh</b>	AIA360	I	Standard	0.060 ng/mL

Despite the plethora of tests available in the market and the convergence of the clinical concept about the high sensitivity troponin I, the majority of these methods relies on the use of natural antibodies

with some limits related to storage stability, sensitivity and detection limits. These issues can be addressed by replacing natural antibodies with stable synthetic analogues. As outlined in the general introduction of this thesis, one promising way of obtaining artificial receptors is the molecular imprinting of polymers (MIPs) [51]. Furthermore, electrochemical sensors based on MIP are characterized by high thermal and chemical stability, low cost, and ease of preparation [82] and has been arising as potential candidates for next generation marketable analytical sensors. In the present work, we study an electrochemical sensor based on molecularly imprinted electrosynthesized polymer for detection of cardiac Troponin I.



## 2. Materials and methods

### 2.1. Materials

*o*-Phenylenediamine (*o*-PD,  $\geq 98\%$ ), ferrocenecarboxylic acid (FcCOOH,  $\geq 97\%$ ), cytochrome *c* (*Cyt c*,  $\geq 95\%$ , Mw = 12.384 kDa, from horse heart), Troponin I (TnI, Mw=23.9 kDa, from human heart, Sigma)) were purchased from Sigma–Aldrich and used as received. Standard stock solution of *Cyt c* (30  $\mu$ M) was prepared in double distilled deionized water and stored at 4 °C if not in use. Standard stock solution of TnI (2 $\mu$ M) was prepared in phosphate buffer saline solution (PBS 1X:  $1 \times 10^{-2}$  M Phosphate Buffer,  $1.37 \times 10^{-1}$  M NaCl,  $2.7 \times 10^{-3}$  M KCl, pH 7.4) and stored at  $-20^{\circ}\text{C}$  if not in use. A 1 mM FcCOOH solution was prepared in PBS 1X at pH 7.4. All other reagents were of analytical grade and solutions were prepared using double distilled deionized water.

### 2.2. Apparatus and Measurements

Cyclic voltammetry (CV) and differential pulse voltammetry (DPV) measurements were performed at room temperature with CH Instruments Potentiostats (CH660B and CH1222a) controlled via personal computer by its own software. A standard three-electrode configuration was used where a gold disk electrode (2.0 mm diameter), a platinum wire and an Ag|AgCl|KCl (1 M) were used as the working, the counter and references electrodes, respectively. Commercial screen printed electrode (SPE) chips were also used where the working, counter and pseudo-references electrode are printed on the same chip. Three different SPEs were used: Dropsens Gold (DRP-220AT), Dropsens Carbon (DRP-110AT) purchased from Metrohm Dropsens, Micrux Carbon (ED-S1PE-C) purchased from Micrux fluidic. The Dropsens Gold electrode is composed of the working electrode and the counter electrode in gold while the reference electrode and the contacts are in silver; the overall dimensions of the chip are  $3.4 \times 1.0 \times 0.05$  cm (length  $\times$  width  $\times$  height). The Dropsens Carbon electrode is composed of the working electrode and the counter electrode in carbon, while the reference electrode is made of silver; the dimensions of this electrode were  $3.4 \times 1.0 \times 0.05$  cm (length  $\times$  width  $\times$  height). The Micrux Carbon electrode is composed of the working electrode and the counter electrode in carbon while the reference electrode is made of silver; the dimensions of this electrode were  $2.75 \times 1.01$  cm (length  $\times$  width).

To electrochemically characterize the SPEs, voltammetric measurements on SPEs were performed by placing a 50 $\mu$ l drop of the corresponding solution onto the working area.

### 2.3 Preparation and electrochemical characterization of imprinted sensors

The electropolymerization of o-PD on a cleaned gold electrode was carried out in acetate buffer solution (pH=5.2), containing 10 mM o-PD and 20 nM TnI, by performing 25 voltammetric cycles between 0 and 1.1 V vs Ag|AgCl using a scan rate of 50 mV s<sup>-1</sup>. To remove the template molecule, the MIP electrode was washed with water and dipped in the template removal solution (0.1 M H<sub>2</sub>SO<sub>4</sub>) for 60 min under mild stirring, followed by repeated washing with water. A control electrode modified with non-imprinted polymer (NIP) was obtained in the same way, but in the absence of TnI. Modified surfaces were stored at room temperature. To investigate dummy imprinting strategy, MIP-modified electrode was electrosynthesized using a solution containing 10 mM o-PD and 1 μM *Cyt c* as dummy template species of TnI. Aiming to develop a portable and low-cost device, electrochemical sensor based on MIP on gold disk electrodes was redesigned on commercial screen-printed electrodes (SPEs). The electrochemical characterization of polymerized films before and after template removal was carried out using 1 mM FcCOOH in PBS 1X, pH 7.4 using different electrochemical techniques, namely cyclic voltammetry (CV) and differential pulse voltammetry (DPV).

### **3.Results and discussion**

#### **3.1. Electrochemical characterization of SPEs**

The development of a successful sensor based on screen-printed electrodes largely depends on the efficiency of the substrate electrode on which the sensing system will be developed. It has been reported that the performance of a SPE is strongly affected by the composition of the material used for its fabrication [188,189], pre-treatment procedures [190], the temperature used for curing the printed layers [190-192], the redox couple chosen to interrogate the sensor [188]. Consequently, we have explored the behaviour of three different SPE strips, bought from different commercial sources. An important parameter to consider when utilising electrochemical sensors is the real electroactive area, especially for fundamental calculations of electrochemical processes, as well as for their benchmarking with respect to the quality control [193]. Indeed, the geometrical area,  $A_{\text{geom}}$  of these SPEs can be physically/visually determined with techniques such as scanning electron microscopy but there is no assurance that the electroactive area and the geometric area coincide [193]. The most appropriate way is to use interfacial techniques such as cyclic voltammetry (CV) to evaluate and study of SPE performances. To this aim we used standardized redox probes, so that by measuring capacitive and faradic currents we can measure and evaluate the analytical performances of different electrochemical platforms.

Moreover, optical and scanning electron microscopy (SEM) were applied to evaluate the morphology of the sensing platforms.

### 3.2. Determining the electroactive area using cyclic voltammetry

#### 3.2.1. Experimental measurement of the active area of Dropsens Gold 220AT

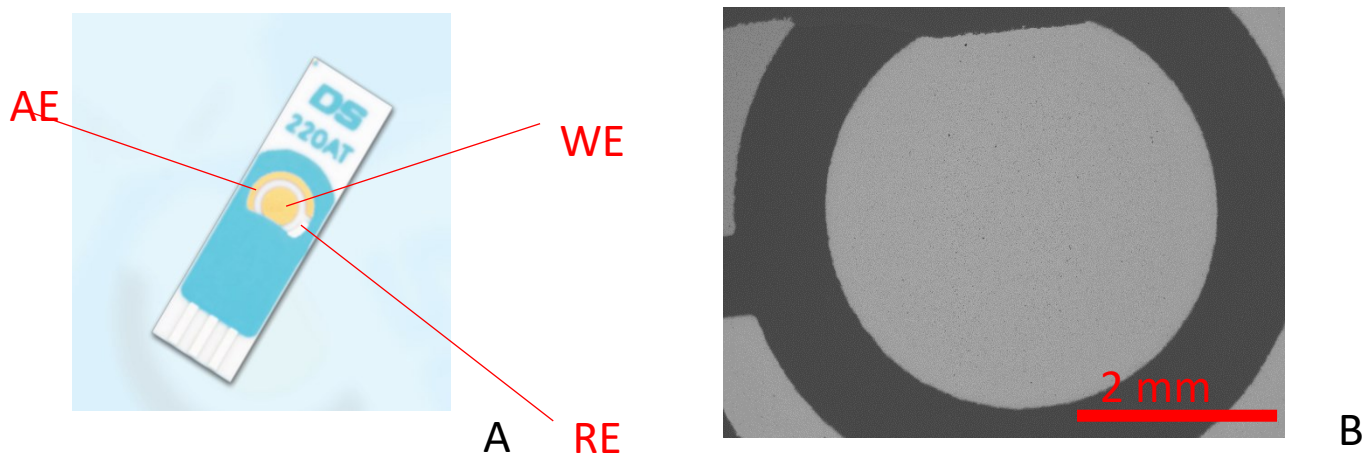


**Figure 37.** (A) Schematic representation of Dropsens Gold 220 AT SPE (adapted from Metrohm); (B) SEM image of the WE of Dropsens gold 220 AT, magnification 30X, 5 kV.

In order to measure experimentally the active area of the SPE, cyclic voltammograms were recorded at different scan rates in a blank solution containing pure supporting electrolyte (0.2 M PBS). Figure 38 shows the recorded voltammograms at the SPE Dropsens Gold 220 AT.

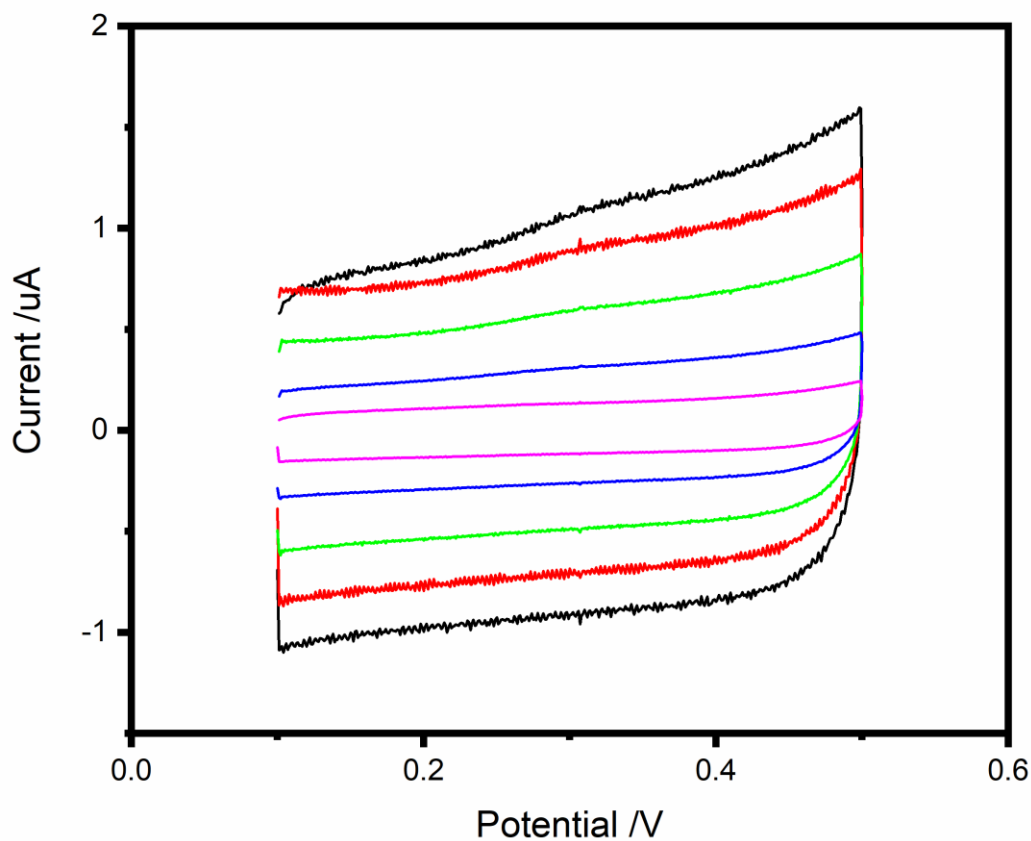


**Figure 38.** Cyclic voltammograms recorded at Dropsens Gold 220 AT SPE in PBS 0.2 M pH 7.4 at different scan rates; from the outer to the inner 200 mV/s, 150 mV/s, 100 mV/s, 50 mV/s, 20 mV/s.

The capacitive current was calculated as half the sum of the forward and the backward background current (see Figure 39 for measurement scheme), measured at 0.225 V, according to Equation 4.1.

$$I_c = \frac{i_{forward} + i_{backward}}{2} \quad (4.1)$$

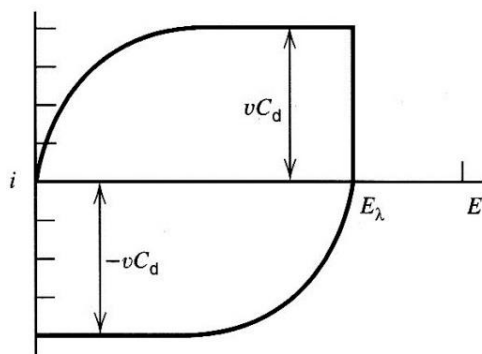


**Figure 39.** Schematic representation of the capacitive current [159].

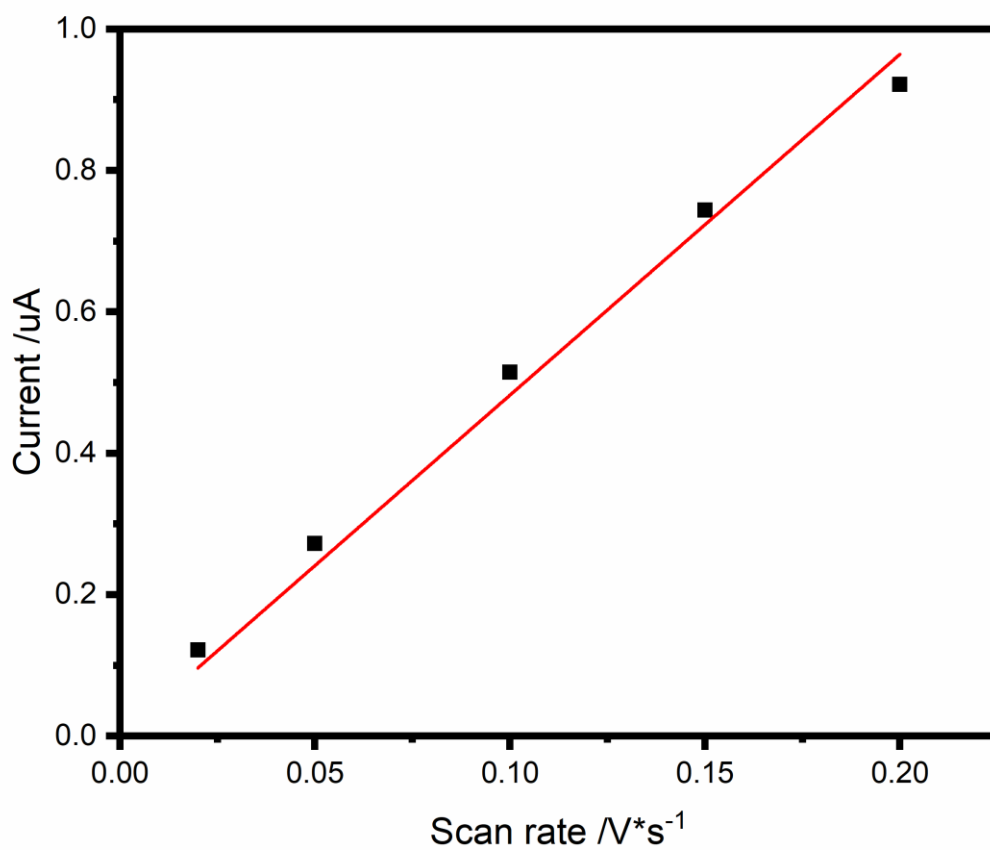


**Figure 40.** Plot of the dependence of capacitive current, measured at 0.225 V, on scan rate.

As shown in Figure 40, at SPE the capacitive current increases linearly with the scan rate. This agrees with Equation 4.2.

$$I_c = A_{act} \times v \times C_{dl} \quad (4.2)$$

where  $I_c$  is the capacitive current,  $A_{act}$  is the active area,  $v$  the scan rate and the  $C_{dl}$  the double layer capacitance which it was considered the the literature value of  $40 \mu\text{F cm}^{-2}$  for gold surfaces [158]. The value of the experimental active area can be calculated dividing the slope value by the double layer capacitance

Considering the plot in Figure 40 and the equation (4.2), the calculated experimental active area was  $1 \times 10^{-1} \text{cm}^{-2}$ .

### 3.2.2. Experimental measurement of the geometric area of DROPSSENS GOLD 220AT

The geometric area of the SPE can be calculated by analysing the scan rate dependence of the CVs recorded in the presence of redox probe.

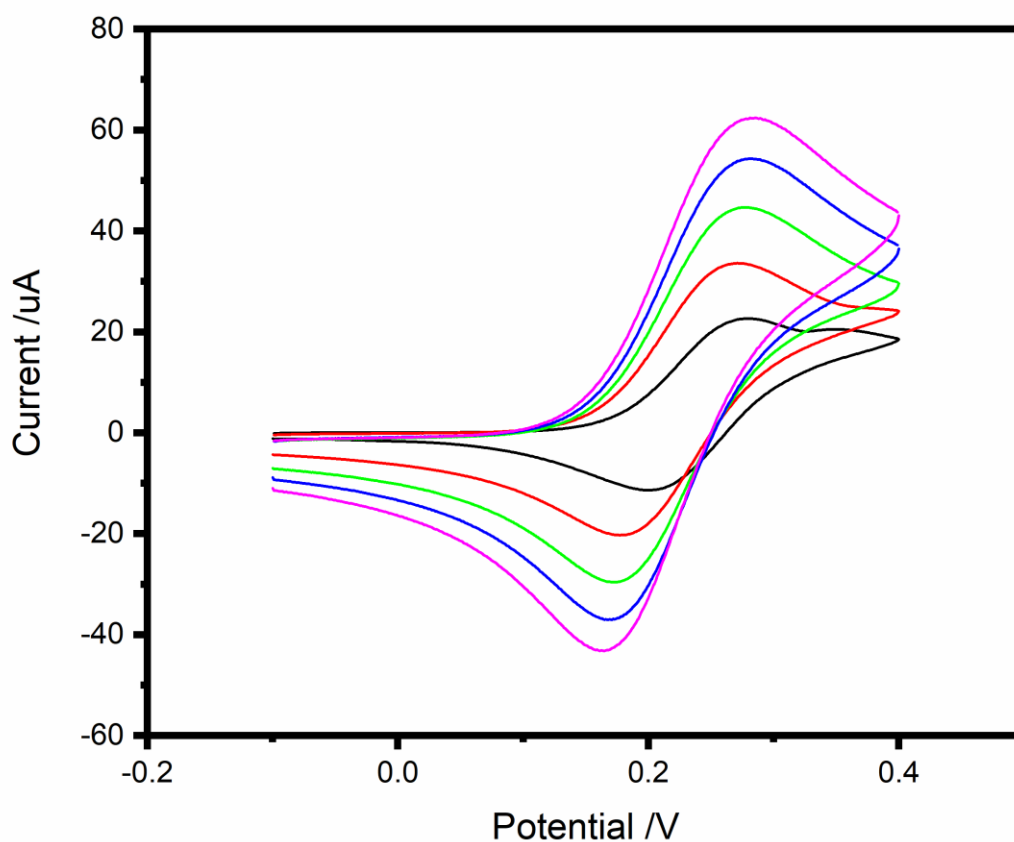


**Figure 41.** Voltammograms obtained from a solution of 2 mM ferrocene carboxylic acid (FcCOOH) in 0.2 M PBS pH 7.4 at different scan rates; from the outer to the inner 200 mV/s, 150 mV/s, 100 mV/s, 50 mV/s, 20 mV/s.

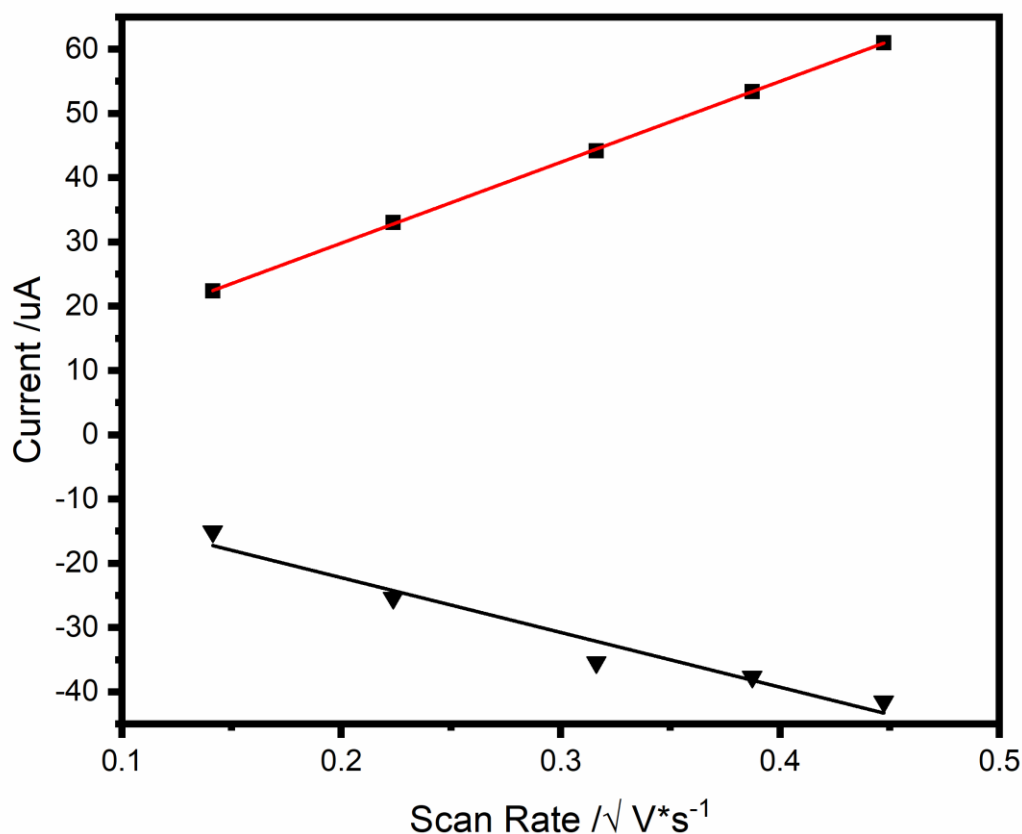


**Figure 42.** Linear correlation between the faradic current and the square root of the scan rate for Dropsens Gold 220 AT in PBS 0.2 M pH 7.4 containing 2 mM FcCOOH.

The peak shape of the CVs shows a typical reversible (Nernstian) electrochemical reaction in which the rate of reaction is governed by the diffusion of the electroactive species to the surface of a planar electrode, confirmed by the experimentally observed linear dependence on  $I_p$  vs.  $v^{1/2}$  reported in Figure 42 which showing the  $i_p$  obeys the Randles-Sevcik equation (Equation 4.3) [103]:

$$I_p = 2.69 \times 10^5 \times n^{3/2} \times D^{1/2} \times C \times v^{1/2} \times A_{geom} \quad (4.3)$$



where  $I_p$  is the faradaic peak current,  $n$  is the number of transferred electrons, that for the FcCOOH is one,  $v$  is the scan rate,  $C$  is the bulk concentration of the electroactive species (FcCOOH),  $A_{\text{geom}}$  is the geometric area and  $D$  is the diffusion coefficient of the FcCOOH that is  $4.30 \times 10^{-6} \text{ cm}^2 \text{ s}^{-1}$  [194].

The measured anodic and cathodic peak currents have been reported in Table 11 which later for the further calculation only the values of anodic peak currents were used.

Knowing the slope value from plot in Figure 42, it is possible to calculate the value of the experimental geometric area of the SPE from Equation 4.3, which the calculated  $A_{\text{geom}}$  was found  $1.04 \times 10^{-1} \text{ cm}^2$ .

**Table 11.** Faradic peak current values recorded at different scan rates at Dropsens Gold 220AT in 0.2 M PBS pH 7.4 containing 2 mM FcCOOH.

Scan rate [V/s]	I forward peak [A]	I backward peak [A]
0.02	$2.238 \times 10^{-5}$	$-1.505 \times 10^{-5}$
0.05	$3.306 \times 10^{-5}$	$-2.543 \times 10^{-5}$
0.1	$4.416 \times 10^{-5}$	$-3.540 \times 10^{-5}$
0.15	$5.340 \times 10^{-5}$	$-3.761 \times 10^{-5}$
0.2	$6.097 \times 10^{-5}$	$-4.127 \times 10^{-5}$

The electrode area calculated is reported in Table 14,

### 3.2.3 Dropsens Carbon 110AT

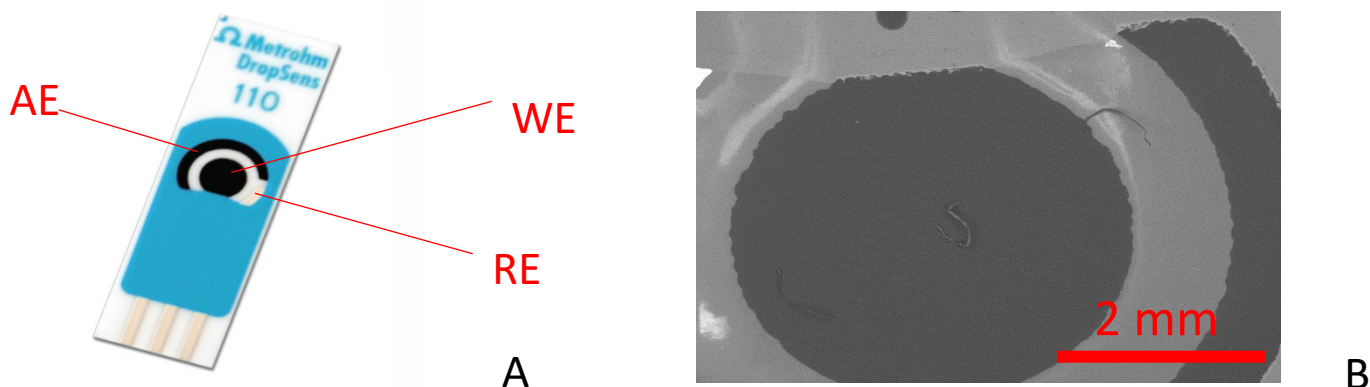


**Figure 43.** (A) Scheme representation of Dropsens Carbon 110 AT SPE (adapted from Metrohm); (B) SEM image of the WE of Dropsens Carbon 110 AT, magnification 30X, 5 kV.

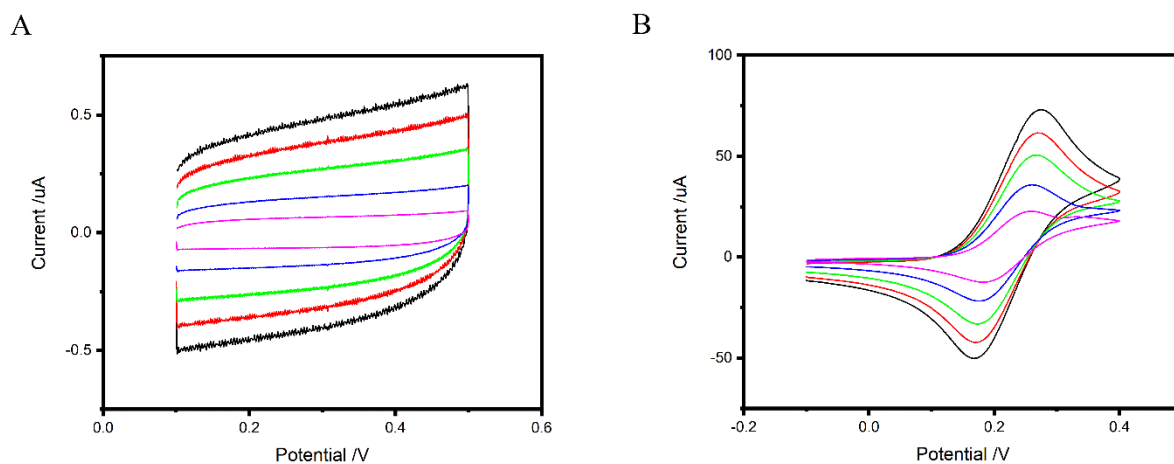


**Figure 44.** Cyclic voltammograms recorded at Dropsens Carbon 110 AT SPE. (A) CVs obtained in 0.2 M PBS pH 7.4 solution at different scan rates; from the outer to the inner 200 mV/s, 150 mV/s, 100 mV/s, 50 mV/s, 20 mV/s, (B) CVs obtained from a solution of 2 mM FcCOOH in 0.2 M PBS pH 7.4 at different scan rates; from the outer to the inner 200 mV/s, 150 mV/s, 100 mV/s, 50 mV/s, 20 mV/s.

Characterization of Dropsens Carbon 110 AT SPE was performed with the same approach described in the previous section. Figure 44 shows the voltammograms recorded at different scan rates with the

SPE Dropsens Carbon 110 AT in pure supporting electrolyte (Figure 44A) and in the presence of ferrocene carboxylic acid (Figure 44B).

Considering the plot in Figure 40 and the equation (4.2), which the  $C_{dl}$  was considered the value of  $24 \mu\text{F cm}^{-2}$  for carbon surfaces determined experimentally on SPE, the calculated experimental active area was  $0.082 \text{ cm}^2$ . The measured anodic and cathodic peak currents have been reported in Table 12 which later for the further calculation only the values of anodic peak currents were used.

Knowing the slope value from plot in Figure 45B and considering the equation (4.3), the value of the experimental geometric area of the SPE ( $A_{\text{geom}}$ ) was found  $0.089 \text{ cm}^2$ .

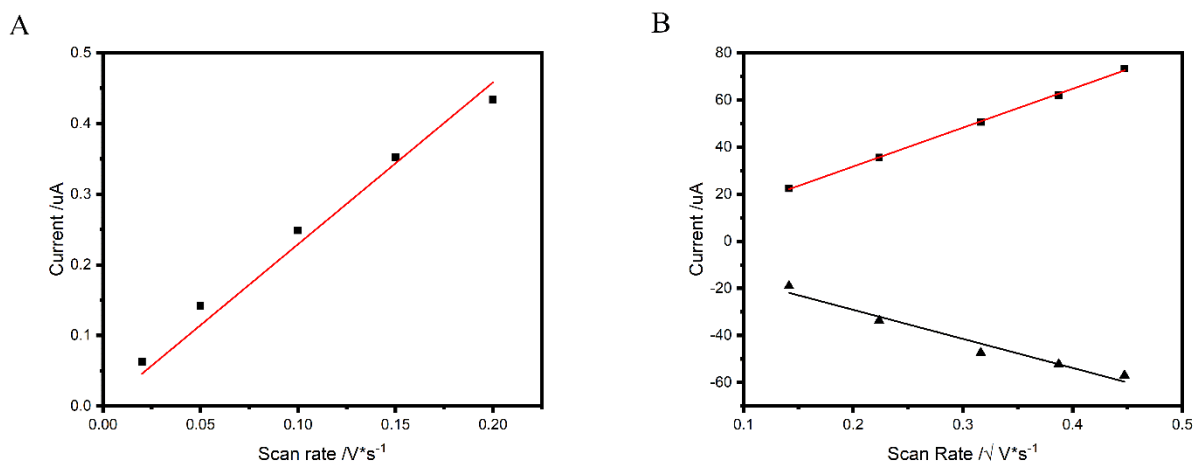


**Figure 45.** Linear correlation between scan rate and current. (A) Linear correlation between capacitive current and the scan rate for Dropsens Carbon 110 AT in 0.2 M PBS pH 7.4 as supporting electrolyte solution, (B) Linear correlation between the Faradic current and the square root of the scan rate for Dropsens Carbon 110 AT in PBS 0.2 M pH 7.4 containing 2 mM FcCOOH.

**Table 12.** Faradic peak current values recorded at different scan rates at Dropsens Carbon 110AT in 0.2 M PBS pH 7.4 containing 2 mM FcCOOH.

Scan rate [V/s]	I forward peak [A]	I backward peak [A]
0.02	$2.246 \times 10^{-5}$	$-1.887 \times 10^{-5}$
0.05	$3.561 \times 10^{-5}$	$-3.368 \times 10^{-5}$
0.1	$5.054 \times 10^{-5}$	$-4.710 \times 10^{-5}$
0.15	$6.196 \times 10^{-5}$	$-5.216 \times 10^{-5}$
0.2	$7.328 \times 10^{-5}$	$-5.689 \times 10^{-5}$

### 3.2.4. Micrux Carbon

The same characterization approach was performed for the Micrux Carbon SPE, with relevant voltammograms and data analysis being presented in Figure 47, Figure 48 and Table 13.

Calculated electrode area values were listed in Table 14, together with those for the other two kind of SPE here characterized.

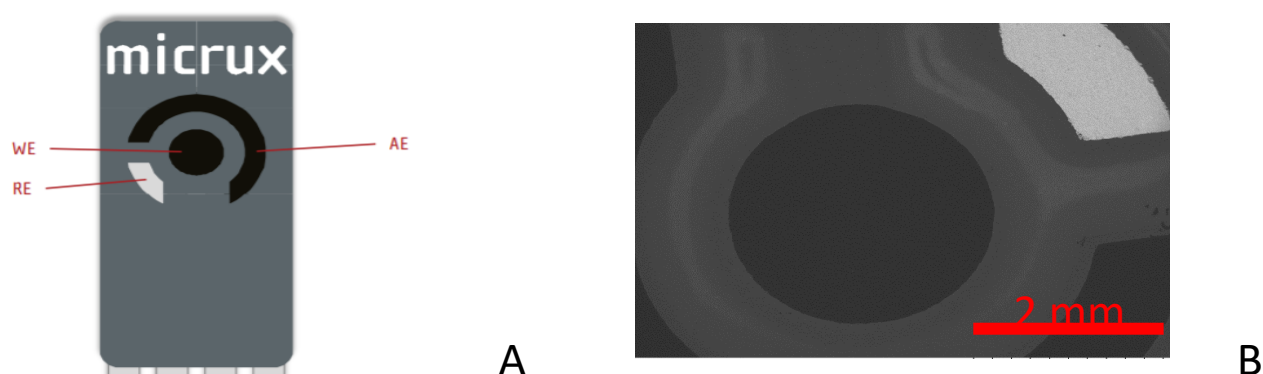


**Figure 46.**(A) schematic representation of Micrux Carbon SPE (adapted from Micrux); (B) SEM image of the WE of Micrux Carbon, magnification 30X, 5 kV

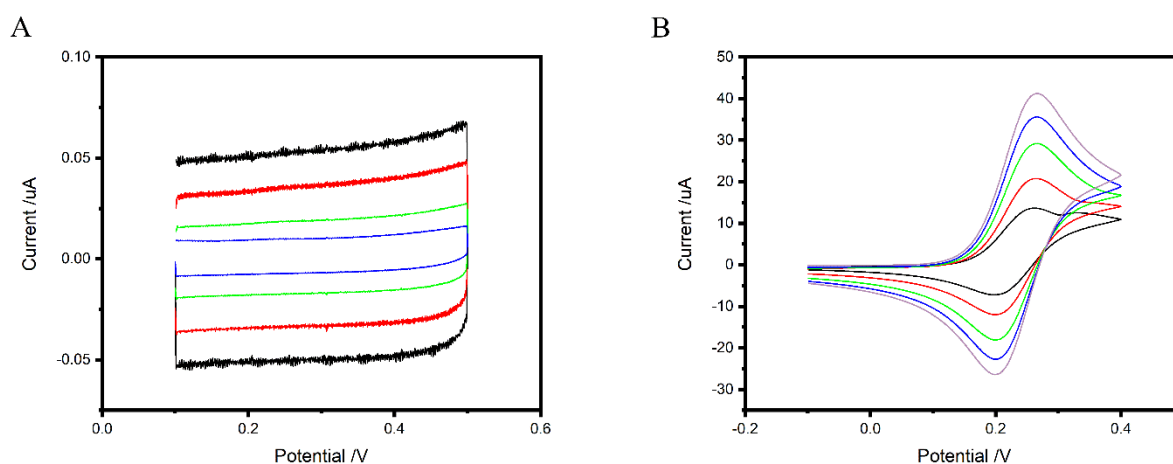


**Figure 47.** Cyclic voltammograms recorded at Micrux Carbon SPE. (A) CVs obtained in 0.2 M PBS, pH 7.4 solution at different scan rates; from the outer to the inner 200 mV/s, 150 mV/s, 100 mV/s, 50 mV/s, 20 mV/s, (B) CVs obtained from a solution of 2 mM FcCOOH in 0.2 M PBS, pH 7.4 at different scan rates; from the outer to the inner 200 mV/s, 150 mV/s, 100 mV/s, 50 mV/s, 20 mV/s.

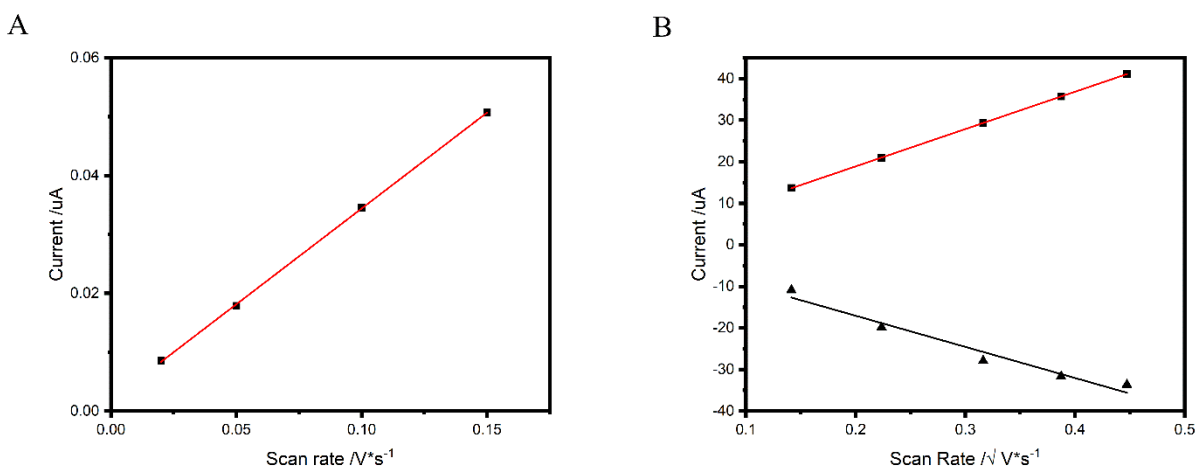


**Figure 48.** Linear correlation between scan rate and current. (A) Linear correlation between the capacitive current and the scan rate for Micrux Carbon SPE in 0.2 M PBS, pH 7.4 solution, (B) Linear correlation between the faradic current and the square root of the scan rate for Micrux Carbon SPE in PBS 0.2 M pH 7.4 containing 2 mM FcCOOH.

Considering the plot in Figure 40 and the equation (4.2), the calculated experimental active area was  $0.053 \text{ cm}^2$ . The measured anodic and cathodic peak currents have been reported in Table 13. Faradic peak current values recorded at different scan rates at Micrux Carbon in 0.2 M PBS, pH 7.4 containing 2 mM FcCOOH. which later for the further calculation only the values of anodic peak currents were used.

Knowing the slope value from plot in Figure 42 and considering the equation (4.2), the value of the experimental geometric area of the SPE ( $A_{\text{geom}}$ ) was found  $0.071 \text{ cm}^2$ .

**Table 13.** Faradic peak current values recorded at different scan rates at Micrux Carbon in 0.2 M PBS, pH 7.4 containing 2 mM FcCOOH.

Scan rate [V/s]	I forward peak [A]	I backward peak [A]
0.02	$1.368 \times 10^{-5}$	$-1.088 \times 10^{-5}$
0.05	$2.091 \times 10^{-5}$	$-1.980 \times 10^{-5}$
0.1	$2.939 \times 10^{-5}$	$-2.778 \times 10^{-5}$
0.15	$3.570 \times 10^{-5}$	$-3.151 \times 10^{-5}$
0.2	$4.102 \times 10^{-5}$	$-3.363 \times 10^{-5}$

### 3.2.5. Comparison between the different SPEs

**Table 14.** Main features derived from the electrochemical characterization of the platforms analyzed with the solution of 0.2 M PBS and the redox probe 2 mM FcCOOH

Electrode	Experimental Capacitive Area[cm <sup>2</sup> ]	Experimental Faradic Area[cm <sup>2</sup> ]	Geometric Area[cm <sup>2</sup> ]	$\Delta E_p$ (at 50 mV/s)[mV]	E <sub>1/2</sub> (at 50 mV/s)[mV]
<b>Dropsens Gold 220 AT</b>	0.100	0.104	0.126	91	225
<b>Dropsens Carbon 110 AT</b>	0.083	0.089	0.126	83	218
<b>Micrux Carbon</b>	0.053	0.071	0.071	65	233

The data obtained from the CVs recorded in the presence of the redox probe reported in Figure 38, Figure 40, Figure 41, Figure 42, Figure 44, Figure 47, Figure 48 were used to calculate the diagnostic parameters and the area values listed in Table 14.

In particular, the E<sub>1/2</sub> and  $\Delta E$  are calculated using the Equation 4.4 and Equation 4.5

$$E_{1/2} = \frac{E_{pa} + E_{pc}}{2} \quad (4.4)$$

$$\Delta E = E_{pc} - E_{pa} \quad (4.5)$$

where E<sub>pa</sub> and E<sub>pc</sub> are the potentials at the anodic and cathodic peaks, respectively. For a reversible redox system E<sub>1/2</sub> should be constant with the scan rate and  $\Delta E_p \approx \frac{0.059}{n} V$  where n is the number of transferred electrons.

Among the SPEs here examined the Micrux Carbon electrode displayed the better performances, showing a highly reversible behavior for the redox probe FcCOOH with  $\Delta E_p$  value very close to the theoretically expected 59 mV value. Moreover, the Micrux Carbon SPE showed a faradic active area which perfectly match the geometrical value.

Note that, at both kind of Dropsens SPEs, quite high  $\Delta E_p$  values were detected. This indicates that at these SPEs, the probe FcCOOH presents a quasi-reversible behavior. Therefore, for rigorous calculations, the Randles-Sevcik equation should be substituted by the following Equation 4.6:

$$I_p = (2.99 \times 10^5) n (\alpha n_\alpha)^{1/2} ACD^{1/2} v^{1/2} \quad (4.6)$$

Where,  $\alpha$  is the transfer coefficient (quantifies the difference in activation energy between the formation reaction of the products and reagents) and  $n\alpha$  is the number of electrons involved in the slower step of the charge transfer process.

However, what was relevant was to identify which SPEs presents an ideal reversible CV behavior, that, in our case, is the Micrux Carbon.

### 3.3. Development of Po-PD modified Screen Printed Electrodes (SPEs)

#### 3.3.1. Electrochemical polymerization on SPEs

The quality of the electrode surface can affect the formation of stable, homogeneous, and compact polymer films suitable to tailor functionalize their surface. In addition to the quality of the surface, the increased electroactive surface area of the SPEs appears to improve their sensor performance. To study the fabrication of an electrochemical sensor based on MIP for detection of Troponin I (TnI), the three types of SPEs, characterized in the previous section, were examined. As the preliminary tests, voltammetric electropolymerization of electroactive o-PD monomer was performed. To reduce the pre-complex solution volume a drop of 80  $\mu\text{L}$  solution was used for NIP or MIP preparation. Figure 49 shows the cyclic voltammograms recorded during the electropolymerization of o-PD on the different SPEs surfaces. The recorded multiscan voltammogram show that the oxidation of o-PD monomer is characterized in the first cycle by one main oxidation peak at about 0.4 V, followed by a second peak at 0.72 V. The anodic current decreases progressively by increasing the number of CV cycles in agreement with the deposition of an insulating coating. All these results agree with the data reported previously by Losito et al. [79, 195], confirming the successful electrodeposition of a polymeric PoPD film on the SPEs surfaces.

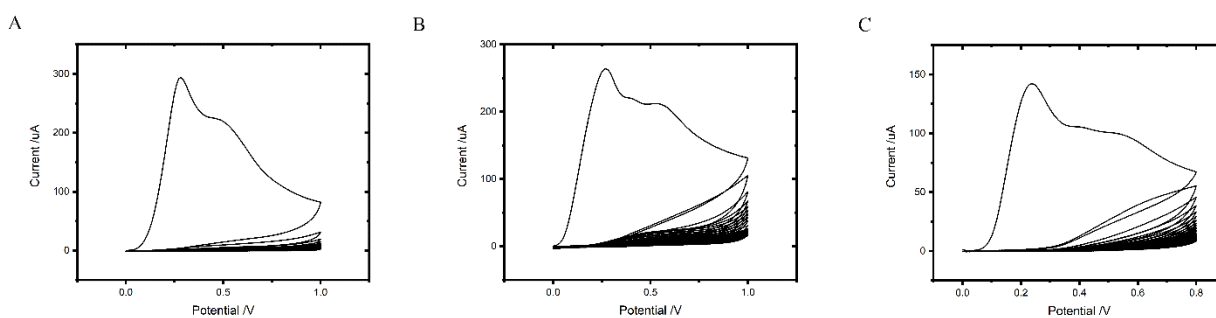


**Figure 49.** Comparison of the electropolymerization pattern of PoPD@SPE using different SPEs. (A) Dropsens Gold 220AT, (B) Dropsens Carbon 110AT, (C) Micrux Carbon. Electrodeposition was performed through the cyclic voltammetry on SPEs in a solution of acetate buffer (pH 5.2), containing 10 mM o-PD, scan rate  $50 \text{ mV s}^{-1}$ ; number of scans 25.



### 3.3.2. Electrochemical characterization of PoPD@SPE

Ferrocene carboxylic acid (FcCOOH) was used as the electroactive redox probe for monitoring and electrochemical characterization of prepared PoPD film@SPE, using the differential pulse voltammetry (DPV) technique. Figure 50 report the DPVs recorded before and after electropolymerization of PoPD at the surface of three different SPEs. putting in evidence some differences, in particular as far as the suppression the mediators signal is concerned.

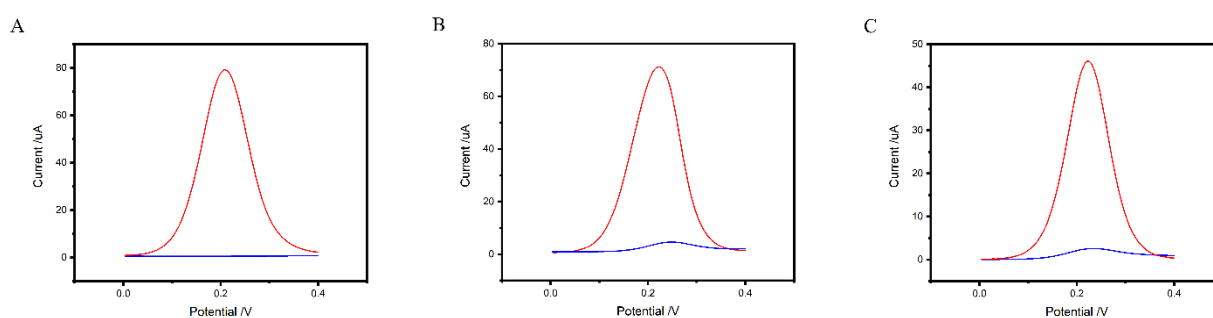


**Figure 50.** Differential pulse voltammograms obtained at SPEs before (red line) and after electrodeposition of PoPD (blue line). (A) Dropsens Gold 220 AT, (B) Dropsens Carbon 110AT, (C) Micrux Carbon. The monitoring was performed in solution 0.2 M PBS, pH 7.4 containing 2 mM FcCOOH.

In these series of measurements, the DPV signal for 2 mM FcCOOH was recorded, before and after the polymerization of o-PD. The parameters used to evaluate the performances of the SPE also with respect to polymerization were:

- i) Peak potential and peak currents before and after polymerization;
- ii) Percent decrease in peak current after the polymerization;
- iii) peak width at half peak height ( $W_{1/2}$ ), before polymerization.

Note that:

$$\text{a) in DPV, } E_p = E_{1/2} - \frac{\Delta E_{pulse}}{2} \quad (4.7)$$

where  $\Delta E_{pulse}$  is the pulse width;

b) parameter iii) is again indicative of the degree of reversibility of the probe redox process, since, theoretically

$$W_{\frac{1}{2}} = \frac{3.52RT}{nF} \quad (4.8)$$

That is about 90mV at 298°K and for  $n = 1$

The obtained results are summarized in Table 15. Analysis of these results indicate that the bare Micrux carbon shows again the most reversible behaviour for the redox probe FcCOOH. All the three SPEs studied showed a significant decrease of the electrochemical signal of the probe after the electropolymerization of PoPD film, from 96 % to 100 %. These results demonstrated that the o-PD is a suitable monomer for the application to create the modified MIP-coated electrodes with the commercially SPEs tested with the Dropsens Gold 220 AT electrode emerging for coverage efficiency (100%) and the Micrux Carbon SPE prevailing for reversible behavior and signal resolution. Moreover, it is worth to stress that carbon electrodes offer a wider accessible potential window than gold electrodes.

**Table 15.** DPV parameters obtained from the analysis of data in Figure 50.

<b>Electrode</b>	<b>I peak before polymerization [A]</b>	<b>Ep [V]</b>	<b>Ep<sub>1/2</sub> [V]</b>	<b>I peak after polymerization [A]</b>	<b>Ep [V]</b>	<b>Ep<sub>1/2</sub> [V]</b>	<b>Signal decrease [%]</b>
<b>Dropsens Gold</b>	$7.766 \times 10^{-5}$	0.208	0.115	//	//	//	100
<b>Dropsens Carbon</b>	$7.002 \times 10^{-5}$	0.224	0.115	$3.014 \times 10^{-6}$	0.248	0.198	96
<b>Micrux Carbon</b>	$4.593 \times 10^{-5}$	0.224	0.100	$2.026 \times 10^{-6}$	0.232	0.182	96

### **3.4. Preparation of Poly o-PD Coatings in the presence of Troponin I on SPE**

#### **Micrux Carbon: Formation of TnI-MIP-SPE**

The preparation of an electrochemical sensor based on MIP for TnI detection was preliminarily investigated using Micrux Carbon SPEs. Attempts to electropolymerize MIPs were performed using different types of electroactive monomers including pyrrole, scopoletin and o-phenylenediamine (o-PD). Based on the results, it was concluded that the optimum monomer was o-PD which is easily electropolymerized on various substrate materials and forms thin films with good chemical and mechanical stability. Furthermore, the presence of neutral or protonated  $-NH_2$  groups may be responsible for interactions with biomolecules such as TnI. To prepare the MIP modified electrodes, a TnI sensitive layer was prepared by electropolymerization of o-PD via cyclic voltammetry technique in the presence of 20 nM TnI on a cleaned gold electrode. Preparing the NIP modified electrodes, no significant difference was observed between cyclic voltammograms recorded in the absence of template which means that the template was electrochemically stable over the scanned potential window and only the monomer underwent electropolymerization. To activate the molecularly imprinted sites in the polymer, the template molecules were removed from the modified electrode surface by washing with different solvent extraction, pure and mixed solvents, such as alkaline solution, acidic solution, alkaline ethanol, acidic methanol, ethanol, methanol, sodium dodecyl sulphate (SDS) and proteinase K.

The MIP electropolymerization was performed in 50  $\mu$ L drop of pre-complex solution by cyclic voltammetry, scanning 25 consecutive cycles on the carbon substrate of SPE. The polymer-encased TnI molecules were then removed from the polymer by a washing step in 0.1 M  $H_2SO_4$ , leaving open cavities containing binding sites suitable to interact again with TnI. The oxidation current of the FcCOOH redox probe was measured on the MIP-SPE using DPV. Indeed, to investigate the capability of the MIP coated SPE to capture TnI, the imprinted SPE was wetted with different 50  $\mu$ L drops of 1 mM FcCOOH (in PBS, pH 7.4) containing increasing concentrations of TnI. The concentration of TnI here examined ranged from 1 pg/mL to 21.8 ng/mL and DPV patterns were recorded after an optimized re-loading time of 10 min.

Data in Figure 49 A show that the DPV peak current decreased with increasing TnI concentration, so indicating the operativity of an efficient competition between non electroactive TnI and the redox probe for the MIP cavities. Figure 49 B report the relevant partition isotherm, which is characterized by an initial linear trend, with very high sensitivity, which tend to flatten at increasing concentrations, probably because of progressive saturation of the TnI specific capture sites present on the MIP.

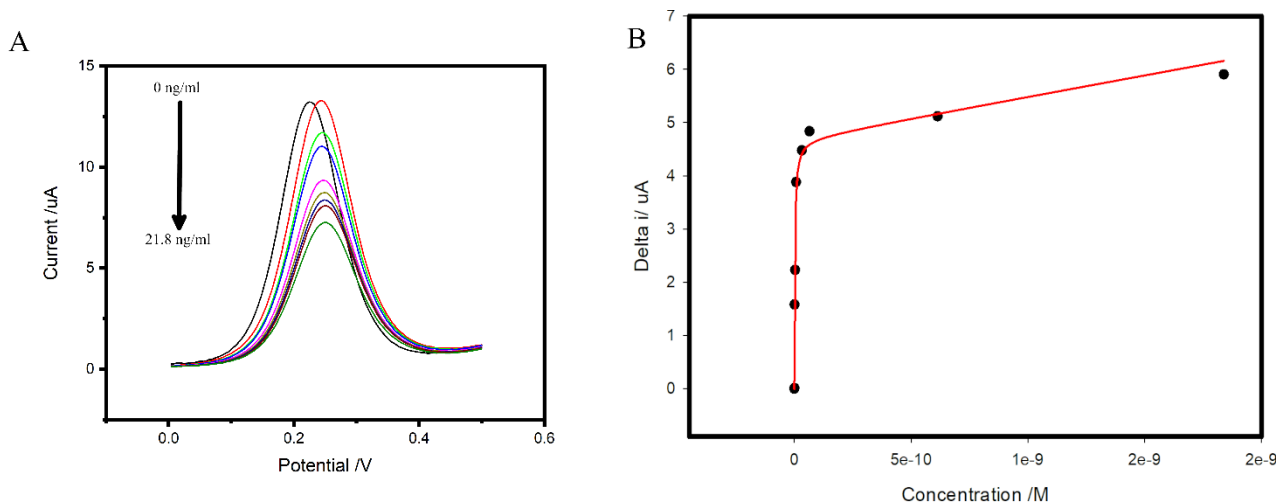


**Figure 51.** (A) DPVs at the MIP electrode after incubation in 1 mM FcCOOH (pH 7.4) containing different TnI concentrations for 5 min. The corresponding curves for TnI addition including: Red curve:  $i_0$ ; green curve: 0.001 ng/mL; blue curve : 0.009 ng/mL; brown curve : 0.04 ng/mL; dark green : 0.09 ng/mL; purple : 0.4 ng/mL; fluo green : 0.6 ng/mL; dark yellow : 7.4 ng/mL; light purple : 21.8 ng/mL, (B) binding isotherm of the MIP electrode at different concentrations of TnI.

Further optimization of the preparation of the sensor, because of the high cost of TnI, was performed by preparing the MIP-SPE sensor by using a potential analogue of the target analyte. After literature research, the *Cyt c* was chosen as the best candidate for similar features with TnI. Thus, we used the *Cyt c* such as dummy template to study the MIP preparation for detection of TnI.

### 3.5. Fabrication of electrochemically sensor based on dummy molecularly imprinted polymers using Cytochrome *c* as a template molecule for TnI detection

Molecular imprinting polymers tailors to an analyte (template) molecule added in the polymerization mixture. From a practical point of view, these protocols often suffer from certain limitations. These may be the poor solubility of the analyte (template) in the imprinting mixture, or the limited availability of the template, of which a considerable amount is needed in order to prepare the MIP in the first place [196]. An innovative strategy to avoid these problems would be replacing the template molecule with a stable, chemically inert, nontoxic, and non-infectious synthetic surrogate, which emulates the size, shape, and surface functionality of the analyte.

In this work, as dummy substitute for TnI we have chosen cytochrome *c* (*Cyt c*) because of its similarity in molecular weight and isoelectric point with TnI. MIP modified electrodes were produced

by replacing the original template (TnI) entirely by cytochrome *c*, used as a dummy template during the MIP synthesis.

The fabrication of the MIP film was achieved by the anodic deposition of o-PD in the presence of *Cyt c* on a cleaned gold substrate as described in chapter 3. After electropolymerization of oPD, the *Cyt c* template was removed by washing with diluted acid (0.1 M H<sub>2</sub>SO<sub>4</sub>). Electrochemical methods were used to monitor the electropolymerization, template removal and TnI binding. To verify the capability of the prepared dummy-MIP sensor to detect the TnI, the MIP-modified electrode was incubated in a solution containing different concentrations of TnI using FcCOOH as competitive redox probe. The DPV patterns reported in Figure 52 show the progressive decrease of the peak current with increasing TnI concentration, from 1 pg/mL to 7.4 ng/mL. These results demonstrate that the signal of the redox probe FcCOOH decreases while increasing TnI concentrations showing the capability to detect TnI concentrations as low as few pg/mL.

This is quite an interesting and promising result, although preliminary, considering that the active sites in the MIP layer were generated using *Cyt c* (and not TnI) as dummy template,

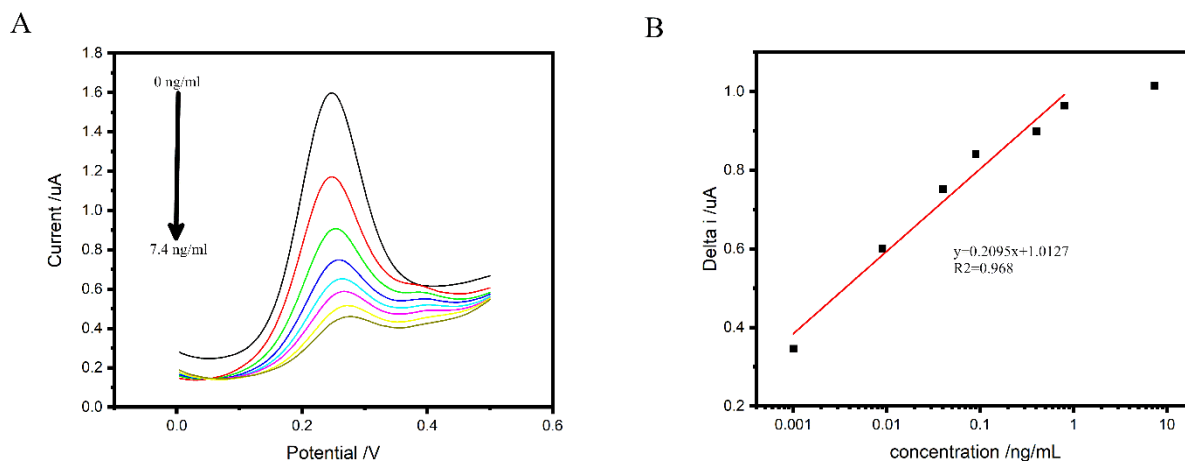


**Figure 52.** TnI binding to dummy template MIP. (A) DPVs at the MIP electrode after incubation in 1 mM FcCOOH in PBS 1X (pH 7.4) containing different TnI concentration. From higher to lower, addition of TnI including: 0 ng/ml, 0.001 ng/ml, 0.009 ng/ml, 0.04 ng/ml, 0.09 ng/ml, 0.4 ng/ml, 0.8 ng/ml, 7.4 ng/ml, respectively. (B) Dependence of the delta peak current on the logarithm of the TnI concentration.

## 4. Conclusions

Here we have reported two proof-of-concept sensors suitable for TnI detection at extremely low concentration levels. Both the prepared sensors have been developed using a MIP film as biorecognition element but using two different kinds of electrochemical platform: SPE and disk gold electrode.

The sensor on SPE showed a signal response in range between 1 ng/L and 21.8 µg/L, demonstrating analytical performances suitable for its potential application as a highly sensitive Troponin I sensor.

Despite this promising achievement, this study is still at a preliminary level. Indeed, further focused studies will be necessary to verify if the sensor can really meet the guidelines accepted by the clinical community (99<sup>th</sup> percentile). Hopefully, the clinical potential of this sensor will be explored in the next future.

Another interesting achievement is the very good TnI detection capability of the MIP sensor prepared using *Cyt c* as dummy template. This second proof-of-concept sensor is characterized by a range of detection between 1 ng/L and 7.4 µg/L, indicating interesting potentialities as a highly sensitive Troponin I sensor, with a much lower preparation cost than the previous one.

Despite this achievement, the obtained results for both the sensors were obtained in synthetic conditions in which the analyte was the only molecule in the medium. Measurements in real samples needs to be performed in order to confirm the analytical performances, to be followed by in-depth clinical studies.

## 5. General Conclusions

Studying the GC-NEA platform, the nanostructured geometry of the surface electrode arised as pivotal in obtaining high quality voltammetric signals, with high S/N ratios. These features, granted by the design, combine positively with the wide potential window accessible with glassy carbon electrodes. Taking in account these two great advantages, GC-NEAs show high potentialities as new generation and efficient bioelectrochemical platforms for the detction of a plethora of analytical targets.

Furthermore, the NEA could be ameliorated by incorporating the reference electrode and the counter electrode onto the platform to conjugate the features above mentioned with the possibility of get an entire electrochemical miniaturized system capable for high sensitivity detection and working with very small volumes of solutions. Small volumes are relevant in bioanalytical analysis for the following reasons: use of one sampling protocol for performing multiple analysis; use of minimal volumes in the case of precious samples; reduce the wastes to be treated.

Considering the second part of this thesis devoted to development of MIP sensor for *Cyt c* detection, it has been reported the successful preparation of a MIP sensor suitable for the detection of cytochrome *c* at trace concentration levels in serum samples. Furthermore, the results achieved highlighted the possibility to use the MIP technology as a potential substitute of the classical antibody-antigen technology used in affinity biosensors. Moreover, MIP sensor could spread the easy and cheap development of biosensing platforms towards non-protein analytes.

The LOD achieved ( $1.4 \times 10^{-15}$  M) could lead the possibility to define the *Cyt c* as a clinical biomarker.

The lack of a clear basal concentration levels of cytochrome *c* in serum could be overcome using this highly sensitive sensor. In particular one of the drawbacks of the *Cyt c* as a clinical biomarker is the discrimination of *Cyt c* levels in serum from not-injury events to apoptotic related events. For this potentially pivotal role, this sensor should be taken in account for a study in clinical conditions in comparison to up-to-date similar sensor, even if no one has been used beyond non-clinical studies.

Finally, the last part of this thesis explored the possible application of the MIP technology to the detection of cardiac biomarker Troponin I, with scaling up the proof-of-concept of a MIP-based Screen Printed Electrodes. The SPEs are low cost and deployable electrochemical sensors easily made by printing with conductive inks. The work on Troponin I revealed the potentiality of these platforms to perform the sensitive analysis of disease biomarkers, like Troponin I, obtaining interesting preliminary results which, in the future, could even evolve into new devices to be applied for Point-of-Care analyses.

The majority of the commercially available sensors used currently in clinical assessment of AMI are working in the class of normal TnI range(ng/mL). In the recent years the clinical community opinion is focused on the new class of troponin I sensors, classified as high sensitivity Troponin I detection sensors(ng/L). This new class shifts the concept of clinical cut-off of AMI, leading to a new model of patient stratification. Within this framework, the sensor developed could be possibly used as a new emerging technology able to substantiate this new clinical concept.



## References

- [1] B. Sellergren, in *Molecularly imprinted polymers: man-made mimics of antibodies and their applications in analytical chemistry*, in: *Tech. Instrum. Anal. Chem.*, Elsevier, Amsterdam, 2001.
- [2] K.M. D. Kriz, O. Ramström, *Analytical Chemistry*, *Anal. Chem.* 69 (1997) 345A-349A.
- [3] P. Ugo, P. Marafini, M. Meneghello, *Bioanalytical chemistry-from biomolecular recognition to nanobiosensing*, De Gruyter, Berlin, 2021.
- [4] D.R. Thvenot, K. Toth, R.A. Durst, G.S. Wilson, *Electrochemical biosensors: Recommended definitions and classification (Technical Report)*, *Pure Appl. Chem.* 71 (1999) 2333–2348. <https://doi.org/10.1351/pac199971122333>.
- [5] J.P. Chambers, B.P. Arulanandam, L.L. Matta, A. Weiss, J.J. Valdes, *Biosensor recognition elements*, *Curr. Issues Mol. Biol.* 10 (2008) 1–12.
- [6] A.C. Laboratories, N. Carolina, C. Hill, *INTERNATIONAL UNION OF PURE AND APPLIED CHEMISTRY ANALYTICAL CHEMISTRY DIVISION COMMISSION ON ELECTROANALYTICAL CHEMISTRY \* CHEMICALLY MODIFIED ELECTRODES : Chemically modified electrodes : terminology and definitions ( IUPAC Recommendations 1997 ) recomm*, 69 (1997) 1317–1323.
- [7] I. Union, A. Chemistry, *Analytical aspects of chemically modified electrodes: Classification, critical evaluation and recommendations (IUPAC Recommendations 1998)*, *Pure Appl. Chem.* 70 (1998) 1301–1318. <https://doi.org/10.1351/pac199870061301>.
- [8] N. Karimian, L.M. Moretto, P. Ugo, *Nanobiosensing with Arrays and Ensembles of Nanoelectrodes*, (2017). <https://doi.org/10.3390/s17010065>.
- [9] M. Ongaro, P. Ugo, *Bioelectroanalysis with nanoelectrode ensembles and arrays*, *Anal. Bioanal. Chem.* 405 (2013) 3715–3729.
- [10] M. De Leo, A. Kuhn, *3D-Ensembles of Gold Nanowires : Preparation , Characterization and Electroanalytical Peculiarities*, (2007) 227–236. <https://doi.org/10.1002/elan.200603724>.
- [11] S.P. Mucelli, M. Zamuner, M. Tormen, G. Stanta, P. Ugo, *Biosensors and Bioelectronics Nanoelectrode ensembles as recognition platform for electrochemical immunosensors*, 23 (2008) 1900–1903. <https://doi.org/10.1016/j.bios.2008.02.027>.
- [12] M. Silvestrini, P. Schiavuta, P. Scopece, G. Pecchiolan, L.M. Moretto, P. Ugo, *Electrochimica Acta Modification of nanoelectrode ensembles by thiols and disulfides to prevent non specific adsorption of proteins*, 56 (2011) 7718–7724. <https://doi.org/10.1016/j.electacta.2011.06.034>.
- [13] D.W.M. Arrigan, *Nanoelectrodes, nanoelectrode arrays and their applications*, *Analyst.* 129 (2004) 1157–1165. <https://doi.org/10.1039/b415395m>.

- [14] R.M. Penner, M.J. Heben, T.L. Longin, N.S. Lewis, R.M. Penner, M.J. Heben, T.L. Longin, N.S. Lewis, *Fabrication and Use of Nanometer-Sized Electrodes in Electrochemistry*, 250 (1990) 1118–1121.
- [15] D.T. Mitchell, C.R. Martin, *Template-Synthesized Nanomaterials in Electrochemistry*, in: A.J. Bard, I. Rubinstein (Eds.), *Electroanal. Chem.*, Marcel Dekker, New York, NY, 1999: pp. 1–74.
- [16] P. Ugo, L.M. Moretto, F. Vezzà, Ionomer-coated electrodes and nanoelectrode ensembles as electrochemical environmental sensors: Recent advances and prospects, *ChemPhysChem*. 3 (2002) 917–925. [https://doi.org/10.1002/1439-7641\(20021115\)3:11<917::AID-CPHC917>3.0.CO;2-U](https://doi.org/10.1002/1439-7641(20021115)3:11<917::AID-CPHC917>3.0.CO;2-U).
- [17] A. Errachid, C.A. Mills, M. Pla-roca, M.J. Lopez, G. Villanueva, Focused ion beam production of nanoelectrode arrays, 28 (2008) 777–780. <https://doi.org/10.1016/j.msec.2007.10.077>.
- [18] M.E. Sandison, J.M. Cooper, Nanofabrication of electrode arrays by electron-beam and nanoimprint lithographies, (2006) 1020–1025. <https://doi.org/10.1039/b516598a>.
- [19] N.S. Losilia, J. Martinez, R. Garcia, Large area nanoscale patterning of silicon surfaces by parallel local oxidation, *Nanotechnology*. 20 (2009) 475304–475308.
- [20] N.S. Losilia, N.S. Oxtoby, J. Martinez, F. Garcia, R. Garcia, M. Mas-Torrent, J. Vecciana, C. Rovia, Sub-50 nm positioning of organic compounds onto silicon oxide patterns fabricated by local oxidation nanolithography, *Nanotechnology*. 19 (2008) 455308–455313.
- [21] N. Godino, X. Borriase, F.X. Mun, F. Javier, R.G. Compton, *Mass Transport to Nanoelectrode Arrays and Limitations of the Diffusion Domain Approach : Theory and Experiment*, (2009) 11119–11125.
- [22] N. Karimian, P. Ugo, Recent advances in sensing and biosensing with arrays of nanoelectrodes, *Curr. Opin. Electrochem.* 16 (2019) 106–116. <https://doi.org/10.1016/j.coelec.2019.04.026>.
- [23] V.P. Menon, C.R. Martin, Fabrication and Evaluation of Nanoelectrode Ensembles, *Anal. Chem.* 67 (1995) 1920–1928. <https://doi.org/10.1021/ac00109a003>.
- [24] P. Ugo, L.M. Moretto, S. Bellomi, V.P. Menon, C.R. Martin, Ion-Exchange Voltammetry at Polymer Film-Coated Nanoelectrode Ensembles, *Anal. Chem.* 68 (1996) 4160–4165. <https://doi.org/10.1021/ac960580b>.
- [25] C. Amatore, J.M. Savéant, D. Tessier, Charge transfer at partially blocked surfaces. A model for the case of microscopic active and inactive sites, *J. Electroanal. Chem.* 147 (1983) 39–51. [https://doi.org/10.1016/S0022-0728\(83\)80055-2](https://doi.org/10.1016/S0022-0728(83)80055-2).
- [26] Hye Jin Lee, C. Beriet, R. Ferrigno, H.H. Girault, Cyclic voltammetry at a regular microdisc electrode array, *J. Electroanal. Chem.* 502 (2001) 138–145. [https://doi.org/10.1016/S0022-0728\(01\)00343-6](https://doi.org/10.1016/S0022-0728(01)00343-6).

- [27] J.C. Hulteen, V.P. Menon, C.R. Martin, Template preparation of nanoelectrode ensembles: Achieving the “pure-radial” electrochemical-response limiting case, *J. Chem. Soc. - Faraday Trans.* 92 (1996) 4029–4032. <https://doi.org/10.1039/FT9969204029>.
- [28] P. Ugo, L.M. Moretto, M. De Leo, A.P. Doherty, C. Vallese, S. Pentlavalli, Diffusion regimes at nanoelectrode ensembles in different ionic liquids, *Electrochimica Acta.* 55 (2010) 2865–2872. <https://doi.org/10.1016/j.electacta.2009.12.059>.
- [29] I.F. Cheng, L.D. Whiteley, C.R. Martin, Ultramicroelectrode Ensembles. Comparison of Experimental and Theoretical Responses and Evaluation of Electroanalytical Detection Limits, *Anal. Chem.* 61 (1989) 762–766. <https://doi.org/10.1021/ac00182a024>.
- [30] E. Sabatani, I. Rubinstein, Organized self-assembling monolayers on electrodes. 2. Monolayer-based ultramicroelectrodes for the study of very rapid electrode kinetics, *J. Phys. Chem.* 91 (1987) 6663–6669. <https://doi.org/10.1021/j100311a021>.
- [31] N. Leibl, K. Haupt, C. Gonzato, L. Duma, Molecularly imprinted polymers for chemical sensing: A tutorial review, *Chemosensors.* 9 (2021) 1–19. <https://doi.org/10.3390/chemosensors9060123>.
- [32] K. Haupt, Molecularly Imprinted Polymers: The Next Generation, *Anal. Chem.* 75 (2003) 376 A-383 A.
- [33] T. Trends, A. Chemistry, A. Merko, New materials for electrochemical sensing IV . Molecular imprinted polymers New materials for electrochemical sensing IV . Molecular imprinted polymers, 9936 (2016) 717–725.
- [34] O. Hayden, P.A. Lieberzeit, D. Blaas, F.L. Dickert, Artificial antibodies for bioanalyte detection - Sensing viruses and proteins, *Adv. Funct. Mater.* 16 (2006) 1269–1278. <https://doi.org/10.1002/adfm.200500626>.
- [35] G. Wulff, Molecular Imprinting in Cross-Linked Materials with the Aid of Molecular Templates— A Way towards Artificial Antibodies, *Angew. Chem. Int. Ed. Engl.* 34 (1995) 1812–1832. <https://doi.org/10.1002/anie.199518121>.
- [36] K. Haupt, K. Mosbach, Molecularly Imprinted Polymers and Their Use in Biomimetic Sensors, *Chem. Rev.* 100 (2000) 2495–2504.
- [37] A.G. Mayes, K. Mosbach, Molecularly imprinted polymers: useful materials for analytical chemistry?, *Trends Anal.* 16 (1997) 321.b.
- [38] C. Malitesta, I. Losito, P.G. Zambonin, Molecularly Imprinted Electrosynthesized Polymers: New Materials for Biomimetic Sensors, *Anal. Chem.* 71 (1999) 1366–1370.

- [39] Y. Fuchs, O. Soppera, K. Haupt, Photopolymerization and photostructuring of molecularly imprinted polymers for sensor applications-A review, *Anal. Chim. Acta.* 717 (2012) 7–20. <https://doi.org/10.1016/j.aca.2011.12.026>.
- [40] L. Chen, X. Wang, W. Lu, X. Wu, J. Li, Molecular imprinting: Perspectives and applications, *Chem. Soc. Rev.* 45 (2016) 2137–2211. <https://doi.org/10.1039/c6cs00061d>.
- [41] C. Alexander, H.S. Andersson, L.I. Andersson, R.J. Ansell, N. Kirsch, I.A. Nicholls, J. O'Mahony, M.J. Whitcombe, Molecular imprinting science and technology: A survey of the literature for the years up to and including 2003, *J. Mol. Recognit.* 19 (2006) 106–180. <https://doi.org/10.1002/jmr.760>.
- [42] T.S. Bedwell, M.J. Whitcombe, Analytical applications of MIPs in diagnostic assays : future perspectives, (2016) 1735–1751. <https://doi.org/10.1007/s00216-015-9137-9>.
- [43] S. Lingxin, As featured in: Molecular imprinting : perspectives and applications, (2016). <https://doi.org/10.1039/c6cs00061d>.
- [44] B. Bräuer, C. Unger, M. Werner, P.A. Lieberzeit, Biomimetic Sensors to Detect Bioanalytes in Real-Life Samples Using Molecularly Imprinted Polymers : A Review, (2021).
- [45] C. Branger, W. Meouche, A. Margailan, Reactive & Functional Polymers Recent advances on ion-imprinted polymers, *React. Funct. Polym.* 73 (2013) 859–875. <https://doi.org/10.1016/j.reactfunctpolym.2013.03.021>.
- [46] G. Theodoridis, P. Manesiotis, Selective solid-phase extraction sorbent for caffeine made by molecular imprinting, *J Chromatogr A.* 948 (2002) 163–169.
- [47] B.T.S. Bui, F. Merlier, K. Haupt, Toward the Use of a Molecularly Imprinted Polymer in Doping Analysis: Selective Preconcentration and Analysis of Testosterone and Epitestosterone in Human Urine, *Anal. Chem.* 82 (2010) 4420–4427.
- [48] L.I. Andersson, R. Müller, G. Vlatakis, K. Mosbach, Mimics of the binding sites of opioid receptors obtained by molecular imprinting of enkephalin and morphine, *Proc Natl Acad Sci USA.* 92 (1995) 4788.
- [49] E. Rosellini, N. Barbani, P. Giusti, G. Ciardelli, C. Cristallini, Novel bioactive scaffolds with fibronectin recognition nanosites based on molecular imprinting technology, *J Appl Polym Sci.* 118 (2010) 3236.
- [50] A. Cutivet, C. Schembri, J. Kovensky, K. Haupt, Molecularly Imprinted Microgels as Enzyme Inhibitors, (2009) 14699–14702.
- [51] N. Karimian, M. Vagin, M.H. Arbab Zavar, M. Chamsaz, A.P.F. Turner, A. Tiwari, An ultrasensitive molecularly-imprinted human cardiac troponin sensor, *Biosens. Bioelectron.* 50 (2013) 492–498.

- [52] A. Mujahid, S. Aigner, F.L. Dickert, *Sensors and Actuators B: Chemical Micro-structured interdigital capacitors with synthetic antibody receptors for ABO blood-group typing*, *Sens. Actuators B Chem.* 242 (2017) 378–383. <https://doi.org/10.1016/j.snb.2016.11.056>.
- [53] D. Refaat, M.G. Aggour, A.A. Farghali, R. Mahajan, J.G. Wiklander, I.A. Nicholls, S.A. Piletsky, *Strategies for Molecular Imprinting and the Evolution of MIP Nanoparticles as Plastic Antibodies — Synthesis and Applications*, *Int J Mol Sci.* 20 (2019) 6304.
- [54] E. Mazzotta, T. Di, G. Cosimino, *Electrochemical sensing of macromolecules based on molecularly imprinted polymers: challenges, successful strategies, and opportunities*, Springer Berlin Heidelberg, 2022.
- [55] J. Wackerlig, R. Schirhagl, *Applications of Molecularly Imprinted Polymer Nanoparticles and Their Advances toward Industrial Use: A Review*, *Anal. Chem.* 88 (2016) 250–261. <https://doi.org/10.1021/acs.analchem.5b03804>.
- [56] Y. Li, H.H. Yang, Q.H. You, Z.X. Zhuang, X.R. Wang, *Protein recognition via surface molecularly imprinted polymer nanowires*, *Anal. Chem.* 78 (2006) 317–320. <https://doi.org/10.1021/ac050802i>.
- [57] H. Nishino, C.S. Huang, K.J. Shea, *Selective protein capture by epitope imprinting*, *Angew. Chem. - Int. Ed.* 45 (2006) 2392–2396. <https://doi.org/10.1002/anie.200503760>.
- [58] I. Perçin, N. Idil, M. Bakhshpour, E. Yılmaz, B. Mattiasson, A. Denizli, *Microcontact imprinted plasmonic nanosensors: Powerful tools in the detection of salmonella paratyphi*, *Sens. Switz.* 17 (2017). <https://doi.org/10.3390/s17061375>.
- [59] A.D. Batista, W.R. Silva, B. Mizaikoff, *Molecularly imprinted materials for biomedical sensing*, *Med. Devices Sens.* 4 (2021) 1–17. <https://doi.org/10.1002/mds3.10166>.
- [60] L. Wan, Z. Chen, C. Huang, X. Shen, *Core-shell molecularly imprinted particles*, *TrAC - Trends Anal. Chem.* 95 (2017) 110–121. <https://doi.org/10.1016/j.trac.2017.08.010>.
- [61] C. Unger, P.A. Lieberzeit, *Molecularly imprinted thin film surfaces in sensing: Chances and challenges*, *React. Funct. Polym.* 161 (2021) 104855. <https://doi.org/10.1016/j.reactfunctpolym.2021.104855>.
- [62] C. Malitesta, F. Palmisano, L. Torsi, P.G. Zambonin, *Glucose Fast-Response Amperometric Sensor Based on Glucose Oxidase Immobilized in an Electropolymerized Poly(o-phenylenediamine) Film*, *Anal. Chem.* 62 (1990) 2735–2740.
- [63] R.D. Crapnell, A. Hudson, C.W. Foster, K. Eersels, B. van Grinsven, T.J. Cleij, C.E. Banks, M. Peeters, *Recent advances in electrosynthesized molecularly imprinted polymer sensing platforms for bioanalyte detection*, *Sens. Switz.* 19 (2019). <https://doi.org/10.3390/s19051204>.

- [64] J. Erdo(double acute)ssy, V. Horváth, A. Yarman, F.W. Scheller, R.E. Gyurcsányi, Electrosynthesized molecularly imprinted polymers for protein recognition, *TrAC - Trends Anal. Chem.* 79 (2016) 179–190. <https://doi.org/10.1016/j.trac.2015.12.018>.
- [65] N. Karimian, A.P.F. Turner, A. Tiwari, Electrochemical evaluation of troponin T imprinted polymer receptor, *Biosens. Bioelectron.* 59 (2014) 160–165.
- [66] G. Ozcelikay, S. Kurbanoglu, A. Yarman, F.W. Scheller, S.A. Ozkan, Au-Pt nanoparticles based molecularly imprinted nanosensor for electrochemical detection of the lipopeptide antibiotic drug Daptomycin, *Sens. Actuators B Chem.* 320 (2020) 128285. <https://doi.org/10.1016/j.snb.2020.128285>.
- [67] M. Mostafavi, M.R. Yaftian, F. Piri, H. Shayani-Jam, A new diclofenac molecularly imprinted electrochemical sensor based upon a polyaniline/reduced graphene oxide nano-composite, *Biosens. Bioelectron.* 122 (2018) 160–167. <https://doi.org/10.1016/j.bios.2018.09.047>.
- [68] M.H. Do, A. Florea, C. Farre, A. Bonhomme, F. Bessueille, F. Vocanson, N.T. Tran-Thi, N. Jaffrezic-Renault, Molecularly imprinted polymer-based electrochemical sensor for the sensitive detection of glyphosate herbicide, *Int. J. Environ. Anal. Chem.* 95 (2015) 1489–1501. <https://doi.org/10.1080/03067319.2015.1114109>.
- [69] T.S.C.R. Rebelo, R. Costa, A.T.S.C. Brandão, A.F. Silva, M.G.F. Sales, C.M. Pereira, Molecularly imprinted polymer SPE sensor for analysis of CA-125 on serum, *Anal. Chim. Acta.* 1082 (2019) 126–135. <https://doi.org/10.1016/j.aca.2019.07.050>.
- [70] B.V.M. Silva, B.A.G. Rodríguez, G.F. Sales, M.D.P.T. Sotomayor, R.F. Dutra, An ultrasensitive human cardiac troponin T graphene screen-printed electrode based on electropolymerized-molecularly imprinted conducting polymer, *Biosens. Bioelectron.* 77 (2016) 978–985. <https://doi.org/10.1016/j.bios.2015.10.068>.
- [71] W.R. Zhao, T.F. Kang, L.P. Lu, S.Y. Cheng, Electrochemical magnetic imprinted sensor based on MWCNTs@CS/CTABr surfactant composites for sensitive sensing of diethylstilbestrol, *J. Electroanal. Chem.* 818 (2018) 181–190. <https://doi.org/10.1016/j.jelechem.2018.04.036>.
- [72] M. Dinc, H. Basan, T. Hummel, M. Müller, H. Sobek, I. Rapp, T. Diemant, R.J. Behm, M. Lindén, B. Mizaikoff, Selective Binding of Inhibitor-Assisted Surface-Imprinted Core/Shell Microbeads in Protein Mixtures, *ChemistrySelect.* 3 (2018) 4277–4282. <https://doi.org/10.1002/slct.201800129>.
- [73] X. Zhang, A. Yarman, J. Erdossy, S. Katz, I. Zebger, K.J. Jetzschmann, Z. Altintas, U. Wollenberger, R.E. Gyurcsányi, F.W. Scheller, Electrosynthesized MIPs for transferrin: Plastibodies or nano-filters?, *Biosens. Bioelectron.* 105 (2018) 29–35. <https://doi.org/10.1016/j.bios.2018.01.011>.

- [74] T. Di Giulio, E. Mazzotta, C. Malitesta, Molecularly imprinted polyscopoletin for the electrochemical detection of the chronic disease marker lysozyme, *Biosensors*. 11 (2021). <https://doi.org/10.3390/bios11010003>.
- [75] Z. Stojanovic, J. Erdössy, K. Keltai, F.W. Scheller, R.E. Gyurecsányi, Electrosynthesized molecularly imprinted polyscopoletin nanofilms for human serum albumin detection, *Anal. Chim. Acta*. 977 (2017) 1–9. <https://doi.org/10.1016/j.aca.2017.04.043>.
- [76] D. Centonze, C. Malitesta, F. Palmisano, P.G. Zambonin, Permeation of solutes through an electropolymerized ultrathin poly(o-phenylenediamine) film used as an enzyme-entrapping membrane, *Electroanalysis*. 6 (1994) 423–429. <https://doi.org/10.1002/elan.1140060511>.
- [77] I. Losito, F. Palmisano, P.G. Zambonin, O-Phenylenediamine Electropolymerization By Cyclic Voltammetry Combined With Electrospray Ionization-Ion Trap Mass Spectrometry, *Anal. Chem.* 75 (2003) 4988–4995. <https://doi.org/10.1021/ac0342424>.
- [78] S.M. Sayyah, M.M. El-Deeb, S.M. Kamal, R.E. Azooz, Electropolymerization of O-Phenylenediamine on Pt-Electrode from Aqueous Acidic Solution: Kinetic, Mechanism, Electrochemical Studies and Characterization of the Polymer Obtained, *J. Appl. Polym. Sci.* 112 (2009) 3695–3706.
- [79] I. Losito, E. De Giglio, N. Cioffi, C. Malitesta, Spectroscopic investigation on polymer films obtained by oxidation of o-phenylenediamine on platinum electrodes at different pHs, *J. Mater. Chem.* 11 (2001) 1812–1817. <https://doi.org/10.1039/b101626l>.
- [80] J.W. Long, C.P. Rhodes, A.L. Young, D.R. Rolison, Ultrathin, protective coatings of poly(o-phenylenediamine) as electrochemical proton gates: Making mesoporous MnO<sub>2</sub> nanoarchitectures stable in acid electrolytes, *Nano Lett.* 3 (2003) 1155–1161. <https://doi.org/10.1021/nl0343598>.
- [81] M.A. Beluomini, N. Karimian, N.R. Stradiotto, P. Ugo, Tailor-made 3D-nanoelectrode ensembles modified with molecularly imprinted poly(o-phenylenediamine) for the sensitive detection of L-arabitol, *Sens. Actuators B Chem.* 284 (2019) 250–257. <https://doi.org/10.1016/j.snb.2018.12.091>.
- [82] N. Karimian, A.M. Stortini, L.M. Moretto, C. Costantino, S. Bogialli, P. Ugo, Electrochemosensor for Trace Analysis of Perfluorooctanesulfonate in Water Based on a Molecularly Imprinted Poly(o-phenylenediamine) Polymer, *ACS Sens.* 3 (2018) 1291–1298.
- [83] R. Liang, R. Zhang, W. Qin, Potentiometric sensor based on molecularly imprinted polymer for determination of melamine in milk, *Sens. Actuators B Chem.* 141 (2009) 544–550. <https://doi.org/10.1016/j.snb.2009.05.024>.

- [84] K. Liu, W.Z. Wei, J.X. Zeng, X.Y. Liu, Y.P. Gao, Application of a novel electrosynthesized polydopamine-imprinted film to the capacitive sensing of nicotine, *Anal. Bioanal. Chem.* 385 (2006) 724–729. <https://doi.org/10.1007/s00216-006-0489-z>.
- [85] D.R. Thévenot, K. Toth, R.A. Durst, G.S. Wilson, Electrochemical biosensors: Recommended definitions and classification, *Anal. Lett.* 34 (2001) 635–659. <https://doi.org/10.1081/AL-100103209>.
- [86] N. Leibl, K. Haupt, C. Gonzato, L. Duma, Molecularly imprinted polymers for chemical sensing: A tutorial review, *Chemosensors.* 9 (2021) 1–19. <https://doi.org/10.3390/chemosensors9060123>.
- [87] R.D. Crapnell, N.C. Dempsey-Hibbert, M. Peeters, A. Tridente, C.E. Banks, Molecularly imprinted polymer based electrochemical biosensors: Overcoming the challenges of detecting vital biomarkers and speeding up diagnosis, *Talanta Open.* 2 (2020) 100018. <https://doi.org/10.1016/j.talo.2020.100018>.
- [88] M. V. Mirkin, A.J. Bard, Multidimensional integral equations: a new approach to solving microelectrode diffusion problems. Part 2. Applications to microband electrodes and the scanning electrochemical microscope, *J. Electroanal. Chem.* 323 (1992) 29–51. [https://doi.org/10.1016/0022-0728\(92\)80002-L](https://doi.org/10.1016/0022-0728(92)80002-L).
- [89] J. Guo, E. Lindner, Cyclic voltammograms at coplanar and shallow recessed microdisk electrode arrays: Guidelines for design and experiment, *Anal. Chem.* 81 (2009) 130–138. <https://doi.org/10.1021/ac801592j>.
- [90] A. Zanut, A. Cian, N. Cefarin, A. Pozzato, M. Tormen, Nanoelectrode Arrays Fabricated by Thermal Nanoimprint Lithography for Biosensing Application, *Biosensors.* 10 (2020). <https://doi.org/10.3390/bios10080090>.
- [91] J.F. Rusling, G. Sotzing, F. Papadimitrakopoulou, Designing nanomaterial-enhanced electrochemical immunosensors for cancer biomarker proteins, *Bioelectrochemistry.* 76 (2009) 189–194. <https://doi.org/10.1016/j.bioelechem.2009.03.011>.
- [92] Y.H. Lanyon, G. De Marzi, Y.E. Watson, A.J. Quinn, J.P. Gleeson, G. Redmond, D.W.M. Arrigan, Fabrication of nanopore array electrodes by focused ion beam milling, *Anal. Chem.* 79 (2007) 3048–3055. <https://doi.org/10.1021/ac061878x>.
- [93] E. Albisetti, D. Petti, M. Pancaldi, M. Madami, S. Tacchi, J. Curtis, W.P. King, A. Papp, G. Csaba, W. Porod, P. Vavassori, E. Riedo, R. Bertacco, Nanopatterning reconfigurable magnetic landscapes via thermally assisted scanning probe lithography, *Nat. Nanotechnol.* 11 (2016) 545–551. <https://doi.org/10.1038/nnano.2016.25>.



- [94] F. Virgilio, M. Prasciolu, P. Ugo, M. Tormen, Development of electrochemical biosensors by e-beam lithography for medical diagnostics, *Microelectron. Eng.* 111 (2013) 320–324. <https://doi.org/10.1016/j.mee.2013.02.026>.
- [95] M. Sentic, F. Virgilio, A. Zanut, D. Manojlovic, S. Arbault, M. Tormen, N. Sojic, P. Ugo, Microscopic imaging and tuning of electrogenerated chemiluminescence with boron-doped diamond nanoelectrode arrays, *Anal. Bioanal. Chem.* 408 (2016) 7085–7094. <https://doi.org/10.1007/s00216-016-9504-1>.
- [96] L.J. Guo, Nanoimprint lithography: Methods and material requirements, *Adv. Mater.* 19 (2007) 495–513. <https://doi.org/10.1002/adma.200600882>.
- [97] S.Y. Chou, P.R. Krauss, P.J. Renstrom, Imprint of sub-25 nm vias and trenches in polymers, *Appl. Phys. Lett.* 67 (1995) 3114. <https://doi.org/10.1063/1.114851>.
- [98] L.M. Moretto, M. Tormen, M. De Leo, A. Carpentiero, P. Ugo, Polycarbonate-based ordered arrays of electrochemical nanoelectrodes obtained by e-beam lithography, *Nanotechnology.* 22 (2011). <https://doi.org/10.1088/0957-4484/22/18/185305>.
- [99] B. Brunetti, P. Ugo, L.M. Moretto, C.R. Martin, Electrochemistry of phenothiazine and methylviologen biosensor electron-transfer mediators at nanoelectrode ensembles, *J. Electroanal. Chem.* 491 (2000) 166–174. [https://doi.org/10.1016/S0022-0728\(00\)00169-8](https://doi.org/10.1016/S0022-0728(00)00169-8).
- [100] A. Lombardo, T.I. Bieber, Ferrocenylmethylation of aniline: nonkinetic determination of a reaction mechanism, *J. Chem. Educ.* 60 (1983) 1080. <https://doi.org/10.1021/ed060p1080>.
- [101] B. Brunetti, P. Ugo, L.M. Moretto, C.R. Martin, Electrochemistry of phenothiazine and methylviologen biosensor electron-transfer mediators at nanoelectrode ensembles, *J. Electroanal. Chem.* 491 (2000) 166–174. [https://doi.org/10.1016/S0022-0728\(00\)00169-8](https://doi.org/10.1016/S0022-0728(00)00169-8).
- [102] A. Zanut, A. Cian, N. Cefarin, A. Pozzato, M. Tormen, Nanoelectrode Arrays Fabricated by Thermal Nanoimprint Lithography for Biosensing Application, *Biosensors.* 10 (2020) 90. <https://doi.org/10.3390/bios10080090>.
- [103] A.J. Bard, L.R. Faulkner, *Electrochemical methods: fundamentals and applications*, 2nd ed, Wiley, New York, 2001.
- [104] G.W. Hance, Theodore. Kuwana, Effect of glassy carbon pretreatment on background double-layer capacitance and adsorption of neutral organic molecules, *Anal. Chem.* 59 (1987) 131–134. <https://doi.org/10.1021/ac00128a027>.
- [105] H. Ji, X. Zhao, Z. Qiao, J. Jung, Y. Zhu, Y. Lu, L.L. Zhang, A.H. MacDonald, R.S. Ruoff, Capacitance of carbon-based electrical double-layer capacitors, *Nat. Commun.* 5 (2014) 3317. <https://doi.org/10.1038/ncomms4317>.

- [106] H. Habtamu, T. Not, L. De Leo, S. Longo, L. Moretto, P. Ugo, Electrochemical Immunosensor Based on Nanoelectrode Ensembles for the Serological Analysis of IgG-type Tissue Transglutaminase, *Sensors*. 19 (2019) 1233. <https://doi.org/10.3390/s19051233>.
- [107] V.P. Menon, C.R. Martin, Fabrication and Evaluation of Nanoelectrode Ensembles, *Anal. Chem.* 67 (1995) 1920–1928.
- [108] A. Shafaat, F. Faridbod, M.R. Ganjali, Label-free detection of cytochrome C by a conducting polymer-based impedimetric screen-printed aptasensor, *New J. Chem.* 42 (2018) 6034—6039-6034—6039.
- [109] P. Manickam, A. Kaushik, C. Karunakaran, S. Bhansali, Recent advances in cytochrome c biosensing technologies, *Biosens. Bioelectron.* 87 (2017) 654–668.
- [110] P. Li, D. Nijhawan, I. Budihardjo, S.M. Srinivasula, M. Ahmad, E.S. Alnemri, X. Wang, Cytochrome c and dATP-Dependent Formation of Apaf-1/Caspase-9 Complex Initiates an Apoptotic Protease Cascade, *Cell*. 91 (1997) 479–489. [https://doi.org/10.1016/S0092-8674\(00\)80434-1](https://doi.org/10.1016/S0092-8674(00)80434-1).
- [111] I. Lee, A.R. Salomon, K. Yu, J.W. Doan, L.I. Grossman, M. Hüttemann, New prospects for an old enzyme: mammalian cytochrome c is tyrosine-phosphorylated in vivo., *Biochemistry*. 45 (2006) 9121–9128. <https://doi.org/10.1021/bi060585v>.
- [112] H. Yu, I. Lee, A.R. Salomon, K. Yu, M. Hüttemann, Mammalian liver cytochrome c is tyrosine-48 phosphorylated in vivo, inhibiting mitochondrial respiration., *Biochim. Biophys. Acta*. 1777 (2008) 1066–1071. <https://doi.org/10.1016/j.bbabi.2008.04.023>.
- [113] G. Benard, N. Bellance, C. Jose, R. Rossignol, Relationships between mitochondrial dynamics and bioenergetics, in: *Mitochondrial Dyn. Neurodegener.*, Springer, 2011: pp. 47–68.
- [114] C. Loreto, G. La Rocca, R. Anzalone, R. Caltabiano, G. Vespasiani, S. Castorina, D.J. Ralph, S. Celtek, G. Musumeci, S. Giunta, R. Djinovic, D. Basic, S. Sansalone, The role of intrinsic pathway in apoptosis activation and progression in Peyronie’s disease., *BioMed Res. Int.* 2014 (2014) 616149. <https://doi.org/10.1155/2014/616149>.
- [115] T. Alleyne, J. Joseph, V. Sampson, Cytochrome-c detection: a diagnostic marker for myocardial infarction, *Appl. Biochem. Biotechnol.* 90 (2001) 97–105.
- [116] K. Barczyk, M. Kreuter, J. Pryjma, E.P. Booy, S. Maddika, S. Ghavami, W.E. Berdel, J. Roth, M. Los, Serum cytochrome c indicates in vivo apoptosis and can serve as a prognostic marker during cancer therapy, *Int. J. Cancer*. 116 (2005) 167–173.
- [117] I. Sakaida, T. Kimura, T. Yamasaki, Y. Fukumoto, K. Watanabe, M. Aoyama, K. Okita, Cytochrome c is a possible new marker for fulminant hepatitis in humans, *J. Gastroenterol.* 40 (2005) 179–185. <https://doi.org/10.1007/s00535-004-1517-4>.

- [118] Z. Ben-Ari, H. Schmilovotz-Weiss, A. Belinki, O. Pappo, J. Sulkes, M.G. Neuman, E. Kaganovsky, B. Kfir, R. Tur-Kaspa, T. Klein, Circulating soluble cytochrome c in liver disease as a marker of apoptosis, *J. Intern. Med.* 254 (2003) 168–175. <https://doi.org/10.1046/j.1365-2796.2003.01171.x>.
- [119] T.J. Miller, A. Knapton, O. Adeyemo, L. Noory, J. Weaver, J.P. Hanig, Cytochrome c: a non-invasive biomarker of drug-induced liver injury, *J. Appl. Toxicol.* 28 (2008) 815–828. <https://doi.org/10.1002/jat.1347>.
- [120] J. Javid, R. Mir, P.K. Julka, P.C. Ray, A. Saxena, Extracellular cytochrome c as a biomarker for monitoring therapeutic efficacy and prognosis of non-small cell lung cancer patients, *Tumor Biol.* 36 (2015) 4253–4260. <https://doi.org/10.1007/s13277-015-3062-6>.
- [121] L. Ma, F. Liu, Z. Lei, Z. Wang, A novel upconversion@polydopamine core@shell nanoparticle based aptameric biosensor for biosensing and imaging of cytochrome c inside living cells, *Biosens. Bioelectron.* 87 (2017) 638–645.
- [122] M. Shamsipur, F. Molaabasi, S. Hosseinkhani, F. Rahmati, Detection of Early Stage Apoptotic Cells Based on Label-Free Cytochrome c Assay Using Bioconjugated Metal Nanoclusters as Fluorescent Probes, *Anal. Chem.* 88 (2016) 2188–2197.
- [123] M.R.K. Pur, M. Hosseini, F. Faridbod, A.S. Dezfuli, M.R. Ganjali, A novel solid-state electrochemiluminescence sensor for detection of cytochrome c based on ceria nanoparticles decorated with reduced graphene oxide nanocomposite, *Sens. Actuators B* 408 (2016) 7193–7202.
- [124] X. Li, H. Liu, X. He, Z. Song, Determination of cytochrome c in human serum and pharmaceutical injections using flow injection chemiluminescence, *Appl. Biochem. Biotechnol.* 160 (2010) 1065–1073.
- [125] S.I. Dikalov, D.G. Harrison, Methods for detection of mitochondrial and cellular reactive oxygen species, *Antioxid. Redox Signal.* 20 (2014) 372–382.
- [126] L.H. Russell, E. Mazzi, R.B. Badisa, Z.P. Zhu, M. Agharahimi, E.T. Oriaku, C.B. Goodman, Autoxidation of Gallic acid Induces ROS-dependant Death in Human Prostate Cancer LNCaP Cells, *Anticancer Res.* 32 (2012) 1595–1602.
- [127] M. Tafani, N.O. Karpinich, K.A. Hurster, J.G. Pastorino, T. Schneider, Russo M.A., J.L. Farber, Cytochrome c release upon Fas receptor activation depends on translocation of full-length bid and the induction of the mitochondrial permeability transition, *J. Biol. Chem.* 277 (2002) 10073–10082.
- [128] F. Appaix, M.-N. Minatchy, C. Riva-Lavieille, J. Olivares, B. Antonsson, V.A. Saks, No Title, *Biochim. Biophys. Acta BBA-Bioenerg.* 1457 (2000) 175–181.

- [129] J. Wang, Portable electrochemical systems, *Trends Anal. Chem.* 21 (2002) 226–232.
- [130] V.V. Shumyantseva, T.V. Bulko, A.V. Kuzikov, R.A. Masamrek, D.V. Pergushov, F.H. Schacher, L.V. Sigolaeva, Electrochemical fingerprint of cytochrome c on a polymer/MWCNT nanocomposite electrode, *Mendeleev Commun.* 30 (2020) 299–301.
- [131] T. Sagara, H. Murakami, S. Igarashi, H. Sato, K. Niki, Spectroelectrochemical Study of the Redox Reaction Mechanism of Cytochrome c at a Gold Electrode in a Neutral Solution in the Presence of 4,4'-Bipyridyl as a Surface Modifier, *Langmuir.* 7 (1991) 3190–3196.
- [132] N. Matsuda, H. Okabe, T. Nagamura, K. Nakano, Direct Electron Transfer Reaction of Cytochrome c Immobilized on a Bare ITO Electrode, *Bull. Chem. Soc. Jpn.* 94 (2021) 433–439.
- [133] M.J. Eddowes, H.A.O. Hill, Novel Method for the Investigation of the Electrochemistry of Metalloproteins : Cytochrome c, *J. Chem. Soc. Chem. Commun.* 747 (1977) 771–772.
- [134] M.J. Eddowes, H.A.O. Hill, Electrochemistry of Horse Heart Cytochrome c, *J. Am. Chem. Soc.* 101 (1979) 4461–4464.
- [135] I. Taniguchi, M. Iseki, T. Eto, K. Toyosawa, H. Yamaguchi, K. Yasukouchi, 722—The effect of pH on the temperature dependence of the redox potential of horse heart cytochrome c at a bis(4-pyridyl)disulfide-modified gold electrode, *Bioelectrochem. Bioenerg.* 13 (1984) 373–383.
- [136] I. Taniguchi, K. Toyosawa, H. Yamaguchi, K. Yasukuoki, Reversible Electrochemical Reduction and Oxidation of Cytochrome c at a Bis(4-pyridyl) Disulphide-modified Gold Electrode, *J. Chem. Soc. Chem. Commun.* 733 (1982) 1032–1033.
- [137] A. Avila, B.W. Gregory, K. Niki, T.M. Cotton, An Electrochemical Approach to Investigate Gated Electron Transfer Using a Physiological Model System: Cytochrome c Immobilized on Carboxylic Acid-Terminated Alkanethiol Self-Assembled Monolayers on Gold Electrodes, *J. Phys. Chem. B.* 104 (2000) 2759–2766.
- [138] J.M. Cooper, K.R. Greenough, C.J. McNeil, Direct electron transfer reactions between immobilized cytochrome c and modified gold electrodes, *J. Electroanal. Chem.* 347 (1993) 267–275.
- [139] E. Lojou, P. Luciano, S. Nitsche, P. Bianco, Poly(ester-sulfonic acid): modified carbon electrodes for the electrochemical study of c-type cytochromes, *Electrochimica Acta.* 44 (1999) 3341–3352.
- [140] P. Ugo, V. Zangrando, L.M. Moretto, B. Brunetti, Ion-exchange voltammetry and electrocatalytic sensing capabilities of cytochrome c at polyestersulfonated ionomer coated glassy carbon electrodes, *Biosens. Bioelectron.* 17 (2002) 479–487.

- [141] L.M. Moretto, P. Bertoncello, F. Vezza, P. Ugo, Electrochemistry of cytochrome c incorporated in Langmuir-Blodgett films of Nafion (R) and Eastman AQ 55 (R), *Bioelectrochem. Bioenerg.* 66 (2005) 29-34-29-34.
- [142] Z.S. Aghamiri, M. Mohsennia, H.A. Rafiee-Pour, Immobilization of cytochrome c on polyaniline/polypyrrole/carboxylated multi-walled carbon nanotube/glassy carbon electrode: biosensor fabrication, *J. Solid State Electrochem.* 23 (2019) 2233-2242.
- [143] F.A. Armstrong, A.M. Bond, H.A.O. Hill, I.S.M. Psalti, C.G. Zoski, A Microscopic Model of Electron Transfer at Electroactive Sites of Molecular Dimensions for Reduction of Cytochrome c at Basal- and Edge-Plane Graphite Electrodes, *J. Phys. Chem. A.* 93 (1989) 6485-6493.
- [144] F.N. Buchi, A.M. Bond, Interpretation of the electrochemistry of cytochrome c at macro and micro sized carbon electrodes using a microscopic model based on a partially blocked surface, *J. Electroanal. Chem.* 314 (1991) 191-206.
- [145] A. Szucs, M. Novak, Stable and reversible electrochemistry of cytochrome c on bare electrodes-Part 1. Effect of ionic strength, *J. Electroanal. Chem.* 383 (1995) 75-84.
- [146] E.F. Bowden, F.M. Hawkrige, H.N. Blount, INTERFACIAL ELECTROCHEMISTRY OF CYTOCHROME c AT TIN OXIDE, INDIUM OXIDE, GOLD, AND PLATINUM ELECTRODES, *J. Electroanal. Chem.* 161 (1984) 355-376.
- [147] T. Voss, P. Grundler, C.M.A. Brett, A.M.O. Brett, Electrochemical behaviour of cytochrome c at electrically heated microelectrodes, *J. Pharm. Biomed. Anal.* 19 (1999) 127-133.
- [148] M. Kudera, A. Aitken, L. Liang, S. Kaneko, H.A.O. Hill, P.J. Dobson, P.A. Leigh, W.S. McIntire, Electron transfer processes of redox proteins at inherently modified microelectrode array devices, *J. Electroanal. Chem.* 495 (2000) 36-41.
- [149] A.K. Abass, J.P. Hart, Direct electrochemistry of cytochrome c at plain and membrane modified screen-printed carbon electrodes, *Electrochimica Acta.* 46 (2001) 829-836.
- [150] K.R. Brown, A.P. Fox, M. Natan, Morphology-Dependent Electrochemistry of Cytochrome c at Au Colloid-Modified SnO<sub>2</sub> Electrodes, *J. Am. Chem. Soc.* 118 (1996) 1154-1157.
- [151] H. Ju, S. Liu, B. Ge, F. Lisdat, F.W. Scheller, Electrochemistry of Cytochrome c Immobilized on Colloidal Gold Modified Carbon Paste Electrodes and Its Electrocatalytic Activity, *Electroanalysis.* 14 (2002) 141-147.
- [152] C.M. Silveira, R. Zumpano, M. Moreira, M.P. de Almeida, M.J. Oliveira, M. Bento, C. Montez, I. Paixão, R. Franco, E. Pereira, M.G. Almeida, Star-Shaped Gold Nanoparticles as Friendly Interfaces for Protein Electrochemistry: the Case Study of Cytochrome c, *ChemElectroChem.* 6 (2019) 4696-4703.

- [153] P. Ugo, N. Pepe, L.M. Moretto, M. Battagliarin, Direct voltammetry of cytochrome c at trace concentrations with nanoelectrode ensembles, *J. Electroanal. Chem.* 560 (2003) 51–58.
- [154] P. Ugo, P. Marafini, M. Meneghello, *Bioanalytical chemistry-from biomolecular recognition to nanobiosensing*, De Gruyter, Berlin, 2021.
- [155] M. Fedurco, Redox reactions of heme-containing metalloproteins: Dynamic effects of self-assembled monolayers on thermodynamics and kinetics of cytochrome c electron-transfer reactions, *Coord. Chem. Rev.* 209 (2000) 263–331. [https://doi.org/10.1016/S0010-8545\(00\)00292-7](https://doi.org/10.1016/S0010-8545(00)00292-7).
- [156] T. Sagara, H. Murakami, S. Igarashi, H. Sato, K. Niki, Spectroelectrochemical Study of the Redox Reaction Mechanism of Cytochrome c at a Gold Electrode in a Neutral Solution in the Presence of 4,4'-Bipyridyl as a Surface Modifier, *Langmuir.* 7 (1991) 3190–3196.
- [157] C. Amatore, J.M. Savéant, D. Tessier, Charge Transfer at Partially Blocked Surfaces. A Model for the Case of Microscopic Active and Inactive Sites, *J. Electroanal. Chem.* 147 (1983) 39–51.
- [158] V.P. Menon, C.R. Martin, Fabrication and Evaluation of Nanoelectrode Ensembles, *Anal. Chem.* 67 (1995) 1920–1928.
- [159] A.J. Bard, L.R. Faulkner, *Electrochemical Methods: Fundamentals and Applications*, Wiley Global Education, New York, 2001.
- [160] N. Karimian, M.H. Arbab Zavar, M. Chamsaz, N. Ashraf, A.P.F. Turner, A. Tiwari, A potential-gated molecularly imprinted smart electrode for nicotinamide analysis, *RSC Adv.* 5 (2015) 35089–35096.
- [161] B.L. Li, J.H. Luo, H.Q. Luo, N.B. Li, A novel strategy for selective determination of d-penicillamine based on molecularly imprinted polypyrrole electrode via the electrochemical oxidation with ferrocyanide, *Sens. Actuators B Chem.* 186 (2013) 96–102.
- [162] A. Nezhadali, L. Mehri, R. Shadmehri, Determination of benzimidazole in biological model samples using electropolymerized-molecularly imprinted polypyrrole modified pencil graphite sensor, *Sens. Actuators B Chem.* 171 (2012) 1125–1131.
- [163] N. Karimian, A.P.F. Turner, A. Tiwari, Electrochemical evaluation of troponin T imprinted polymer receptor, *Biosens. Bioelectron.* 59 (2014) 160–165. <https://doi.org/10.1016/j.bios.2014.03.013>.
- [164] R. Kazemi, E.I. Potts, J.E. Dick, Quantifying Interferent Effects on Molecularly Imprinted Polymer Sensors for Per- and Polyfluoroalkyl Substances (PFAS), *Anal. Chem.* 92 (2020) 10597–10605.

- [165] X. Hong, Y. Meng, S.N. Kalkanis, Serum proteins are extracted along with monolayer cells in plasticware and interfere with protein analysis, *J. Biol. Methods.* 3 (2016) e51. <https://doi.org/10.14440/jbm.2016.129>.
- [166] X. Han, S. Li, Z. Peng, A.M. Othman, R. Leblanc, Recent Development of Cardiac Troponin I Detection, *ACS Sens.* 1 (2016) 106–114. <https://doi.org/10.1021/acssensors.5b00318>.
- [167] P.A. Heidenreich, T. Alloggiamento, K. Melsop, K.M. McDonald, A.S. Go, M.A. Hlatky, The prognostic value of troponin in patients with non-ST elevation acute coronary syndromes: A meta-analysis, *J. Am. Coll. Cardiol.* 38 (2001) 478–485. [https://doi.org/10.1016/S0735-1097\(01\)01388-2](https://doi.org/10.1016/S0735-1097(01)01388-2).
- [168] A. Jeremias, The utility of troponin measurement to detect myocardial infarction: review of the current findings, *Vasc. Health Risk Manag.* (2010) 691. <https://doi.org/10.2147/VHRM.S5306>.
- [169] F.S. Apple, Cardiac Troponin Assays: Analytical Issues and Clinical Reference Range Cutpoints, *Cardiovasc. Toxicol.* 1 (2001) 093–098. <https://doi.org/10.1385/CT:1:2:093>.
- [170] A. Nezami, S. Dehghani, R. Nosrati, N. Eskandari, S.M. Taghdisi, G. Karimi, Nanomaterial-based biosensors and immunosensors for quantitative determination of cardiac troponins, *J. Pharm. Biomed. Anal.* 159 (2018) 425–436. <https://doi.org/10.1016/j.jpba.2018.07.031>.
- [171] P.K. Bhavsar, G.K. Dhoot, D.V. Cumming, G.S. Butler-Browne, M.H. Yacoub, P.J. Barton, Developmental expression of troponin I isoforms in fetal human heart., *FEBS Lett.* 292 (1991) 5–8. [https://doi.org/10.1016/0014-5793\(91\)80820-s](https://doi.org/10.1016/0014-5793(91)80820-s).
- [172] S. Sasse, N.J. Brand, P. Kyprianou, G.K. Dhoot, R. Wade, M. Arai, M. Periasamy, M.H. Yacoub, P.J. Barton, Troponin I gene expression during human cardiac development and in end-stage heart failure., *Circ. Res.* 72 (1993) 932–938. <https://doi.org/10.1161/01.res.72.5.932>.
- [173] S.J. Maynard, I.B.A. Menown, A.A.J. Adgey, Troponin T or troponin I as cardiac markers in ischaemic heart disease, *Heart.* 83 (2000) 371–373. <https://doi.org/10.1136/heart.83.4.371>.
- [174] A.R. Chapman, D. Sandeman, A.V. Ferry, S. Stewart, F.E. Strachan, R. Wereski, A. Bularga, A. Anand, A.S.V. Shah, N.L. Mills, Risk Stratification Using High-Sensitivity Cardiac Troponin T in Patients With Suspected Acute Coronary Syndrome, *J. Am. Coll. Cardiol.* 75 (2020) 985–987. <https://doi.org/10.1016/j.jacc.2019.12.036>.
- [175] A. Bagai, K.P. Alexander, J.S. Berger, R. Senior, C. Sajeev, R. Pracon, K. Mavromatis, J.L. Lopez-Sendón, G. Gosselin, A. Diaz, G. Perna, J. Drozd, D. Humen, B. Petrauskiene, A.N. Cheema, D. Phaneuf, S. Banerjee, T.D. Miller, S. Kedev, H. Schuchlenz, G.W. Stone, S.G. Goodman, K.W. Mahaffey, A.S. Jaffe, Y.D. Rosenberg, S. Bangalore, L.K. Newby, D.J. Maron, J.S. Hochman, B.R. Chaitman, Use of troponin assay 99th percentile as the decision level for

- myocardial infarction diagnosis, *Am. Heart J.* 190 (2017) 135–139. <https://doi.org/10.1016/j.ahj.2017.04.016>.
- [176] B. Cummins, M.L. Auckland, P. Cummins, Cardiac-specific troponin-I radioimmunoassay in the diagnosis of acute myocardial infarction, *Am. Heart J.* 113 (1987) 1333–1344. [https://doi.org/10.1016/0002-8703\(87\)90645-4](https://doi.org/10.1016/0002-8703(87)90645-4).
- [177] I.-H. Cho, E.-H. Paek, Y.-K. Kim, J.-H. Kim, S.-H. Paek, Chemiluminometric enzyme-linked immunosorbent assays (ELISA)-on-a-chip biosensor based on cross-flow chromatography, *Anal. Chim. Acta.* 632 (2009) 247–255. <https://doi.org/10.1016/j.aca.2008.11.019>.
- [178] G.-R. Han, M.-G. Kim, Highly Sensitive Chemiluminescence-Based Lateral Flow Immunoassay for Cardiac Troponin I Detection in Human Serum, *Sensors.* 20 (2020) 2593. <https://doi.org/10.3390/s20092593>.
- [179] C.A. Marquette, F. Bouteille, B.P. Corgier, A. Degiuli, L.J. Blum, Disposable screen-printed chemiluminescent biochips for the simultaneous determination of four point-of-care relevant proteins, *Anal. Bioanal. Chem.* 393 (2009) 1191–1198. <https://doi.org/10.1007/s00216-008-2503-0>.
- [180] S.-W. Kim, I.-H. Cho, J.-N. Park, S.-M. Seo, S.-H. Paek, A High-Performance Fluorescence Immunoassay Based on the Relaxation of Quenching, Exemplified by Detection of Cardiac Troponin I, *Sensors.* 16 (2016) 669. <https://doi.org/10.3390/s16050669>.
- [181] V.T. Tran, H. Ju, Fluorescence Based on Surface Plasmon Coupled Emission for Ultrahigh Sensitivity Immunoassay of Cardiac Troponin I, *Biomedicines.* 9 (2021) 448. <https://doi.org/10.3390/biomedicines9050448>.
- [182] Y. Ma, X.-L. Shen, H.-S. Wang, J. Tao, J.-Z. Huang, Q. Zeng, L.-S. Wang, MIPs-graphene nanoplatelets-MWCNTs modified glassy carbon electrode for the determination of cardiac troponin I, *Anal. Biochem.* 520 (2017) 9–15. <https://doi.org/10.1016/j.ab.2016.12.018>.
- [183] S. Ko, B. Kim, S.S. Jo, S.Y. Oh, J.K. Park, Electrochemical detection of cardiac troponin I using a microchip with the surface-functionalized poly(dimethylsiloxane) channel, *Biosens. Bioelectron.* 23 (2007) 51–59. <https://doi.org/10.1016/j.bios.2007.03.013>.
- [184] V. Bhalla, S. Carrara, P. Sharma, Y. Nangia, C. Raman Suri, Gold nanoparticles mediated label-free capacitance detection of cardiac troponin i, *Sens. Actuators B Chem.* 161 (2012) 761–768. <https://doi.org/10.1016/j.snb.2011.11.029>.
- [185] H. Jo, H. Gu, W. Jeon, H. Youn, J. Her, S.K. Kim, J. Lee, J.H. Shin, C. Ban, Electrochemical Aptasensor of Cardiac Troponin i for the Early Diagnosis of Acute Myocardial Infarction, *Anal. Chem.* 87 (2015) 9869–9875. <https://doi.org/10.1021/acs.analchem.5b02312>.



- [186] H. Jo, J. Her, H. Lee, Y.B. Shim, C. Ban, Highly sensitive amperometric detection of cardiac troponin I using sandwich aptamers and screen-printed carbon electrodes, *Talanta*. 165 (2017) 442–448. <https://doi.org/10.1016/j.talanta.2016.12.091>.
- [187] N. Karimian, A.M. Stortini, L.M. Moretto, C. Costantino, S. Bogialli, P. Ugo, Electrochemosensor for Trace Analysis of Perfluorooctanesulfonate in Water Based on a Molecularly Imprinted Poly(o-phenylenediamine) Polymer, *ACS Sens.* 3 (2018) 1291–1298. <https://doi.org/10.1021/acssensors.8b00154>.
- [188] J. Wang, B. Tian, V.B. Nascimento, L. Angnes, Performance of screen-printed carbon electrodes fabricated from different carbon inks, *Electrochimica Acta*. 43 (1998) 3459–3465. [https://doi.org/10.1016/S0013-4686\(98\)00092-9](https://doi.org/10.1016/S0013-4686(98)00092-9).
- [189] R.O. Kadara, N. Jenkinson, C.E. Banks, Characterisation of commercially available electrochemical sensing platforms, *Sens. Actuators B Chem.* 138 (2009) 556–562. <https://doi.org/10.1016/j.snb.2009.01.044>.
- [190] M.D. Osborne, B.J. Seddon, R.A.W. Dryfe, G. Lager, U. Loyall, H. Schäfer, H.H. Girault, Excimer laser-induced electrochemical activity in carbon ink films, *J. Electroanal. Chem.* 417 (1996) 5–15. [https://doi.org/10.1016/S0022-0728\(96\)04781-X](https://doi.org/10.1016/S0022-0728(96)04781-X).
- [191] M. Stiene, U. Bilitewski, Electrochemical characterization of screen-printed carbonaceous electrodes for the determination of peroxidase activity in novel screen-printed flow-through modules, *Fresenius J. Anal. Chem.* 372 (2002) 240–247. <https://doi.org/10.1007/s00216-001-1208-4>.
- [192] J. Wanga, M. Pedrera, H. Sakslund, O. Hammerich, *Analyst*, March 1996, Vol. 121 (345–350) 345, I (1996) 345–350.
- [193] A.G.M. Ferrari, C.W. Foster, P.J. Kelly, D.A.C. Brownson, C.E. Banks, Determination of the electrochemical area of screen-printed electrochemical sensing platforms, *Biosensors*. 8 (2018) 1–10. <https://doi.org/10.3390/bios8020053>.
- [194] Z. Nie, C.A. Nijhuis, J. Gong, X. Chen, A. Kumachev, A.W. Martinez, M. Narovlyansky, G.M. Whitesides, Electrochemical sensing in paper-based microfluidic devices, *Lab. Chip*. 10 (2010) 477–483. <https://doi.org/10.1039/B917150A>.
- [195] I. Losito, F. Palmisano, P.G. Zambonin, o-Phenylenediamine Electropolymerization by Cyclic Voltammetry Combined with Electrospray Ionization-Ion Trap Mass Spectrometry, *Anal. Chem.* 75 (2003) 4988–4995.
- [196] B. Fresco-Cala, B. Mizaikoff, Surrogate Imprinting Strategies: Molecular Imprints via Fragments and Dummies, *ACS Appl. Polym. Mater.* 2 (2020) 3714–3741.

[197] H. Guo, D. Yang, C. Gu, Z. Bian, N. He, J. Zhang, Development of a low density colorimetric protein array for cardiac troponin i detection, *J. Nanosci. Nanotechnol.* 5 (2005) 2161–2166.

## Acknowledgements

I would like to thank Prof. Paolo Ugo for the support in this journey, because he started to teach me the electrochemistry even if my level was less than the book “electrochemistry for dummies”.

I would like to thank Dr. Najmeh Karimian, PhD because she taught me all the expertise needed to carry out a PhD; for all the times I was struggling with the experiments, electrodes and for all the times when electrochemistry was annihilating my patience and self-control.

I would like to thank Dr. Dino Paladin, PhD and AB Analitica for their support in this thesis.

I would like to thank all the staff of ThunderNIL for providing me the electrodes NEA for doing the experiments in this thesis.

I would like to thank Dr. Angela Maria Stortini, PhD for sharing to me the secrets of SEM analysis. For all tip and tricks learned during the long experiment sessions. Also for the useful science discussions. Angela, Please remember the golden answer to everything: “let’s bring two euros of gasoline”.

I would like to thank Giada Bedendi for all the support during the summer of the 2020 entirely spent in Lab.

I would like to thank Thomas Scattolin, Enrica Bortolamiol, Rachele Piccolo, Francesco Fama, Giacomo Isetta, Luca Munarin, Davide organic lab, Valeria Gagliardi, Daniele amico del legno, Chiara Gaetani and Sole Zalaffi for all the meals at 13.00 pm, for the happiness, friendship and Pizza gamberetti and fried potatoes in these three years.

I am especially grateful to Margherita Donnici, without her presence surviving this PhD would not be possible.

I would like to thank Sara Linciano for discovering the best recipe in the world: “Patate, riso and Cozze”; also for useful discussions on why Puglia is the best place to live in the world.

I would like to thank Zhanna Romanyuk for the cursed Thursday myth, which is handed down from PhD student to PhD student through the centuries.

I would like to thank Ylenia Mazzocato for pressing me and continuously asking “Davide, have you started to write the thesis?”. She kept me on the way.

I would like to thank Giulia Moro for giving me the best pencil case in the world!!!!!!!!!!

I would like to thank Veronica Cacco for the best player in a sushi team ever!!!!!!

I would like to thank Trasporti Territoriali for giving me the opportunity to have a different idea of what are the possible shades of transport services.

I would like to thank Marco Polo Airport for its supporting in giving me an escape plan B if something would be in the wrong way.

I would like to thank my parents and their support even if they are still trying to understand what is a PhD.

I would like to thank Alvisè Menegazzo for all the support given in these three years.

I would like to thank Stefano Zanutta and Alessandro Persello, because they encouraged me to finish the PhD even when it was draining all my energies.

I would like to thank Elena Campaner, because given me the opportunity to demonstrate how resilient I am.

## Estratto per riassunto della tesi di dottorato

L'estratto (max. 1000 battute) deve essere redatto sia in lingua italiana che in lingua inglese e nella lingua straniera eventualmente indicata dal Collegio dei docenti.

L'estratto va firmato e rilegato come ultimo foglio della tesi.

Studente: Campagnol Davide \_\_\_\_\_ matricola: 956451

Dottorato: Science and Technology of Bio and Nanomaterials

Ciclo: XXXIV

Titolo della tesi<sup>1</sup>: *Advanced bioelectrochemical sensors based on nanostructured surfaces*

Abstract:

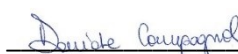
### English Abstract

In this thesis the preparation and characterization of nanostructured polymer films on different electrode materials are studied with focus on their potential application for biochemical analysis. With this goal both nanoelectrode arrays and molecular imprinted polymers were examined. The analytes of interest have been focused on same redox mediators used in bioelectrochemistry as well as proteins such as Cytochrome C and Troponin I. In particular the use of MIP showed very promising capabilities for the detection of Cytochrome C at trace concentrations levels ( $< \mu\text{M}$ ). Preliminary result indicates the possibility to extend this approach to high sensitivity detection of Troponin I as a cardiac disease potential biomarker.

### Italian Abstract

In questa tesi è stata studiata la preparazione e caratterizzazione di film polimerici nanostrutturati su differenti materiali elettrodi mantenendo focalizzato l'interesse sul loro potenziale uso nell'ambito della analisi biochimiche. Considerando questo obiettivo, si sono preparati, caratterizzati ed applicati sia array di nanoelettrodi sia polimeri a stampo molecolare. Gli analiti su cui i sensori sono stati sperimentati sono stati sia mediatori comunemente usati in bioelettrochimica, sia proteine come il Citocromo C e la Troponina I. In particolare i polimeri a stampo molecolare hanno mostrato una promettente capacità di rilevare il Citocromo C a concentrazione a livello di tracce ( $< \mu\text{M}$ ). Inoltre è stato effettuato uno studio preliminare volto ad estendere l'applicazione del medesimo approccio alla rilevazione ad alta sensibilità della Troponina I come potenziale biomarker nell'infarto del miocardio.

Firma dello studente



---

<sup>1</sup> Il titolo deve essere quello definitivo, uguale a quello che risulta stampato sulla copertina dell'elaborato consegnato.